SQT

INCOMPLETE DOCUMENT: MISSING PAGES

II, IV, V, IX, 46 and A-1

UNABLE TO OBTAIN FROM NASA CENTER

May 14, 1984 - DOCUMENT EVALUATOR

WYLE LABORATORIES — RESEARCH STAFF
REPORT WR 73-9

PREDICTION OF VIBRO-ACOUSTIC LOADING CRITERIA FOR SPACE VEHICLE COMPONENTS

By

K. Y. Chang
J. C. Cockburn
G. C. Kao

Work Performed Under Contract NAS8-25811

September 1973

WYLE LABORATORIES

COPY NO. 35

ABSTRACT

This report presents a technique to estimate driving force spectra of equipment packages attached to cylindrical structures subjected to broadband random acoustic excitations. This procedure is considered indicative of the present state-of-the-art and will provide satisfactory predictions of the vibratory environment.

The force-spectrum equation was derived from a one-dimensional mechanical impedance model and is expressed in terms of structural impedance, acoustic mobility and blocked pressure spectra. A set of nomograms and computational charts was developed to compute the force spectrum graphically with minimum amount of manual computation. Two example problems with different structural configurations were used to demonstrate computation procedures. Satisfactory agreements between analytical predictions and experimental measurements were observed.

LIST OF FIGURES

LIST OF FIGURES (Continued)

LIST OF FIGURES (Concluded)

M	=	Total mass
M_m	=	Modal mass
$\left[P_{block} \right]$	=	Blocked sound pressure levels
$\left[P_{far} \right]$	=	Far-field sound pressure levels
$\left[P_{flex} \right]$	=	Surface sound pressure levels
Q	=	Dynamic magnification factor
R	=	Radius
S_p	=	Pressure mean-square spectral density
$S_{\dot{u}}$	=	Velocity mean-square spectral density
ω	=	Circular frequency in rad/sec
ω_0	=	Resonance frequency of undamped system
x, y	=	Displacement
z	=	Specific structural impedance of transmission
Z	=	Input impedance
Z_B	=	Characteristic impedance of beams
Z_R	=	Characteristic impedance of rings
Z_S	=	Characteristic impedance of cylindrical shells
Z_L	=	Input impedance of component package
Z_P	=	Plate impedance
α	=	Acoustic mobility
α'	=	Normalized acoustic mobility
ρ	=	Mass density

ν	=	Poisson's ratio
Φ_L	=	Predicted driving force spectrum
Φ_P	=	Blocked sound pressure spectrum
Φ_R	=	Velocity response spectrum

1.0 INTRODUCTION

The prediction of localized vibratory criteria for space vehicle components due to acoustic excitation has been accomplished based on the empirical techniques as described in References 1 and 2. These techniques provide standardized approaches to predict vibro-acoustic environments with sufficient conservatism to satisfy design and test requirements for unloaded primary structures. The testing of components to such criteria is valid only when the impedance of a primary structure is sufficiently higher than that of the attached component. Otherwise, there is a strong possibility that the specimen would be overtested.

The objective of this program is to present a complementary technique by which the vibratory criteria are to be specified in terms of actual forces acting on components. Test specifications are given in terms of the power spectral density of a force environment and the approach is designated as the "Force-Spectrum" method. The method utilizes one-dimensional mechanical impedance models to describe dynamic characteristics of components and primary structures in the direction normal to supporting surfaces. These impedances together with the acoustic mobility and blocked pressure spectra form the basic elements to compute vibratory force environments.

The development of the Force-Spectrum method was accomplished in three phases. In the first phase, the one-dimensional Force-Spectrum equation was developed (Reference 3). An experimental program was conducted to validate the prediction equation. A stiffened aluminum cylinder with the dimensions of 3 ft (diameter) x 3 ft (height) x 0.02 in. (skin thickness) was used in acquiring input impedances and acoustic mobilities. An 8 in. x 8 in. x 1/2 in. aluminum plate was used as a simulated component. The plate was supported by four sets of leaf springs, and a loadwasher was attached to the bottom of each spring for measuring loads. The aluminum plate and the spring assemblies were used to measure the component package impedance. The blocked sound pressure spectra were obtained from microphone measurements on a rigid dummy concrete cylinder. Three equipment mounting positions and six acoustic excitation levels were used in the tests. All test data were acquired on-line to analog/digital data acquisition systems. Computer programs were written to reduce and analyze the acquired data, and also to make predictions on interaction force spectra. Good agreements between the predicted and measured force spectra were obtained.

The work performed in the second phase (Reference 4) consisted of evaluating the effectiveness of different vibration specifications and control techniques to qualify flight components for vibro-acoustic environments. The objectives of the evaluation are two-fold: the first is to investigate the ability of analog control systems in simulating vibro-acoustic environments as described above; and the second is to evaluate the severities of different component testing methods under different vibration specifications. The scope of this program is limited to the study of the one-dimensional simulation of vibro-acoustic environments by an electro-dynamic exciter in the frequency range of 50 Hz to 2000 Hz. The control techniques considered in this study included: the motion-control, the force-control and the current-control techniques. A total of eighteen (18) vibration specifications were used to perform testing on two component specimens excited by an electro-dynamic exciter. The test results suggest several possible solutions to meet realistic component testing requirements.

The work performed in the third phase consisted of developing simplified computation techniques to allow performing quick estimates on force spectra without involving computer runs. It is recognized that several analytical methods, such as the direct integration method and other numerical methods, can be used for the prediction of loads on finite cylindrical structures. Nevertheless, the resulting equations are either too sophisticated or too general and are not practical for performing quick estimates with adequate accuracies. Considering the fact that an average engineer does not have ample time to thoroughly analyze each individual problem; therefore, simplified methods are needed to solve complex problems with a minimum amount of calculations and yet provide adequate accuracy. This is accomplished by the use of charts and nomograms to reduce complex computations. The details of the simplified methods are presented in this report.

The force-spectrum predicting equation was derived from a one-dimensional mechanical impedance model. The equation contains four parameters defined at component mounting locations; namely:

- Input impedance of primary structure
- Input impedance of component package
- Acoustic mobility of primary structure
- Blocked pressure spectrum

The derivation of the prediction equation is given in Section 2.0.

Due to structural complexities of space vehicles, precise analytical approaches to obtain the above indicated parameters are not practical. Therefore, approximate formulae were used to compute these parameters. The design equations used in the computation are summarized in Section 3.0. The design equations were further converted into nomographic and computation charts so that lengthly computations can be avoided. The resulting charts and application guidelines are presented in Section 4.0. In Section 5.0, two example problems used to demonstrate the application design procedures are discussed. Finally, a summary of the research program and the concluding remarks on the prediction procedures are described in Section 6.0. The details of the development of these approximate equations are described in detail in Appendices A, B and C. During the performance of this research program, several computer programs were developed for dynamic analysis of cylindrical structures. The listing of these computer programs and their usages are presented in Appendix D.

2.0 EQUATIONS FOR PREDICTING DRIVING FORCE SPECTRUM

The equation used in predicting driving force spectra of components is defined by Equation (2.1) as follows:

$$\Phi_L(\omega) = \left| \frac{Z_L Z_S}{Z_L + Z_S} \right|^2 \cdot \left| \alpha(\omega) \right|^2 \cdot \Phi_p(\omega) \qquad (2.1)$$

where

$\Phi_L(\omega)$ = Predicted driving force spectrum

$Z_S(\omega)$ = Input impedance of primary structures

$Z_L(\omega)$ = Input impedance of component

$\alpha(\omega)$ = Acoustic mobility of the primary structure at component mounting points

$\Phi_p(\omega)$ = Blocked sound pressure spectrum

The derivation of Equation (2.1) is presented in Appendix A.

Input impedances of Equation (2.1) are specified in terms of the "force/velocity" format. Therefore, the unit for input impedances is lb-sec/in. Design charts used to estimate input impedances are provided in Section 4.0.

The acoustic mobility term, $\alpha(\omega)$, is defined as the ratio of rms velocity response and the driving acoustic pressure spectra at component mounting points. For a given cylindrical structure, the acoustic mobility is dependent on the system damping factor, Q , the diameter of the cylinder and the unit surface weight. By entering the design values for these quantities, the α-term can be obtained by the method outlined in Section 3.3.

The blocked pressure spectrum, $\Phi_p(\omega)$, is defined as the effective acoustic pressure acting on a primary structure. The pressure is equivalent to that acting on a rigid cylinder which has the identical geometrical dimensions as the primary structure. The method used to compute the blocked-pressure spectrum is presented in Section 3.4.

An alternate approach to compute the driving force spectrum could be achieved by replacing the product of $\left|\alpha(\omega)\right|^2 \cdot \Phi_p(\omega)$ by $\Phi_R(\omega)$, which is defined as the velocity response spectrum at the component mounting points of the unloaded primary structure. Thus, Equation (2.1) can be written as follows:

$$\Phi_L(\omega) = \left| \frac{Z_L Z_S}{Z_L + Z_S} \right|^2 \cdot \Phi_R(\omega) \qquad (2.2)$$

The computation of the driving force spectrum is illustrated by two examples as described in Section 5.0. A flow chart indicating the computation sequence to determine the force spectrum is shown in Figure 2.1.

3.0 ENGINEERING DESIGN EQUATIONS

3.1 Prediction of Structural Impedance

The cylindrical type support structures considered in this report consists of the following three primary components:

- Stringers,
- Circular ring frames, and
- Unstiffened cylindrical shells.

The derivation of the design equations is based on the following assumptions:

- Dimensions of cylindrical shells are assumed to be such that the usual thin shell theories are valid, that is, the thickness-to-radius ratio is small;
- Shells are stiffened by stringers in the axial direction, and ring frames are attached inside the shell wall;
- The skin panel of shells is directly excited by impinging acoustic pressures;
- The direction of vibratory response under consideration is referred to that normal to the skin;
- The stiffeners are not directly excited by acoustic forces but is driven by the motion of adjacent panels.
- The modulus of impedance is used in the design computation.

The evaluation of the driving-point impedances may be subdivided into three different frequency ranges:

- Low frequency range or frequencies below the fundamental frequency of the shell,
- Intermediate frequency range, and
- High frequency range or frequencies above the ring frequency of the shell.

The equations for predicting the input impedance of structures are discussed in detail in Appendix B. The resulting equations are presented in the subsequent sections and are summarized in Table 3.1.

3.1.1 Beam (or Stringer) Impedances — The static stiffness of a beam defines the input impedance at frequencies below the fundamental resonance frequency of the beam. The static stiffness at the mid-length point of a simply supported beam is given by

$$K = 48 \frac{EI}{\ell^3} \tag{3.1A}$$

where

E = Young's modulus of elasticity

I = moment of inertia of stringer cross-section

ℓ = effective length of stringer*

Then the input impedance is obtained as:

$$Z = K/i\omega \tag{3.1B}$$

where

ω = circular frequency

$i = \sqrt{-1}$

The fundamental resonance frequency of the beam can be computed from the following equation:

$$f_L = \frac{1}{2\pi} \left(\frac{\pi}{\ell}\right)^2 \sqrt{\frac{EI}{\rho A}} \tag{3.2}$$

where

ρ = mass density

A = cross-section area of stringer

At high frequencies or frequencies above the fundamental frequency, the average input impedance can be approximated as the characteristic impedance of an infinite beam and is given by Cremer (Reference 5) as follows:

$$Z = 2(1+i)\,\rho A \left(\frac{EI}{\rho A}\right)^{1/4} \sqrt{\omega} \tag{3.3}$$

---

* Note: If the distance, ℓ, between two adjacent supports is different from the entire length of a stringer, the stiffness should be computed in according to the shortest support distance.

The impedance curve defined by the above equation is represented by the line that passes through the points of inflection of the impedance curve as shown in Figure 3.1. The peaks and valleys are proportional to the damping coefficient, Q, and are located above or below the average impedance line; their amplitudes, in respect to the average impedance line, decrease with increasing frequency and the order of reduction in relative amplitudes is proportional to $1/\sqrt{\omega}$. The equation used to compute the ratio of peak values is defined as:

$$\frac{|Z_{peak}|}{|Z_{avg}|} = 4\sqrt{2}\ \frac{1}{\ell}\left(\frac{EI}{\rho A}\right)^{1/4}\ \frac{Q}{\sqrt{\omega}} \tag{3.4}$$

3.1.2 Ring Impedances — The in-plane static stiffness of a simply supported ring is given by (Reference 6):

$$K = \frac{EI}{0.15R^3} \tag{3.5}$$

where

I = moment of inertia of ring cross-section area

R = median radius of ring

However, the low frequency response of a free ring is associated with rigid-body motion which is along the mass line in the impedance plot and is given by:

$$Z = i\omega M \tag{3.6}$$

where M is the total mass of the ring and is expressed as:

$M = 2\pi\ \rho R A$

A = cross-section area of ring

The lowest resonance frequency of the fundamental mode of rings is defined as follows:

$$f_L = 0.427\ \frac{1}{R^2}\ \sqrt{\frac{EI}{\rho A}} \tag{3.7}$$

at frequencies above the fundamental frequency, the impedance curve approaches the impedance of an infinite beam whose value is given by:

$$Z = i\,2\sqrt{2}\;\rho A\left[\frac{EI}{\rho A}\right]^{1/4}\sqrt{\omega} \tag{3.8}$$

Similarly, the peak responses at resonance frequencies are proportional to structural damping and its peak/average ratio is obtained as:

$$\frac{|Z_{peak}|}{|Z_{avg}|} = 2\sqrt{2}\;\frac{1}{\pi R}\left[\frac{EI}{\rho A}\right]^{1/4}\frac{Q}{\sqrt{\omega}} \tag{3.9}$$

The impedance curve obtained from the approximate equations is illustrated in Figure 3.2 along with the analytic solution which is obtained from the general expression as discussed in Appendix B.

3.1.3 Shell Impedances — The static input stiffness of a simply supported cylindrical shell defines the input impedance at frequencies below the fundamental resonance frequency of the shell. The static point input stiffness at the midlength of a cylindrical shell can be estimated by the following approximate formula (Reference 7):

$$K = 2.50\,Eh\left(\frac{R}{\ell}\right)^{1/2}\left(\frac{h}{R}\right)^{5/4} \tag{3.10}$$

where

h = thickness of shells

R = radius of shell

ℓ = effective length of shell

E = Young's modulus of elasticity

The fundamental frequency of a thin shell with simply supported ends is

$$f_L = 0.375\;\frac{C_L}{\ell}\left(\frac{h}{R}\right)^{1/2} \tag{3.11}$$

where

C_L = speed of sound in shell wall

$$= \sqrt{\frac{E}{\rho (1-\nu^2)}}$$

and

ρ = mass density

ν = Poisson's ratio

At high frequencies, the impedance becomes asymptotic to a constant value and is given by the expression:

$$Z_p = \frac{4}{\sqrt{3}} \rho h^2 C_L \tag{3.12}$$

which is identical to the impedance of a semi-infinite plate of width πR. The frequency for which the corresponding mode shape shows no dependence on the axial direction is defined as the ring breathing frequency. The equation used to compute the ring frequency is given by:

$$f_R = \frac{1}{2\pi} \frac{C_L}{R} \tag{3.13}$$

Within the intermediate frequency range, which extends from the fundamental frequency to the ring frequency, the impedance curve can be approximated by the straight line which joins two points representing the input impedances at the fundamental frequency and the ring frequency, respectively. The expression which describes this impedance curve was derivated and is expressed below.

$$\begin{aligned} |Z| &\simeq Z_p \cdot \left(f_R/f\right)^{1/2} \\ &= \frac{4}{\sqrt{3}} \rho h^2 C_L^{3/2} \Big/ \sqrt{R\omega} \end{aligned} \tag{3.14}$$

An alternate theoretical method employing the concept of the modal density can also be used for estimating the impedance at intermediate frequencies. The modal density of a structure is

defined as the average number of resonance frequencies that occur within a unit frequency band. The inverse of the modal density is equal to the average separation between resonance frequencies. Heckl (Reference 8) derived a closed form expression for the modal density of a uniform cylindrical shell using a simple approximation to the frequency equation; and these expressions are used tc obtain the average separation between resonance frequencies (see also Reference 9) as follows:

$$\Delta f = \frac{8\pi}{9\sqrt{3}} \frac{h}{\ell} \frac{f_R^{3/2}}{f^{1/2}} \quad \text{for} \quad f < f_R \tag{3.15}$$

and the input impedance can be approximated by the following equation (Reference 10).

$$\begin{aligned} |Z| &= \frac{2}{\pi} \cdot 2\pi\Delta f \cdot M_m \\ &= \frac{8\pi}{9\sqrt{3}} \rho h^2 C_L^{3/2} \Big/ \sqrt{R\omega} \end{aligned} \tag{3.16}$$

in which M_m represents the modal mass and is approximately equal to one-quarter of the total mass of shell.

Comparison of Equations (3.14) and (3.16) shows that the theoretically derived expression in Equation (3.14) is essentially the same result as the empirical equation obtained by fitting the desired curve. A comparison of the resulting impedances obtained either from the approximate and analytical equations is shown in Figure 3.3.

3.1.4 Stiffened Shell Impedances — The evaluation of the stiffened shell impedances may be made for three different frequency ranges classified as follows (Reference 11):

- Low frequency range or frequencies below the fundamental frequency of the shell,
- Intermediate frequency range, and
- High frequency range or frequencies above the ring frequency of the shell.

3.1.4.1 Low Frequency Impedances — The static stiffness is the predominant factor which influences the input impedance. Due to the lack of theoretical expressions for input impedances of stiffened cylindrical shells, it is assumed that at low frequencies the input impedance at any location follows the stiffness line, this stiffness being equal to the summation of the stiffness of the individual structural elements that are present in that location. Two cases are considered in this frequency range, namely;

Case I — If the stiffness of the ring is small in comparison to the stiffness of the stringer or the unstiffened shell, the overall stiffness can be computed by adding the stiffness of the properly modeled structural elements that are present at the input location, as follows:

$$K = K_s + \sum K_B + \sum K_R \tag{3.17}$$

where

K_s = static stiffness of shells

K_B = static stiffness of stringers or beams

K_R = static stiffness of rings

Thus the input impedance of a stiffened cylindrical shell at low frequency follows a stiffness line whose value can be computed from the sum of stiffnesses of structural elements at that point.

Case II — For a stiffened cylindrical shell, if rings are sufficiently stiff in comparison with the entire shell, these rings act like the boundary of structure panels. Then the characteristic impedance of the shell can be determined from the length of the spacing between two adjacent rings.

$$K = K_s + \sum K_B \tag{3.18}$$

The characteristic impedance represents the impedance of a structure of such a length that reflections from the boundaries are negligible. In other words, the resonance modes of a structure with any nondissipative boundary conditions are identical to the resonance modes of a supported structure whose length is equal to the distance between the node lines.

3.1.4.2 Intermediate Frequency Impedances — Within the intermediate frequency range, which extends from the fundamental frequency to the ring frequency, the input impedances of the test specimens can be evaluated as the combination of the characteristic impedances of the primary structural components. The equation is written as:

$$Z = Z_s + \sum Z_B + \sum Z_R \tag{3.19}$$

where

Z_s = characteristic impedance of shells

Z_B = characteristic impedance of stringers

Z_R = characteristic impedance of rings

3.1.4.3 High Frequency Impedances — The input impedance of a stiffened shell at high frequencies depends on the location of a measurement point and is evaluated by the following rules:

- Unstiffened (skin) Point — The input impedance approaches that of an infinite plate of the same thickness.
- Stiffened Point — The skin and the stiffener(s) decouple dynamically at high frequencies, therefore, the input impedance approaches that of the stiffener(s).
- Stiffened Intersection Point — The input impedance at the centers of short stiffeners segments are generally higher than those of longer stiffener segments; and the impedance at an intersection of the stiffeners is approximately equal to the sum of the individual impedances of the two stiffeners - the ring impedance and stringer impedance.

3.2 Impedance of Payload Structure

The Payload structure can be assumed as a lumped-mass system. The mathematical model is shown in Figure 3.4 and the differential equations of motion can then be written as

$$\begin{cases} M\ddot{x} + C(\dot{x} - \dot{y}) + K(x - y) = 0 \\ C(\dot{x} - \dot{y}) + K(x - y) = -Fe^{i\omega t} \end{cases} \tag{3.20}$$

in which M represents the total mass, K is the stiffness, and C denotes the damping of the system. The frequency of the steady-state motion is the same as the force excitation frequency, ω, therefore, the mechanical impedance of the system is obtained as follows:

$$Z = \frac{Fe^{i\omega t}}{\dot{y}} = \frac{1}{\frac{1}{i\omega M} + \frac{1}{C + \frac{K}{i\omega}}}$$

$$= i\omega M \frac{\left[1 + \frac{i}{Q}\left(\frac{\omega}{\omega_0}\right)\right]}{\left[\left(1 - \frac{\omega^2}{\omega_0^2}\right) + \frac{i}{Q}\left(\frac{\omega}{\omega_0}\right)\right]} \qquad (3.21)$$

$$= \frac{K}{i\omega} \frac{\left[1 + \frac{i}{Q}\left(\frac{\omega}{\omega_0}\right)\right]}{\left[\left(1 - \frac{\omega_0^2}{\omega^2}\right) - \frac{i}{Q}\left(\frac{\omega_0}{\omega}\right)\right]}$$

where

$\omega_0 = \sqrt{K/M}$ = resonance frequency of undamped system

$Q = \sqrt{KM}/C$ = dynamic magnificant factor

For the region, $\omega \ll \omega_0$, Equation (3.21) can be approximated by

$$Z \simeq i\omega M \qquad (3.22)$$

Equation (3.22) shows that the impedance is a purely mass line. For the region, $\omega \gg \omega_0$, it is possible to obtain an approximate formula for the impedance and this approximation yields the following impedance formula:

$$Z \simeq \frac{K}{i\omega}\left[1 + \frac{i}{Q}\left(\frac{\omega}{\omega_0}\right)\right] = C + \frac{K}{i\omega} \qquad (3.23)$$

A typical example of the component impedance plot is shown in Figure 3.5 as a function of the frequency of the driving force. The approximated curve is also shown in the same figure for comparison. A computer program has been developed to compute the impedance and is shown in Appendix D.

3.3 Prediction of Acoustic Mobility

Acoustic mobility, $\alpha(\omega)$, is defined as the ratio of the mean-square spectral density of the velocity to the mean-square spectral density of the fluctuating pressure driving the structure. This quantity is expressed by Equation (3.24) as follows:

$$\alpha(\omega) = \frac{S_{\dot{U}}(\omega)}{S_p(\omega)} \tag{3.24}$$

where $S_{\dot{U}}(\omega)$ has units of $(\text{in./sec})^2/\text{Hz}$, and $S_p(\omega)$ is the blocked pressure spectral density having units of $(\text{psi})^2/\text{Hz}$. The blocked pressure includes the effects of reflection and thus accounts for the pressure doubling effect when an object is immersed in a random pressure field.

Generally, the acoustic mobility for a given structure would be calculated based upon modal analysis or statistical energy analysis as described in Appendix C. However, for the purposes of presenting simplified design techniques, empirical curves may be used for defining acoustic mobility. The development of these empirical curves from abroad range of available vibro-acoustic data is described in detail in Appendix C. Only the main results will be presented in this section. The basic design curves for acoustic mobility are shown in Figure 3.6 for three values of damping; Q = 20, Q = 100 and Q = 200. The modified acoustic mobility, which was derived from acceleration data from a wide range of vibro-acoustic measurements, is expressed as:

$$\alpha'(\omega) = \frac{S_{\dot{U}}}{S_p} \frac{(\mu g)^2}{D^2} \tag{3.25}$$

and has units of $(\text{in./sec})^2/\text{ft}^2$. The abscissa of Figure 3.6 is fD, i.e., frequency times vehicle diameter in units of Hz-ft. The surface weight term, (μg), has units of (lb/in.^2), and the vehicle diameter, D, is in feet.

In order to use the empirical curves of Figure 3.6, an estimate of the structural damping, Q, must first be obtained. Then by substituting for vehicle diameter, D, and surface weight, (μg), the

acoustic mobility $\frac{S_{\dot{u}}}{S_p}$ (or α) may be determined as a function of frequency, f Hz. For structural Q values other than those shown in Figure 3.6, the acoustic mobility term may be interpolated since an increase in Q by a factor of 10 results in an increase in the acoustic mobility term of one decade.

3.4 Evaluation of Blocked Pressure

The blocked pressure, which is the effective acoustic pressure load acting on a flexible structure, can be determined from the far-field and the near-field pressure sources. The following equations were derived for an infinite panel and do not account for diffraction effects of structures with finite length. However, the error dut to diffraction effects is considered as insignificant and will not influence the final results.

3.4.1 Far-Field Sound Pressure — The mean squared sound pressure on the surface of a reflecting object such as cylindrical shells in a reverbrant sound field can be determined from the far-field sound pressure measurement. The ratio of two RMS sound pressure levels can also be defined as the normalized blocked pressure spectrum and is given by (Reference 12):

$$\frac{\left[P^2_{block}\right]}{\left[P^2_{far}\right]} = 4\,(\pi k R)^{-2} \sum_{m=0}^{\infty} \epsilon_m \left|H'_m (kR)\right|^{-2} \qquad (3.26)$$

where

$\left[P_{far}\right]$ = measured sound pressure levels without the presence of flexible structures

k = wave number = $2\pi f/c$

f = frequency, Hz

c = speed of sound in acoustic medium; for air $c = 13{,}400$ in./sec

R = radius of cylinder

ϵ_m = Neumann factor = 1 for $m = 0$, 2 for $m > 0$

$H'_m (kR)$ = derivative of Hankel function of order, m

The curve representing the expression of Equation (3.26) versus ka is shown in Figure 3.7 and can be used to evaluate the blocked pressure spectra on the surface of cylinders in a reverberant acoustic environment.

The same curve can also be used to convert measured far-field sound pressure levels into blocked pressure levels. In the frequency range of interest, the RMS blocked sound pressure is approximately 40% higher than the measured sound pressure and such a conversion factor generally leads to conservative estimates of the force spectra.

3.4.2 Near-Field Sound Pressure — The blocked sound pressure can also be determined from the pressure measured at the surface of the flexible structure. An approximate formula for converting sound pressure levels measured on flexible structures into blocked sound pressure levels is shown below (Reference 13).

$$\frac{\left[P_{block}\right]}{\left[P_{flex}\right]} = \frac{1}{1 + \frac{\rho c}{z} \ell n \left[\frac{\rho c}{\rho c + z}\right]} \qquad (3.27)$$

where

$\left[P_{flex}\right]$ = measured sound pressure levels at the surface of flexible structures

ρ = density of acoustic medium

z = specific structural impedance of transmission

The sum $(\rho c + z)$ is the total impedance and is equal to the inverse of the acoustic mobility, α, of the cylindrical structures. Also, the acoustic impedance, ρc, is usually much smaller than the structural impedance and Equation (3.25) can, therefore, be written as

$$\frac{\left[P_{block}\right]}{\left[P_{flex}\right]} = \frac{1}{1 + \rho c \alpha \ell n (\rho c \alpha)} \qquad (3.28)$$

4.0 COMPUTATION CHARTS AND GUIDELINES

In order to minimize manual efforts in performing force-spectrum computations, it is necessary to reduce the derived equations described in Section 3.0 into the forms of graphs or nomograms so that lengthly computations can be avoided.

All equations listed in Table 3.1 contain a frequency dependent and a frequency independent terms. Therefore, by evaluating the frequency independent terms, and later, combining with the frequency dependent term, the impedance curve can be easily constructed. The approaches, which are based on the separation of the frequency dependency to simplify the impedance prediction, are presented below.

4.1 Nomographic Charts

A nomograph, in its simplest and most common form, is a chart on which one can draw a straight line that will intersect three or more scales in values that satisfy an equation or a given set of conditions. The equations summarized in Table 3.1 can be converted into nomographic forms, and are shown in Figures 4.1 through 4.10. Figure 4.1 evaluates the static stiffness of the ring frame based on the expression of Equation (3.5). By knowing the values of radius, R, and the flexibility, EI, of the ring, and connecting these two values on the R scale and the EI scale with a straight line, the intersection point in the K scale represents the computational result of the given equation.

Figures 4.2 and 4.3 perform similar computations for Equation (3.1A) and the frequency independent part of Equations (3.3) and (3.8) which is defined as:

$$Z_r = 2\sqrt{2}\,\rho A \left[\frac{EI}{\rho A}\right]^{1/4} \tag{4.1}$$

Figure 4.4 is a four-variable type nomogram for the expression of Equation (3.10). By using one additional axis, T, which lies between the ℓ and R axes and need not be graduated, Equation (3.10) was broken into two three-variable equations and are handled as the proceeding way, i.e., connecting the ℓ scale and the R scale with a straight line, then joining the intersection point on the T axis and the h scales with another straight line, the intersection point on the K scale is the resulting value.

Figure 4.5 is used to evaluate the frequency independent part of the shell impedance as defined below:

$$Z_f = \frac{4}{\sqrt{3}}\,\rho h^2 C_L^{3/2} \Big/ \sqrt{R} \tag{4.2}$$

Figure 4.6 is used to evaluate the infinite plate impedance, Z_p, according to the expression of Equation (3.14).

Figures 4.7 through 4.10 are used to compute the lowest fundamental resonance and ring frequencies of structural components. These fundamental frequencies are not required in the prediction of impedances. Nevertheless, frequencies obtained from Figures 4.7 through 4.10 can be used to check the accuracy of the computation procedure.

The application of impedance data obtained from Figures 4.1 through 4.6 to compute vibro-acoustic loadings by computation charts is described in the next section.

4.2 Computation Charts

4.2.1 Charts for Computing Structural Impedance — The impedance of an ideal damping, spring and mass system may be represented by three straight lines as shown in Figure 4.11. By using this approach, the driving-point impedance for beams and rings based on the equations of Table 3.1 can be represented by two sets of intersection lines varying with the frequency as shown in Figure 4.12. In this figure, the line representing the proper stiffness value is obtained either from the result of Figure 4.1 or 4.2 for rings and beams, respectively, and the line defining the proper Z_p value of the structure is determined from Figure 4.3. The stiffness lines represent the impedance at low frequencies and the Z_p lines represent the impedance at high frequencies. The intersection of these two lines determines the fundamental resonant frequency of the structural system. In this figure and the following figures, a scale factor is used to obtain correct scale values for the standard diagrams.

The driving-point impedance for unstiffened cylindrical shells is shown in Figure 4.13, where the Z_p lines are replaced by the Z_f lines. The lines represented the proper stiffness, Z_f and infinite-plate impedance are obtained from Figures 4.4, 4.5 and 4.6, respectively. At low frequencies, the impedance of cylinders follows a stiffness line and at high frequencies the impedance is equal to the impedance of an infinite plate which has a constant value. Within the intermediate frequency range, the input impedance may be represented by the Z_f line. The fundamental frequency and the ring frequency of cylinders are determined by the intersection of these three characteristic lines.

Figure 4.14 represents the impedance lines for the component package which are defined by the stiffness, mass and damping. The graph shown on the upper portion of these three charts will be used to compute the logarithmic sums of two impedance curves. The application of the logarithmic summation chart is explained in Section 5.0.

4.2.2 Charts for Computing Blocked Pressure Spectrum — The conversion of a far-field sound pressure spectrum into a corresponding blocked pressure spectrum is achieved by multiplying the far-field spectrum by the correction coefficient β, as shown in Figure 3.7. To facilitate graphical computation, Figure 3.7 is converted to Figure 4.15, in which the abscissas scale is expressed in terms of fD; where f is the frequency in Hz and D is the cylinder diameter in inches. To obtain the $\sqrt{\beta}$ - coefficient for a particular cylinder in the frequency scale,

it is accomplished by shifting the fD scale in Figure 4.15 to the left for the amount corresponding to the cylinder diameter, D. For example, if the diameter of a cylinder is 72 inches, the $\sqrt{\beta}$ - coefficient for that cylinder is obtained by shifting the fD scale by a factor of 72 to the left, as shown by the $\sqrt{\beta}$-curve in Figure 4.16. The blocked pressure spectrum of the far-field pressure spectrum, shown in Figure 4.16, is obtained by adding the $\sqrt{\beta}$ values at each frequency point to the far-field pressure spectrum. The resulting blocked pressure spectrum is shown by the dashed line in Figure 4.16.

4.2.3 Charts for Computing Response Spectrum — The velocity response spectrum is obtained by the product of the blocked pressure spectrum and the velocity acoustic mobility. The normalized acoustic mobility curves for Q = 20 and 200 are shown in Figure 4.17. These curves must be converted to $|\alpha|^2$ versus frequency format for use in response computation. The conversion can be accomplished graphically by shifting the abscissas scale to the left corresponding to the diameter of a cylinder, D; and shifting the ordinate scale downward corresponding to the quantity $(m/D)^2$. For example, by applying the above procedures to an aluminum cylinder with D = 72 inches, Q= 20, and $(m/D)^2 - 10^{-6}$ lb/m^3, the velocity mobility for the cylinder curve is obtained as shown in Figure 4.18. The velocity response spectrum is obtained by summing up logarithmically the velocity acoustic mobility curve and the blocked pressure spectrum curve. The response spectrum is indicated by the dashed-line in Figure 4.18.

In practice, it is often necessary to convert the acceleration PSD into velocity PSD for computing force responses. This can be achieved graphically by plotting the response curve on the conversion chart as shown in Figure 4.19. The equivalent velocity response is read-off from the vertical scale on the left-hand side.

4.2.4 Chart for Computing Force Spectrum — The response spectra and the structural impedance obtained from Figure 4.14 are again plotted on Figure 4.20 for final computation. The curve representing the sum of these two curves, as shown in Figure 4.20, is the resulting force spectrum for the design structural system.

4.3 Summary of Computation Procedures

The computation procedures presented in this section provide simplified techniques to predict vibratory environments for space vehicle components. A summary of the computation procedures is presented below for quick references.

STEP 1: Determine and compute the geometrical and material properties of cylinders and their components.

STEP 2: Evaluate the parameters of structural impedances of primary structural components, employing Figures 4.1 through 4.6. Figures 4.7 through 4.10 may be used to compute resonant frequencies. These impedances are summed in accordance with the guidelines described in Section 3.1.4 by using Figures 4.12 and 4.13.

STEP 3: Estimate the impedance of the component package and construct the component impedance curve by Figure 4.13.

STEP 4: Determine the blocked pressure spectrum by means of charts as shown in Figures 4.15 and 4.16. The response spectrum is computed by utilizing charts as shown in Figures 4.17 and 4.18, or the response spectra may be obtained from the experimental measured data plotted in Figure 4.19 directly.

STEP 5: Plot the response spectra and the structural impedance on Figure 4.20. The force spectra for the design system is obtained by summing these two individual curves.

5.0 EXAMPLE PROBLEMS

To aid in understanding the computation procedure, two examples are illustrated in this section. The first example is used to demonstrate the procedures used to predict structural impedances of a stiffened cylinder. The predicted results were then compared with the measured data obtained previously (Reference 11) to evaluate the accuracy of impedance prediction equations. The second example is used to illustrate the procedures in computing a force spectrum based on the structural configurations and the loading criteria used in Reference 3. The measured force response data was used to evaluate the accuracy and conservatism of the predicted force spectrum.

5.1 Example of Prediction of Structural Impedance

The cylindrical structure consisted of a basic cylindrical shell, longitudinal stringers and ring frames. The impedance data were measured under a total of seven different structural configurations as described below:

- Bare shell
- Shell with one ring frame
- Shell with two ring frames
- Shell with two ring frames and one stringer
- Shell with two ring frames and two stringers
- Shell with two ring frames and four stringers
- Shell with two ring frames and eight stringers

Figure 5.1 depicts the last structural configuration described above. All structural elements were made of aluminum. The stringers and ring frames were fastened to the shell by means of rivets. Details of structural configuration for each test set up and corresponding test results can be found in Reference 11. Overall dimensions of the specimens are listed in Table 5.1.

The computations of static stiffness, Z_p and Z_f for the primary structure components have been demonstrated previously as shown in Figures 4.1 through 4.6. The impedance computations for the configuration with two ring frames and four stringers are illustrated in Figures 5.2 and 5.3. In the computation, it was assumed that these two rings act like end bulkheads with high structural rigidity so that the effective length of cylinder becomes the length of the middle segment which is equal to 32 inches. In Figure 5.2, the impedance for one stringer and four stringers are plotted based on the values obtained from Figures 4.2 and 4.3. Similarly, the impedance curve representing the unstiffened cylindrical shell is plotted in Figure 5.3, in which the impedance representing the sum of four stringers is also shown, except that at high frequencies where the structural system decouples dynamically and the impedance approaches that of one stiffener only. The impedance of the stiffened shell is equal to the linear summation of these two component impedance curves and it is obtained in the following way:

- At any frequency point, measure the difference of two impedance values and use this length as the abscissas value in the logarithmic summation chart (LSC).

- The ordinate corresponding to the abscissas in the LSC is the resulting value for these two curves in logarithmic summation.

- Add the length of the ordinate to the upper impedance curve, the resulting curve denotes the linear combination of these two impedances.

Based on the procedure as described in the above, the computed results are presented in Figure 5.4. The experimental data obtained from Reference 11 are also shown in the same figure for comparison. Generally speaking, the comparison is considered quite satisfactory both in low frequency and high frequency ranges. Fair agreement is also observed for frequencies just below the ring frequency. Some discrepancies are observed in the intermediate frequency region. Such discrepancies are attributed to the errors incurred in summing the impedances of the stringers. Further refinements in predicting techniques to achieve a higher degree of accuracy in this frequency range are needed. The comparisons of the remaining six configurations are illustrated in Figures 5.5 through 5.10. These results show a satisfactory agreement between the predicted and measured data. Therefore, it may be concluded that the equations and guidelines outlined in Section 3.0 are adequate for determining the structural impedances for design purposes.

5.2 Example for Prediction of Force Spectra

The structure used in the second example was a stiffened aluminum cylinder, as shown in Figure 5.11. The cylinder's dimensions were 36 in. (diameter) x 36 in. (length) x 0.02 in. (thick). Its structural configuration is shown in Figure 5.12. The cylinder consisted of five aluminum rings spaced at 6 inches in the longitudinal direction and 24 longitudinal stringers spaced at 4.7 inches in the circumferential direction. All stiffeners were mounted to the cylinder wall by rivets. The dimensions of the curved panels formed by the stiffeners were 6 inches and 4.75 inches. Two steel rings of 1 in. x 1 in. x 1/8 in. angle section were rivetted at both ends and two circular sandwich plates were bolted to the end rings by 1/4 in. diameter hex bolts and nuts. Each sandwich plate consisted of two steel end plates of 1/8 in. thickness and 1/2 in. plywood as its center core. Overall dimensions of the cylindrical structure are listed in Table 5.2.

The simulated component package consisted of a 1/2 in. aluminum plate with lateral dimensions of 8 in. x 8 in. The plate was supported by four sets of leaf springs at its corners. The bottom of each spring was fitted with a load washer assembly. Each assembly consisted of a Kistler 901A load washer which was sandwiched between an anti-friction washer on the top and an aluminum stud at the bottom. These elements were held together with the top clamping strips by a center bolt. Each loadwasher was pre-compressed to approximately 1000 pounds level, so that the tensile and compressive forces induced during testing could be measured.

The total weight of the component package was 3.81 pounds; the resonances of the package were measured at 110 Hz and 1200 Hz, respectively. The latter frequency is the fundamental resonance of the 1/2 in. plate. Detailed descriptions of the structural configurations can be found in Reference 3.

The resultant impedances at the center of longitudinal stiffener segments were measured and are shown in Figure 5.14. The analytic procedures used to predict the impedance are essentially the same as that described in the proceeding section. Hence, no analytical prediction on stiffness was made for this example. The impedance of the component package is estimated and is shown in Figure 5.15. The fundamental resonant frequency of the component package as seen from the shaker is located at 110 Hz. The measured impedance for the stiffened cylinder is also presented in the same figure, which is approximated by two inclined straight lines as shown. In Figure 5.15 the plotting scale is 100 times the correct value as denoted by Factor = 0.01. These two impedance curves are then combined according to the procedure as described in Section 5.1 for the impedance of the stiffened shell except that the resultant curve is obtained by subtracting the length of the ordinate coordinate from the lower impedance curve, i.e., by summing the two individual mobility curves. The summed curve given is the impedance term in the computation of the force-spectrum equation.

The blocked pressure and the acoustic mobility data for this example have been obtained according to the procedure as described in Section 4.2.2, and are shown in Figures 5.16 and 5.17, respectively. The response spectra is then obtained by summing these two individual curves and is shown in Figure 5.17.

Based on Figures 5.15 and 5.17, the force spectrum was computed and the resultant curve is shown in Figure 5.18. The measured force response data obtained from Reference 3 are also presented in the same figure for comparison. Good agreements between the predicted and measured force spectra were obtained.

6.0 SUMMARY AND CONCLUSIONS

6.1 Summary

A method was developed to compute the interaction force between a component and its support structure (space vehicle) which is subjected to broad band random acoustic excitations. The method was derived from a one-dimensional impedance model and the force environment was computed based on a total of four parameters as described below:

- Input impedance of component
- Input impedance of support structure
- Acoustic mobility at component mounting points on the support structure
- Blocked acoustic pressure spectrum acting on the support structure

A set of nomograms was developed to compute impedances and computational charts were prepared to obtain the force spectrum graphically with minimum amount of manual computation. Two example problems were given to demonstrate computation procedures to obtain input impedances of structural elements and the force spectrum. The computed results were verified with experimental data. Good agreements between the two sets of data were observed.

6.2 Conclusions

The following conclusions may be drawn from the results of this program:

- The force-spectrum equation provides satisfactory results on the predicted force environments of components mounted on space vehicles. This equation is valid for the prediction of forces in the radial direction of the support structure. However, the same concept can be expanded to include the coupling effects induced from the longitudinal and tangential directions so that the complete description of forces in all three directions is feasible.

- The simplified computation method as presented in this report has been shown to be accurate and conservative within current acceptable tolerance limits. The computation process requires minimum manual effort and no computer assistance is required.

REFERENCES

1. Barrett, R. E., "Techniques for Predicting Localized Vibratory Environments of Rocket Vehicles," NASA TN D-1836, October 1963.

2. Barrett, R. E., "Statistical Techniques for Describing Localized Vibratory Environments of Rocket Vehicles," NASA TN D-2158, July 1964.

3. Kao, G. C., "Prediction of Force Spectra by Mechanical Impedance and Acoustic Mobility Measurement Techniques," Wyle Laboratories Research Staff Report WR 71-16, October 1971.

4. Kao, G. C., "Evaluation of Force-Control, Response-Control and Current-Control Vibro-Acoustic Simulation Testing Techniques," Wyle Laboratories Research Staff Report WR 72-9, October 1972.

5. Heckl, M.A., "Compendium of Impedance Formulas," BBN Report No. 774, May 1961.

6. Bozich, D.J. and White, R.W., "A Study of the Vibration Response of Shells and Plates to Fluctuating Pressure Environments," NASA CR-1515, March 1970.

7. Roark, R.J., "Formulas for Stress and Strain," McGraw-Hill Book Co., Fourth Edition, 1965.

8. Heckl, M.A., "Vibrations of Point-Driven Cylindrical Shells," JASA, Vol. 34, No. 10, October 1962.

9. Miller, D.K. and Harf, F.D., "Modal Density of Thin Circular Cylinders," NASA CR-897, December 1967.

10. Skudrzyk, E., "Simple and Complex Vibratory Systems," Pennsylvania State University Press, 1968.

11. Conticelli, V.M., Kao, G.C. and White, R.W., "Experimental Evaluation of Input Impedances of Stiffened Cylindrical Shells," Wyle Laboratories Research Staff Report WR 70-2, August 1970.

12. Waterhouse, R.V., "Diffraction Effects in a Random Sound Field," JASA, Vol. 35, pp. 1610-1620, October 1963.

13. Conticelli, V.M., "Evaluation of Blocked Pressure Spectra on Stiffened Cylindrical Shells," Wyle Laboratories Research Staff Technical Memorandum, TM 71-1, September 1971.

TABLES

TABLE 3.1. SUMMARY OF INPUT-IMPEDANCE EQUATIONS OF BEAMS, RINGS AND SHELLS

Structure \ Frequency	Low Frequency Range $(f \le f_L)$	Fundamental Frequency, f_L	Intermediate Frequency Range $(f_L < f \le f_R)$	Ring Frequency, f_R	High Frequency Range $(f > f_R)$
Beam	$K_B = \frac{48EI}{\ell^3}$	$\frac{1}{2\pi}\left(\frac{\pi}{\ell}\right)^2\sqrt{\frac{EI}{\rho A}}$	$Z_B = 2(1+i)\ \rho A\left[\frac{EI}{\rho A}\right]^{1/4}\sqrt{\omega}$		Same as Intermediate
Ring	$K_R = \frac{EI}{0.15R^3}$	$\frac{0.427}{R^2}\sqrt{\frac{EI}{\rho A}}$	$Z_R = i2\sqrt{2}\ \rho A\left[\frac{EI}{\rho A}\right]^{1/4}\sqrt{\omega}$		Same as Intermediate
Shell	$K_S = 2.5\,Eh\left(\frac{R}{L}\right)^{1/2}\left(\frac{h}{R}\right)^{1.25}$	$\frac{0.375}{L}\sqrt{\frac{Eh}{\rho R}}$	$\lvert Z_S\rvert = \frac{4}{\sqrt{3}}\ \rho h^2\sqrt{\frac{E}{\rho R}}\left(\frac{E}{\rho}\right)^{1/4}\frac{1}{\sqrt{\omega}}$	$\frac{1}{2\pi R}\sqrt{\frac{E}{\rho}}$	$Z_S = \frac{4}{\sqrt{3}}\ h^2\sqrt{E\rho}$
Stiffened Shell	$K = K_S + \sum K_B$ (or $+\sum K_R$) $\lvert Z\rvert = K/\omega$		$Z = Z_S + \sum Z_B + \sum Z_R$		$Z = Z_S$, $Z = Z_B$, $Z = Z_R$

TABLE 5.1. SUMMARY OF DIMENSIONS, STIFFNESS AND MASS PROPERTIES OF CYLINDER AND ITS COMPONENTS

Property	Dimension	Structural Items		
		Ring	Stringer	Shell
Mean Radius, R	(in.)	23.0	---	24.0
Overall Length, ℓ	(in.)	144.5	96.0	96.0
Shell Skin Thickness, h	(in.)	---	---	0.08
Cross-section Area, A	($in.^2$)	0.215	0.123	---
Moment of Inertia, I	($in.^4$)	0.135	0.012	---
Weight per Unit Volume, ρ	($lb/in.^3$)	0.1	0.1	0.1
Modulus of Elasticity, E	($lb/in.^2$)	10^7	10^7	10^7
Weight per Stiffener *	(lb)	3.10	1.18	116.0

* Two rings spaced at 32" in the longitudinal direction and eight longitudinal stringers spaced at 18.8" in the circumferential direction.

TABLE 5.2. SUMMARY OF DIMENSIONS, STIFFNESS AND MASS PROPERTIES OF CYLINDRICAL STRUCTURES

Property	Dimension	Structural Items		
		Ring	Stringer	Shell
Mean Radius, R	(in.)	16.0	--	18.0
Overall Length, ℓ	(in.)	100.5	48.0	48.0
Shell Skin Thickness, h	(in.)	--	--	0.02
Cross-section Area, A	($in.^2$)	0.942	0.049	--
Moment of Inertia, I	($in.^4$)	1.7715	0.00051	--
Elasticity Modulus, E	($lb/in.^2$)	10^7	10^7	10^7
Weight Density, ρ	($lb/in.^3$)	0.1	0.1	0.1
Weight per Stiffener *	(lb)	9.467	0.235	10.857

* The cylinder consisted of five rings spaced at 6" in the longitudinal direction and 24 stringers spaced at 4.75" in the circumferential direction.

FIGURES

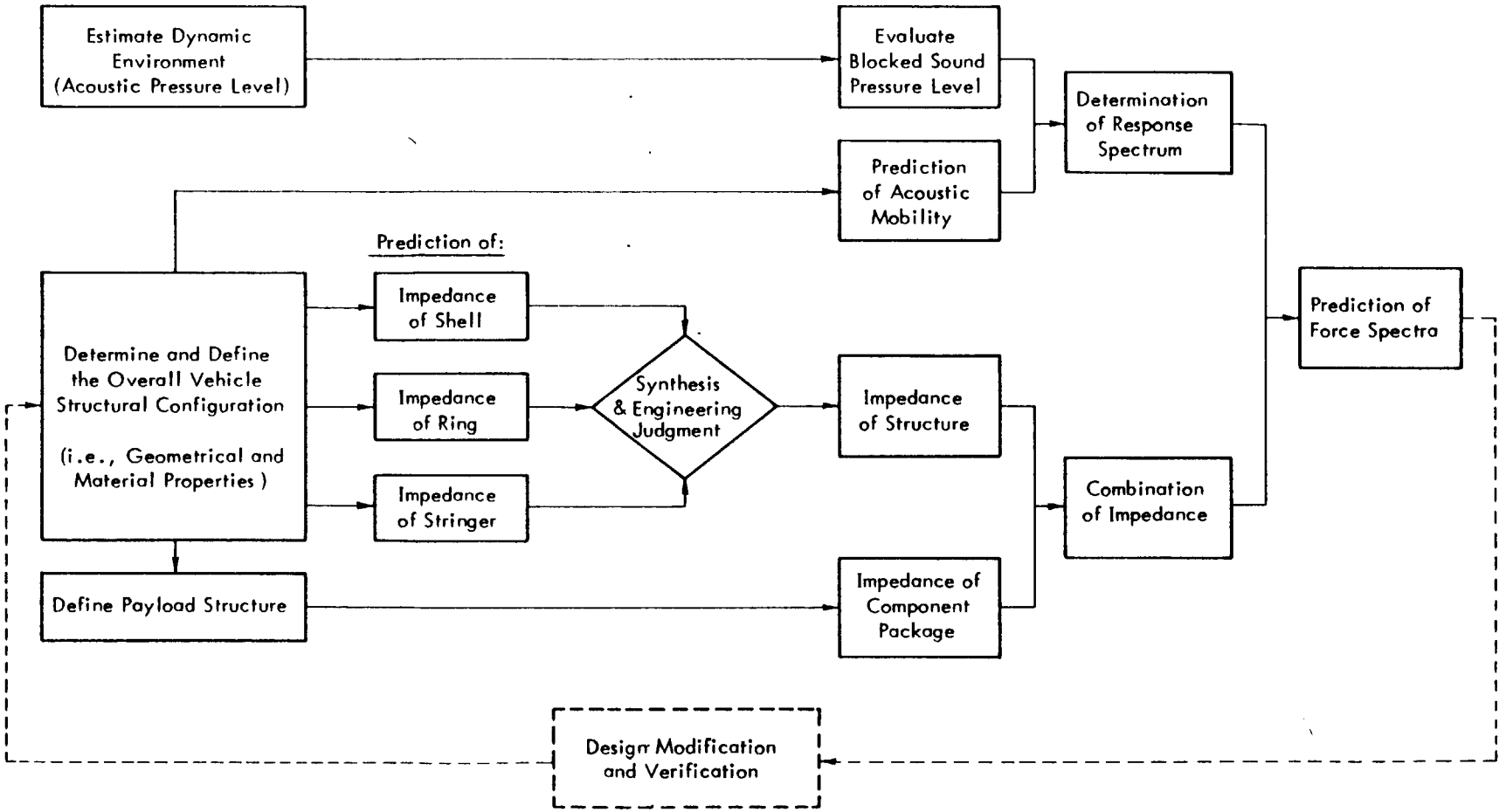

Figure 2.1. Flow Chart for Predicting the Force Spectra of Structures

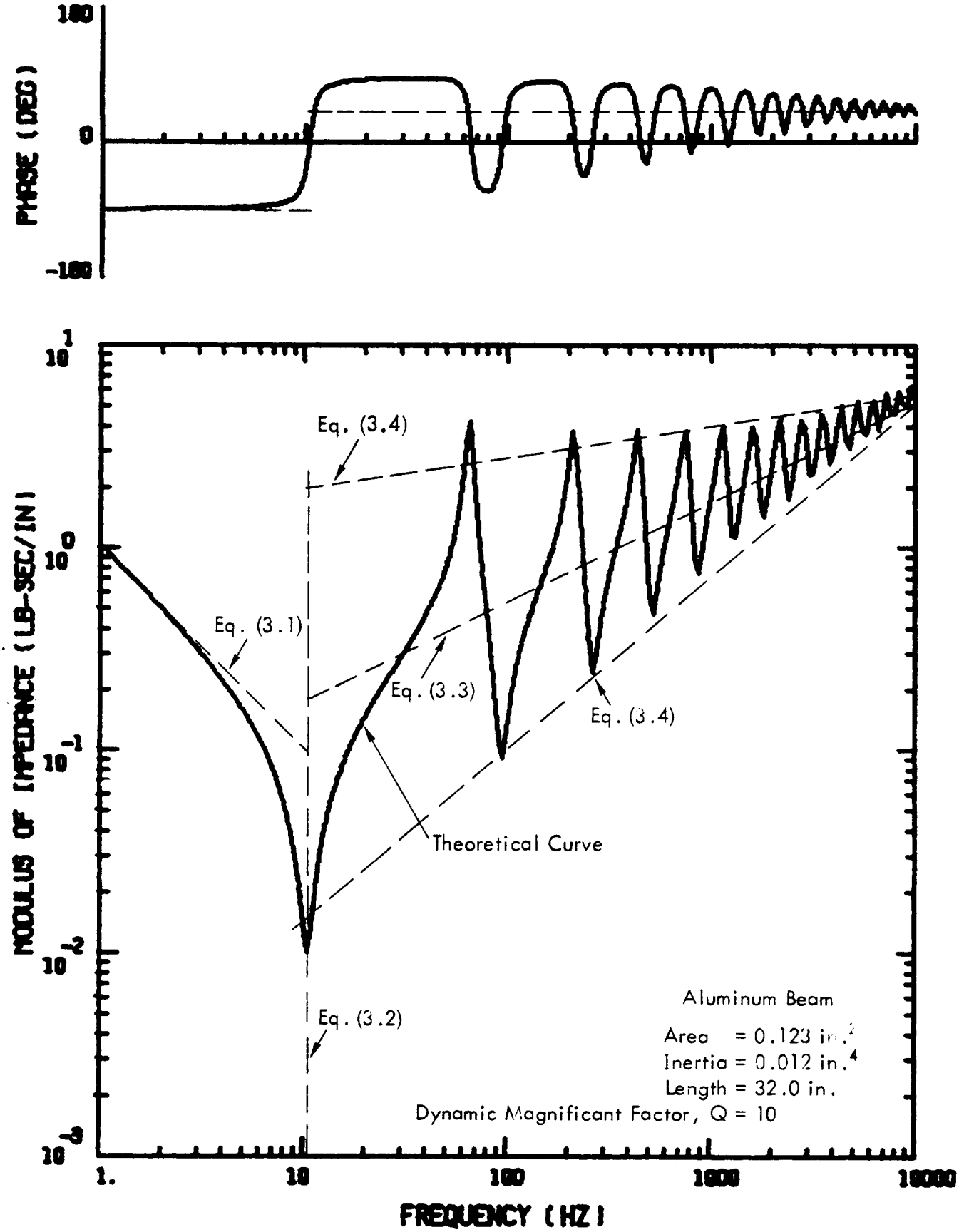

Figure 3.1. Comparison of Design Equations with the Analytic Solution for the Impedance of Beam-Type Structures

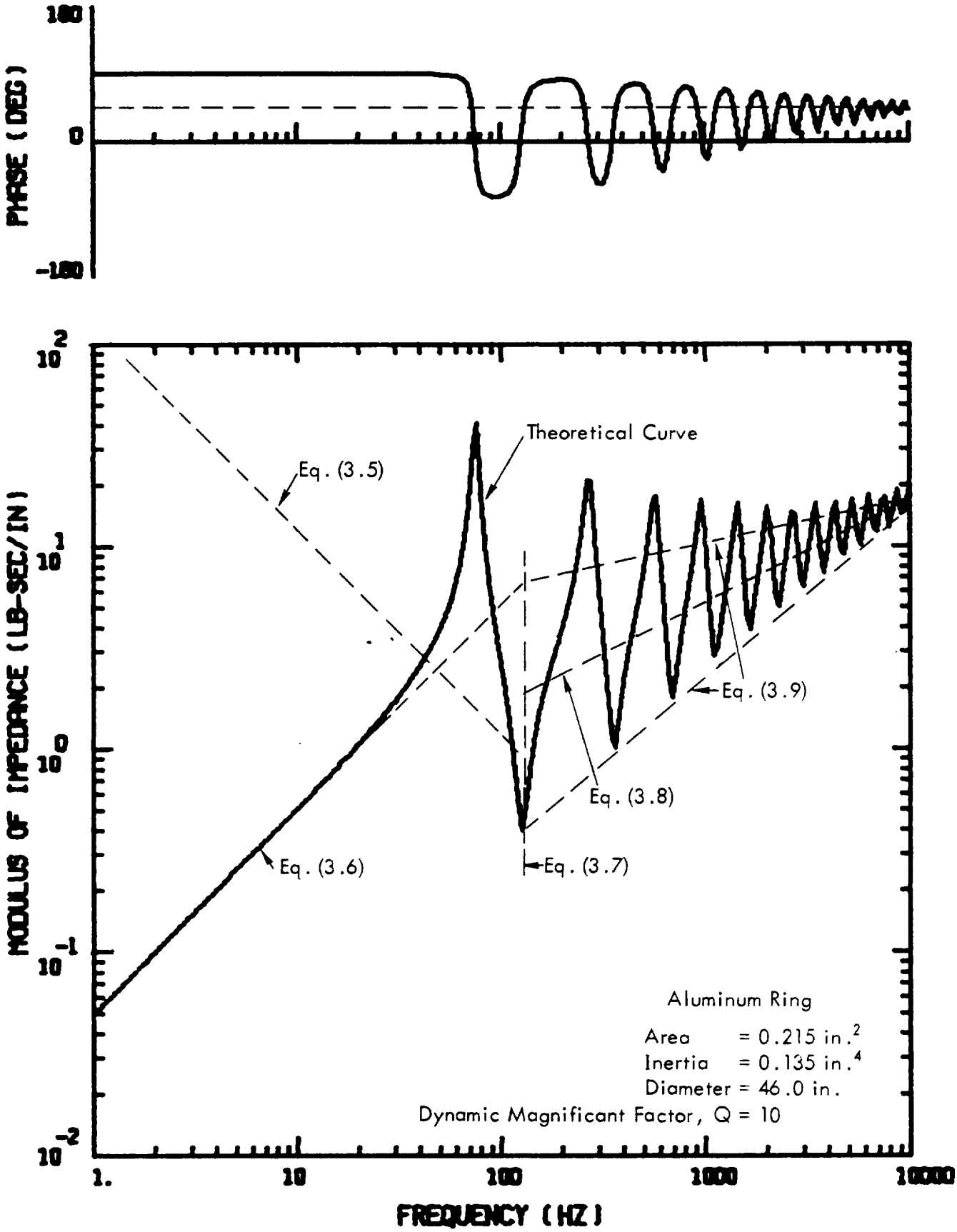

Figure 3.2. Comparison of Design Equations with the Analytic Solution for the Impedance of Ring-Type Structures

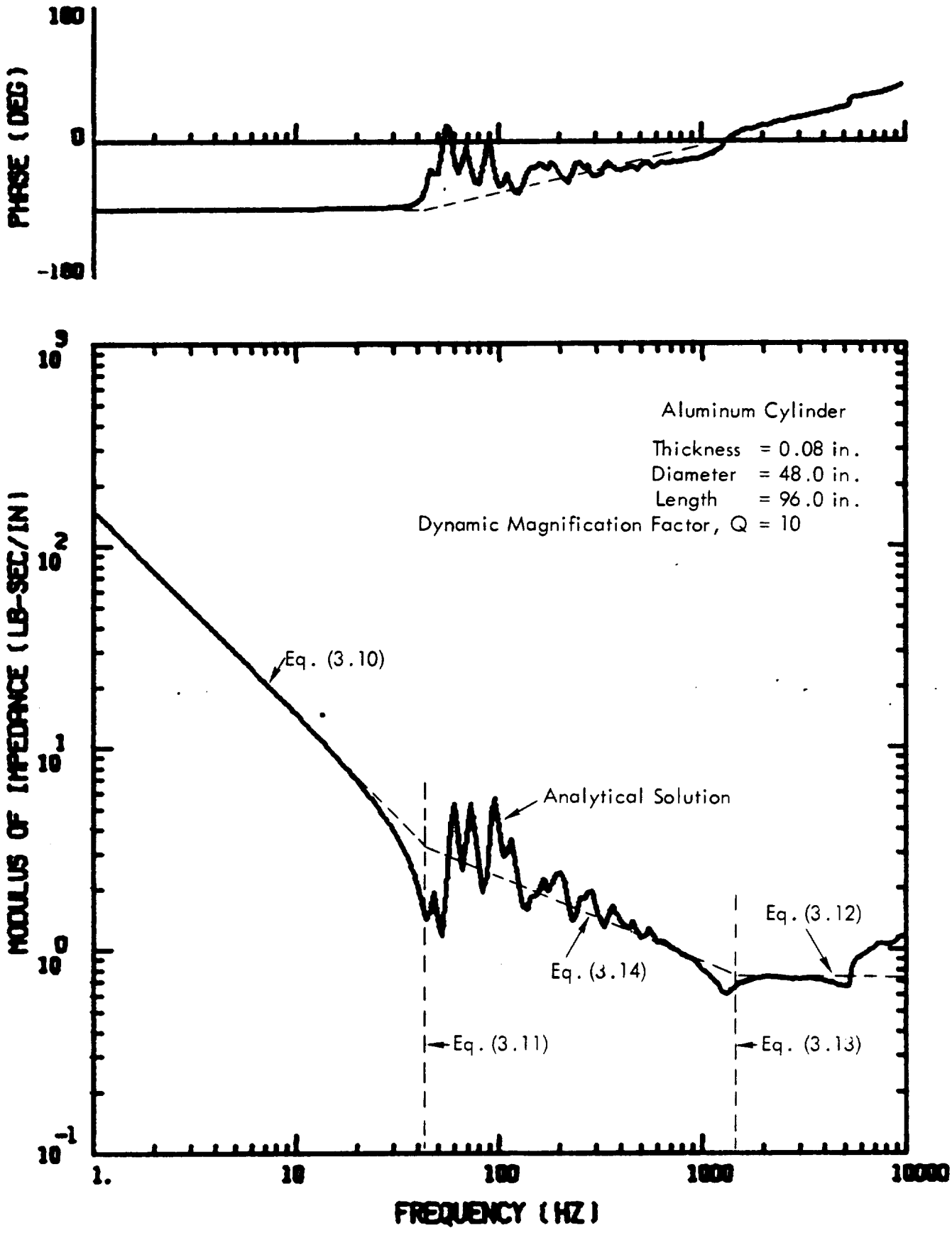

Figure 3.3. Design Equations and Analytical Solution of Input Impedance at Mid-Length of an Unstiffened Cylinder

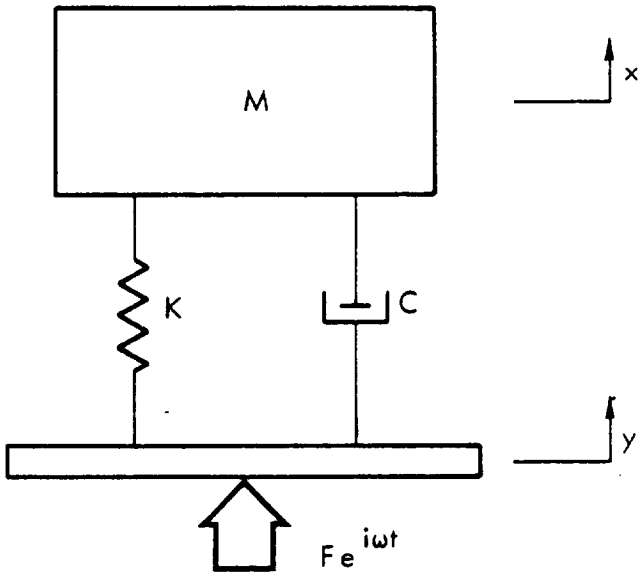

Figure 3.4. Mass-Spring — Dashpot Model

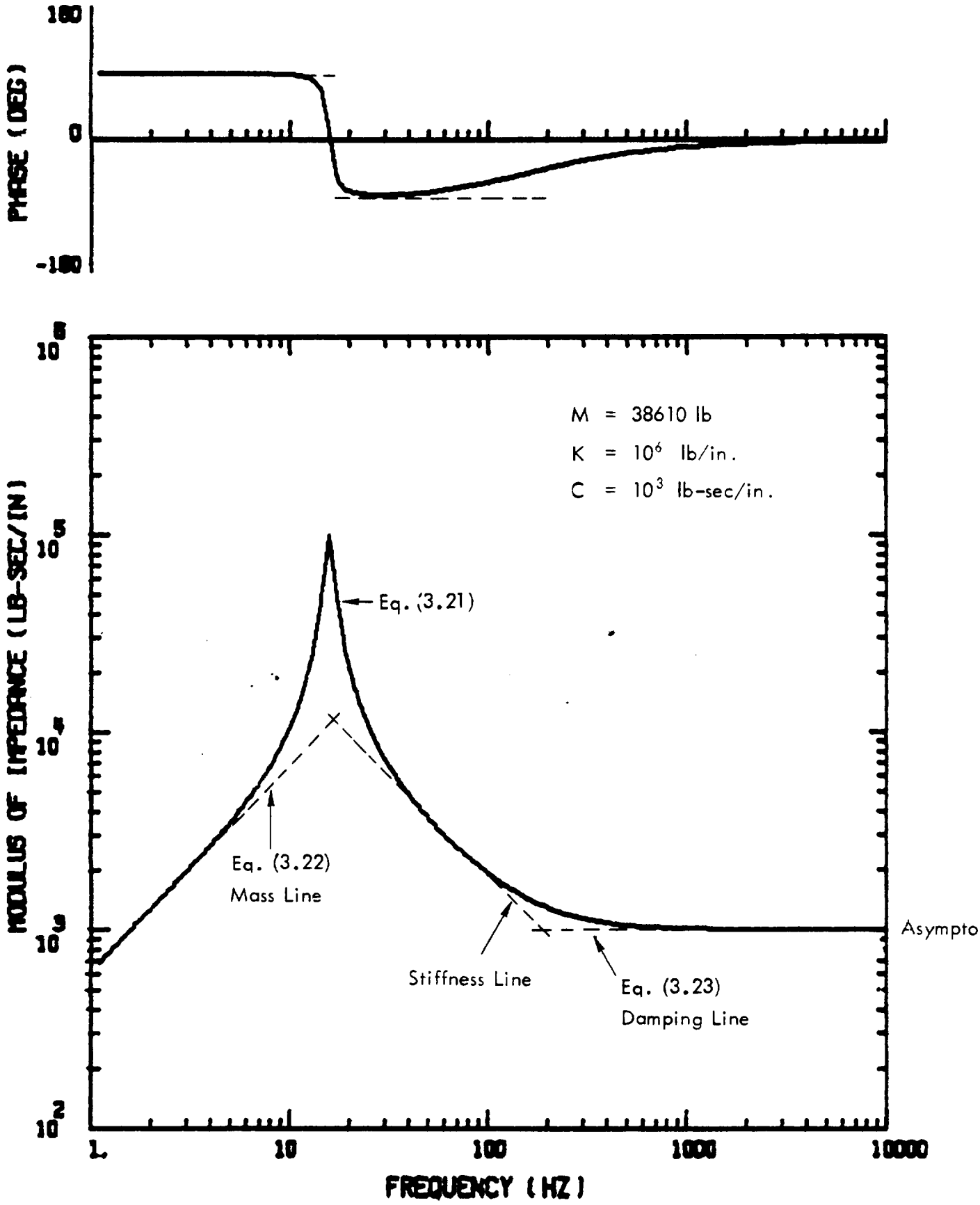

Figure 3.5. Impedance of Component Package

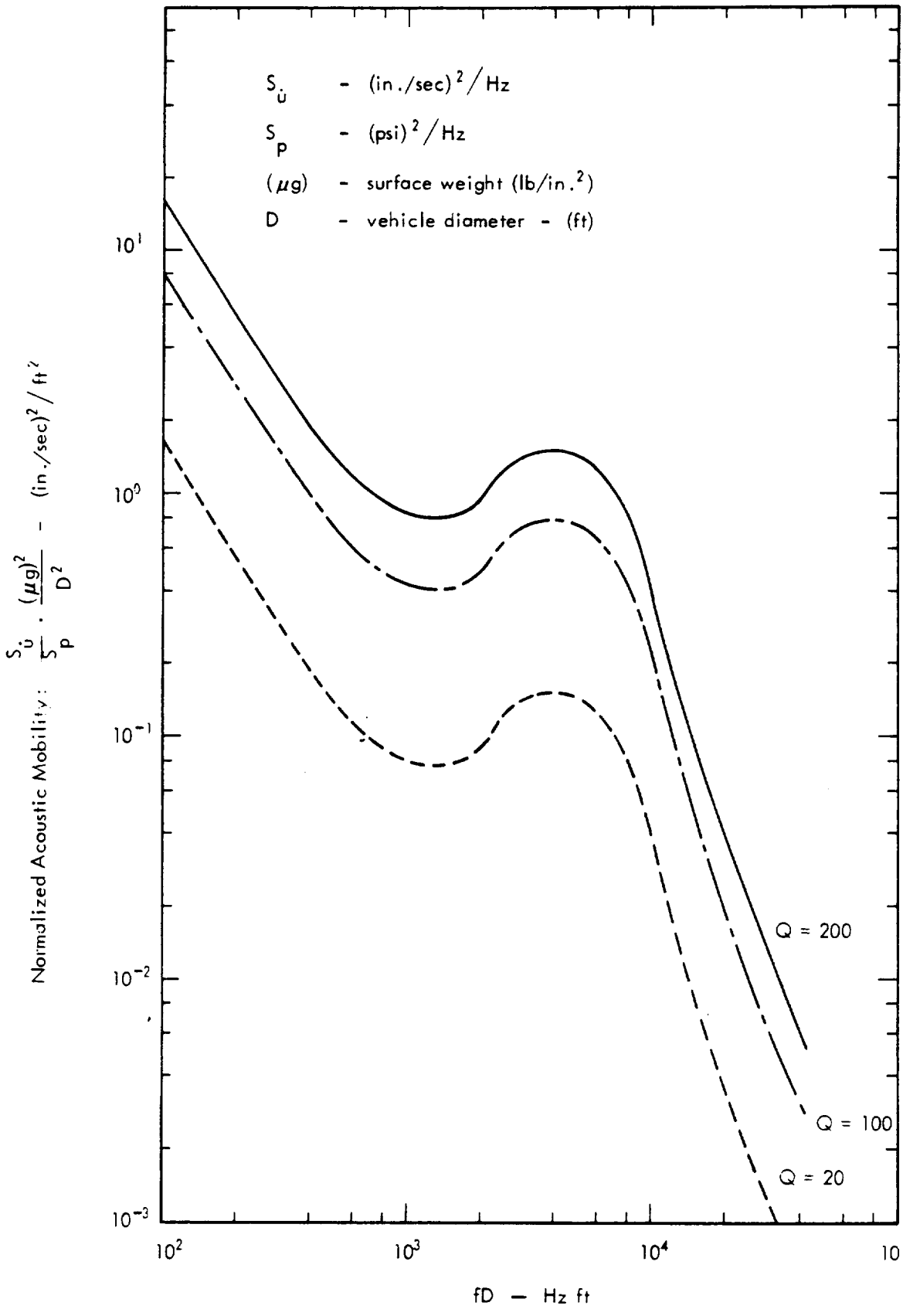

Figure 3.6. Acoustic Mobility for Cylindrical Vehicle Structures (Based on Blocked Pressures)

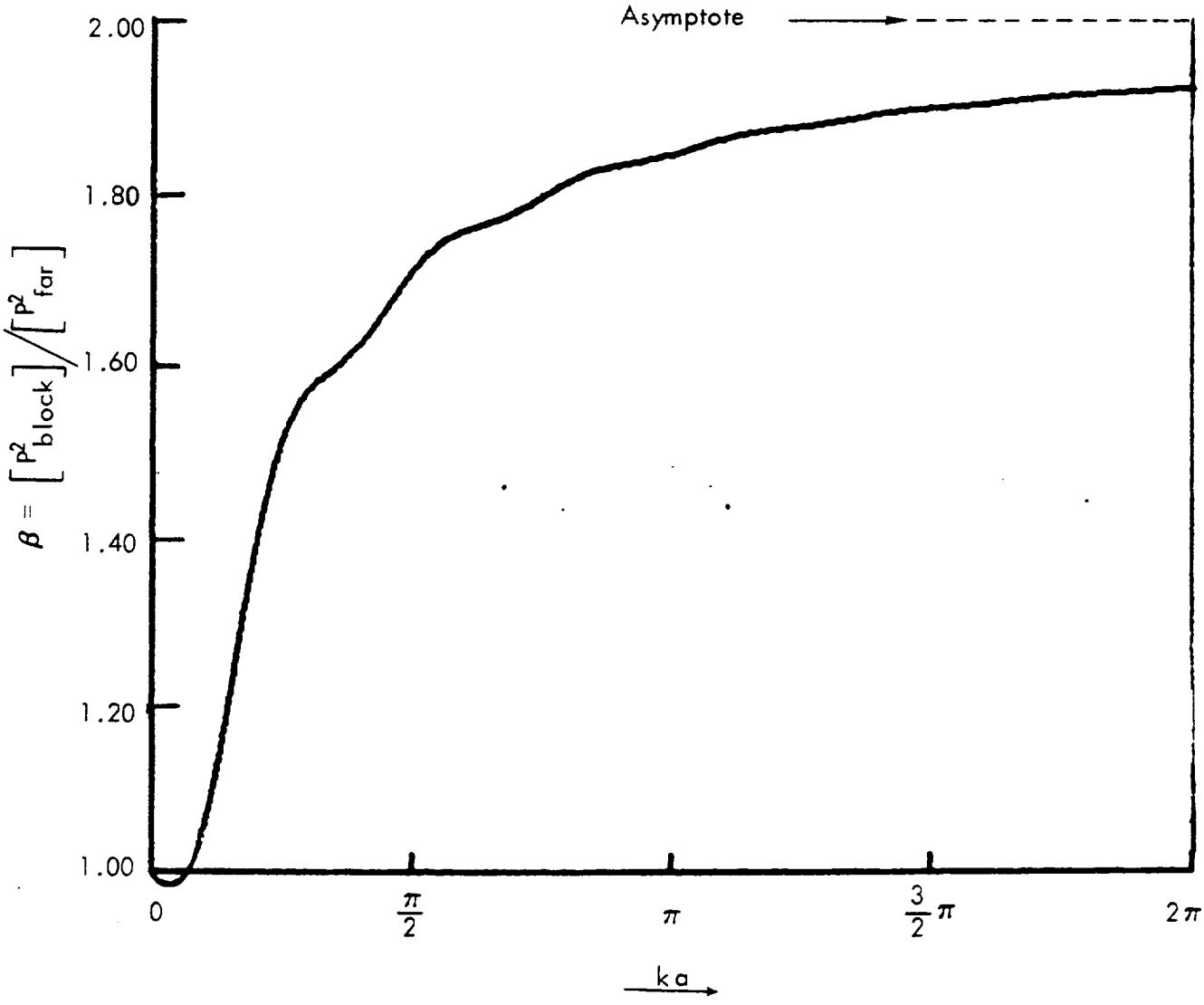

Figure 3.7. Normalized Mean Squared Blocked Pressure on Cylindrical Surfaces in a Reverberant Field

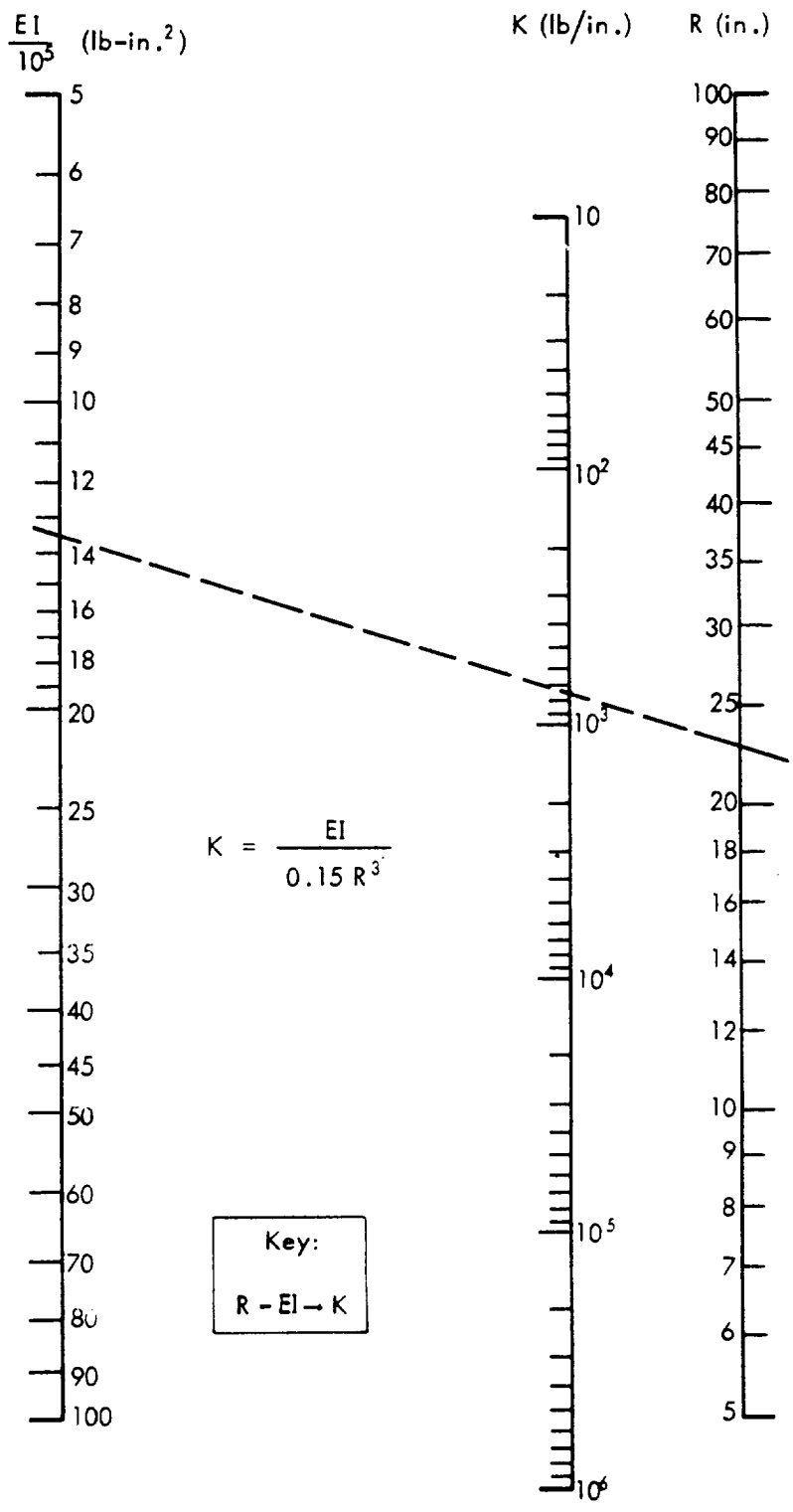

Figure 4.1. Nomograph for Determining Static Stiffness of Rings

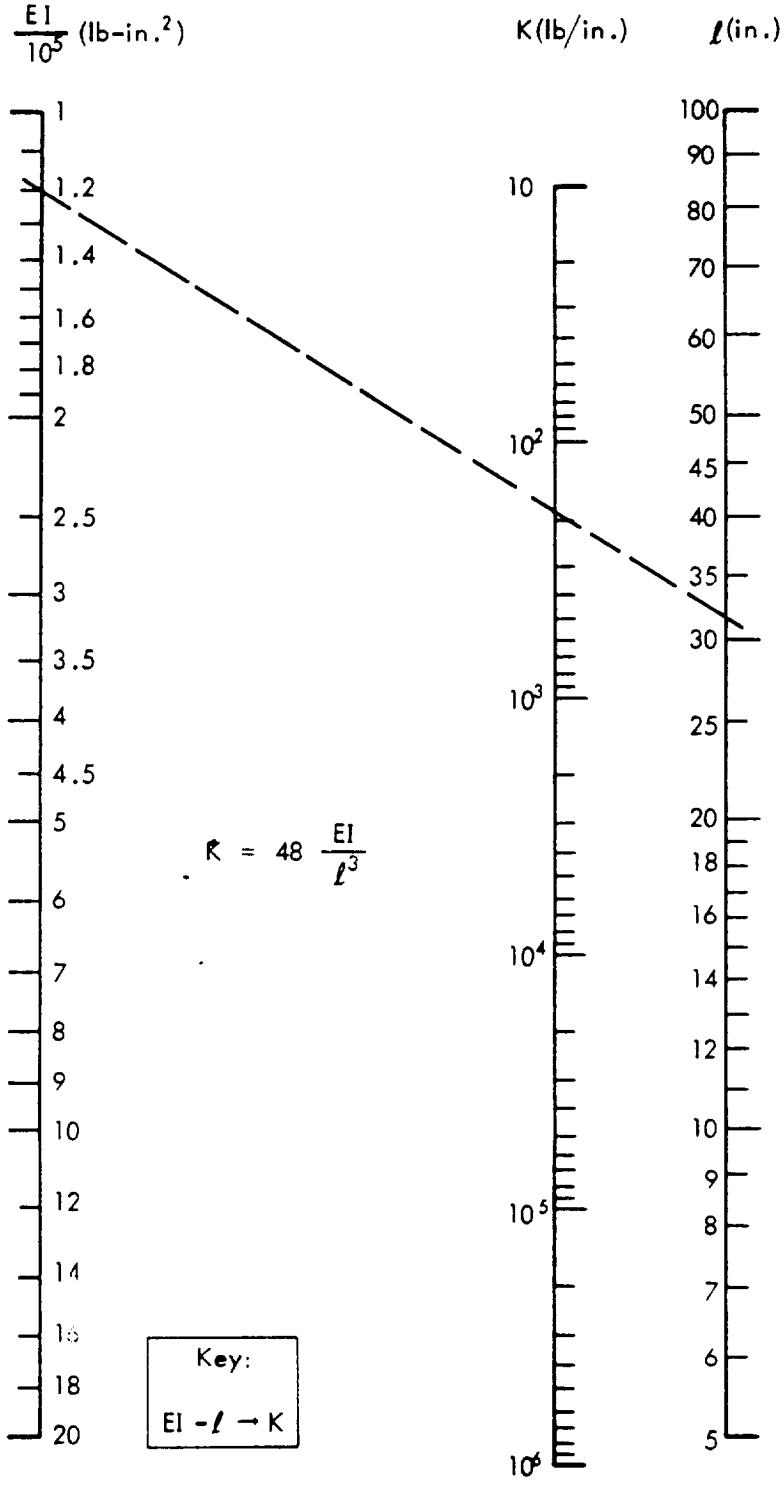

Figure 4.2. Nomograph for Determining Static Stiffness of Beams

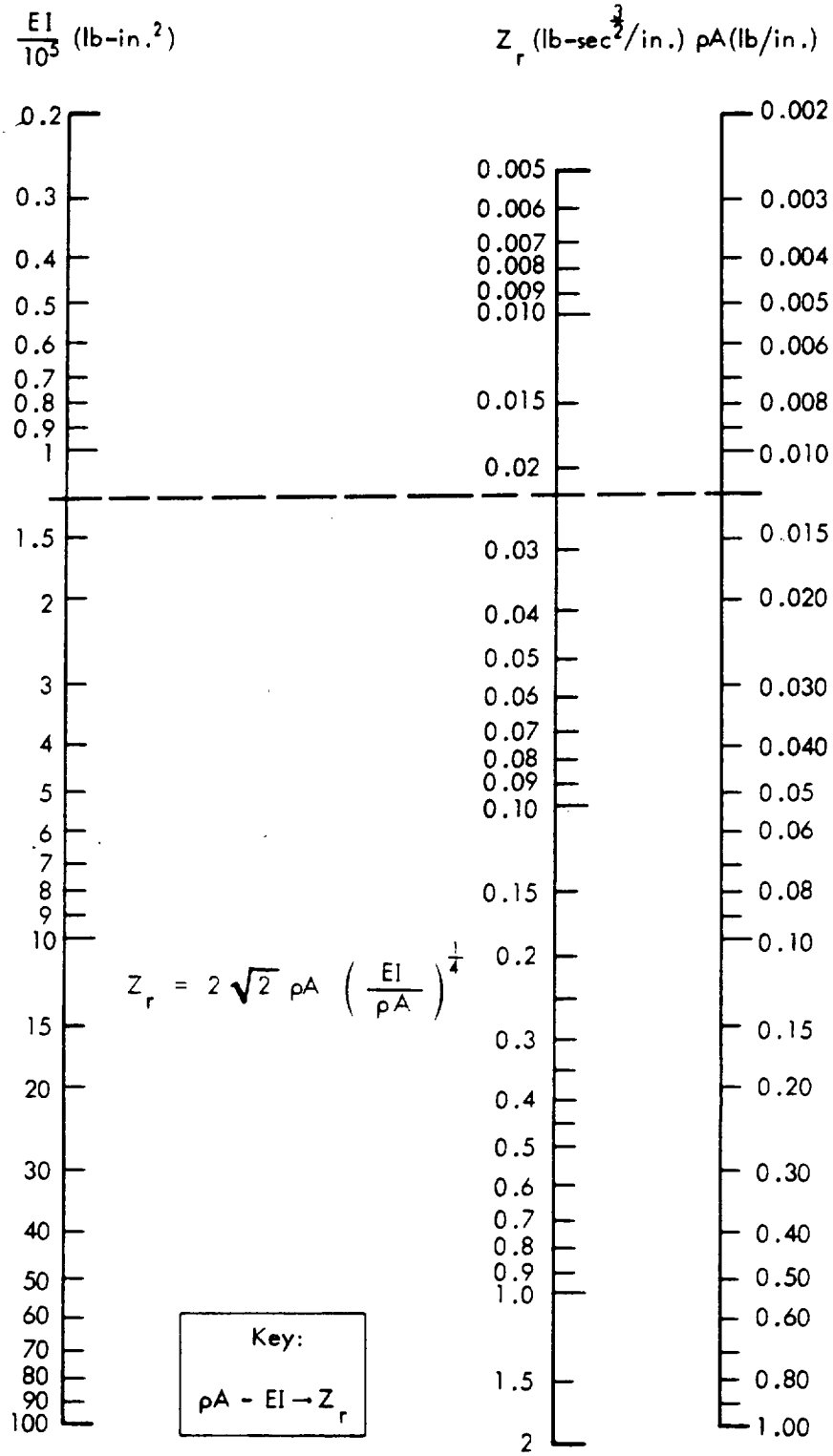

Figure 4.3. Nomograph for Determining Z_r of Beams and Rings

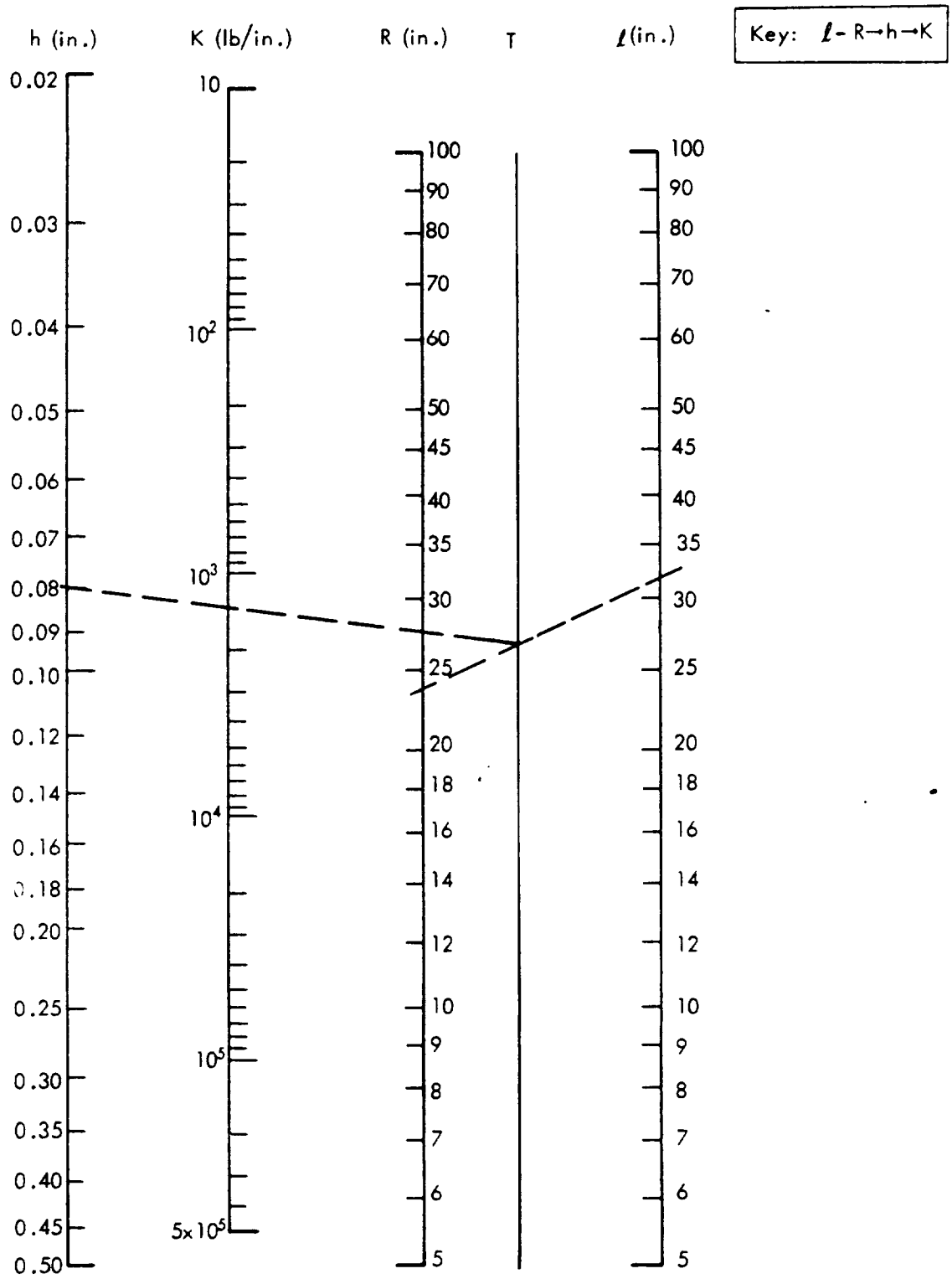

Figure 4.4 . Nomograph for Evaluating Static Stiffness of Unstiffened Cylinders

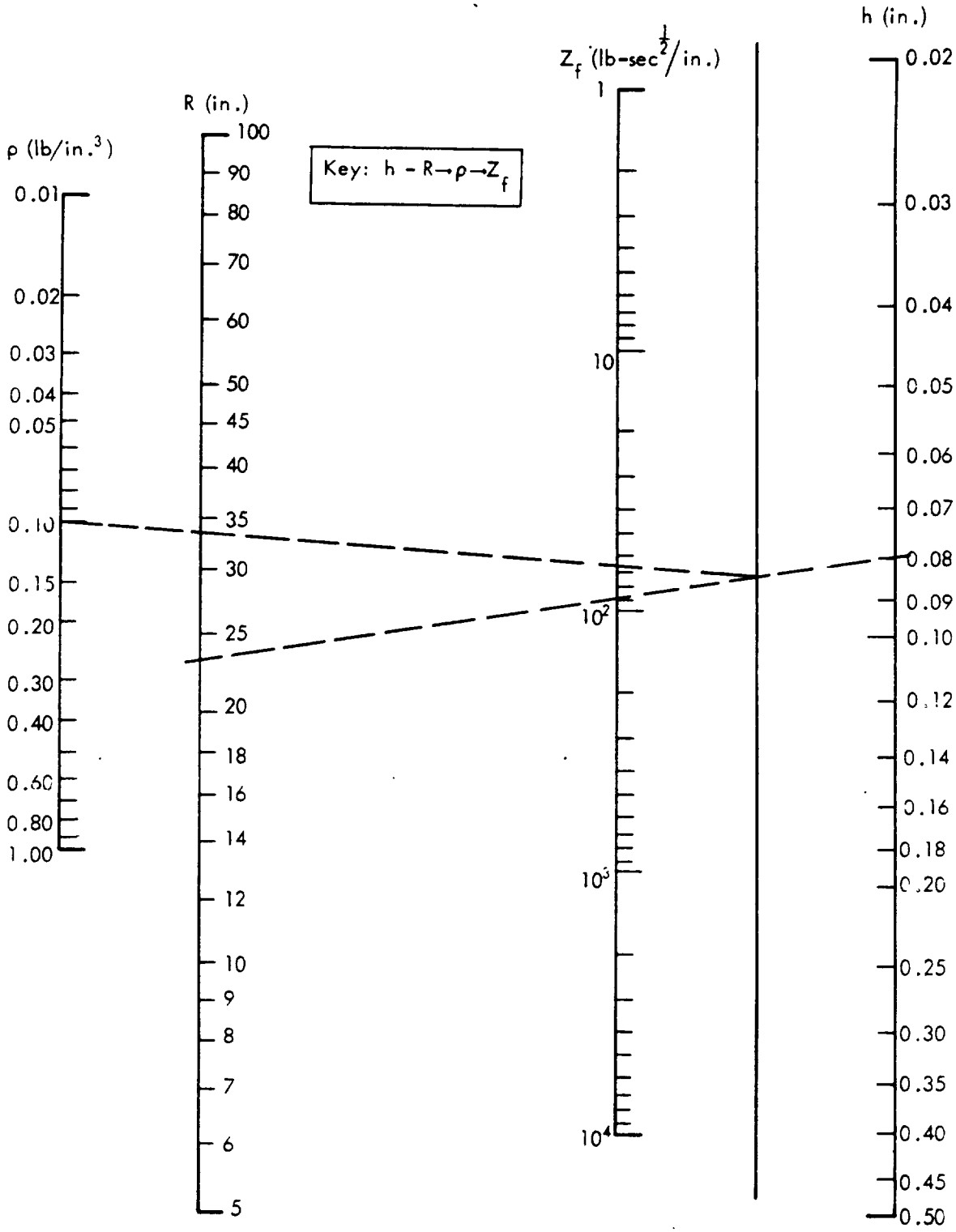

$$Z_f = \frac{4}{\sqrt{3}} \rho h^2 \sqrt{\frac{E}{\rho}} \left(\frac{E}{\rho R^2} \right)^{\frac{1}{4}} , \quad (E = 10^7 \text{ psi for Al})$$

Figure 4.5. Nomograph for Determining Z_f of Unstiffened Cylinders

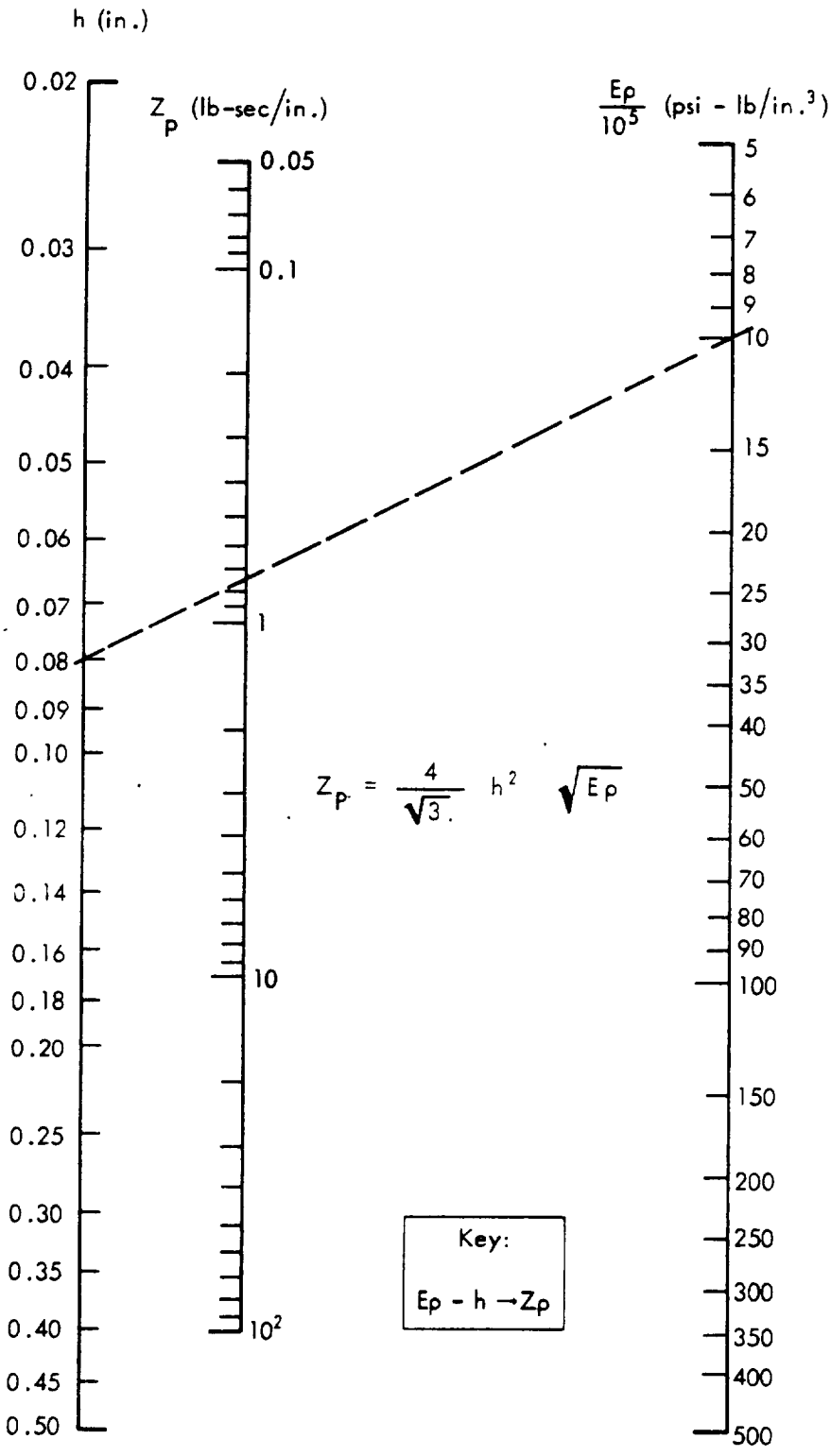

Figure 4.6. Nomograph for Evaluating Impedance of Infinite Plate

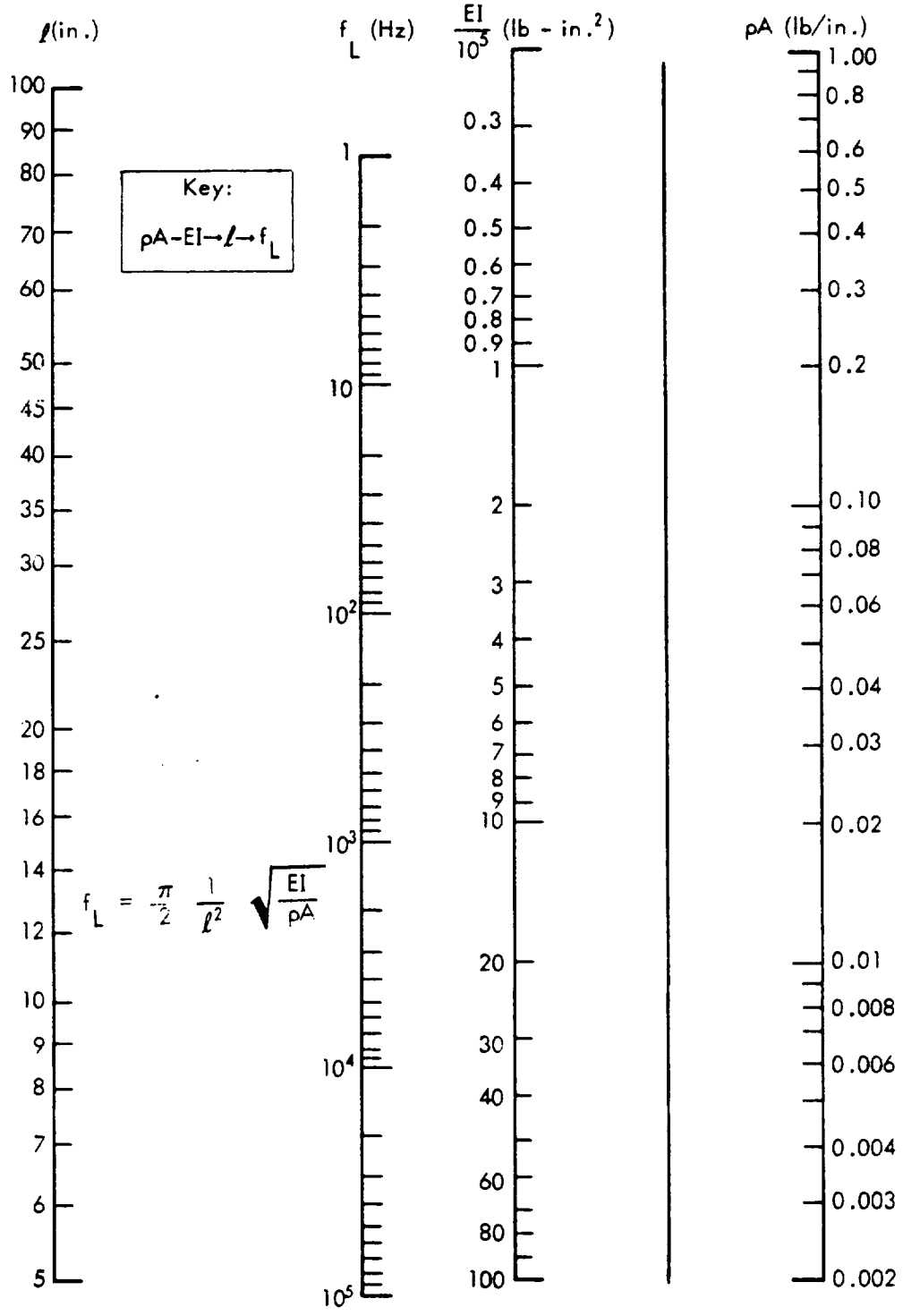

Figure 4.7. Alignment Chart for Determining the Lowest Fundamental Frequency of Beams

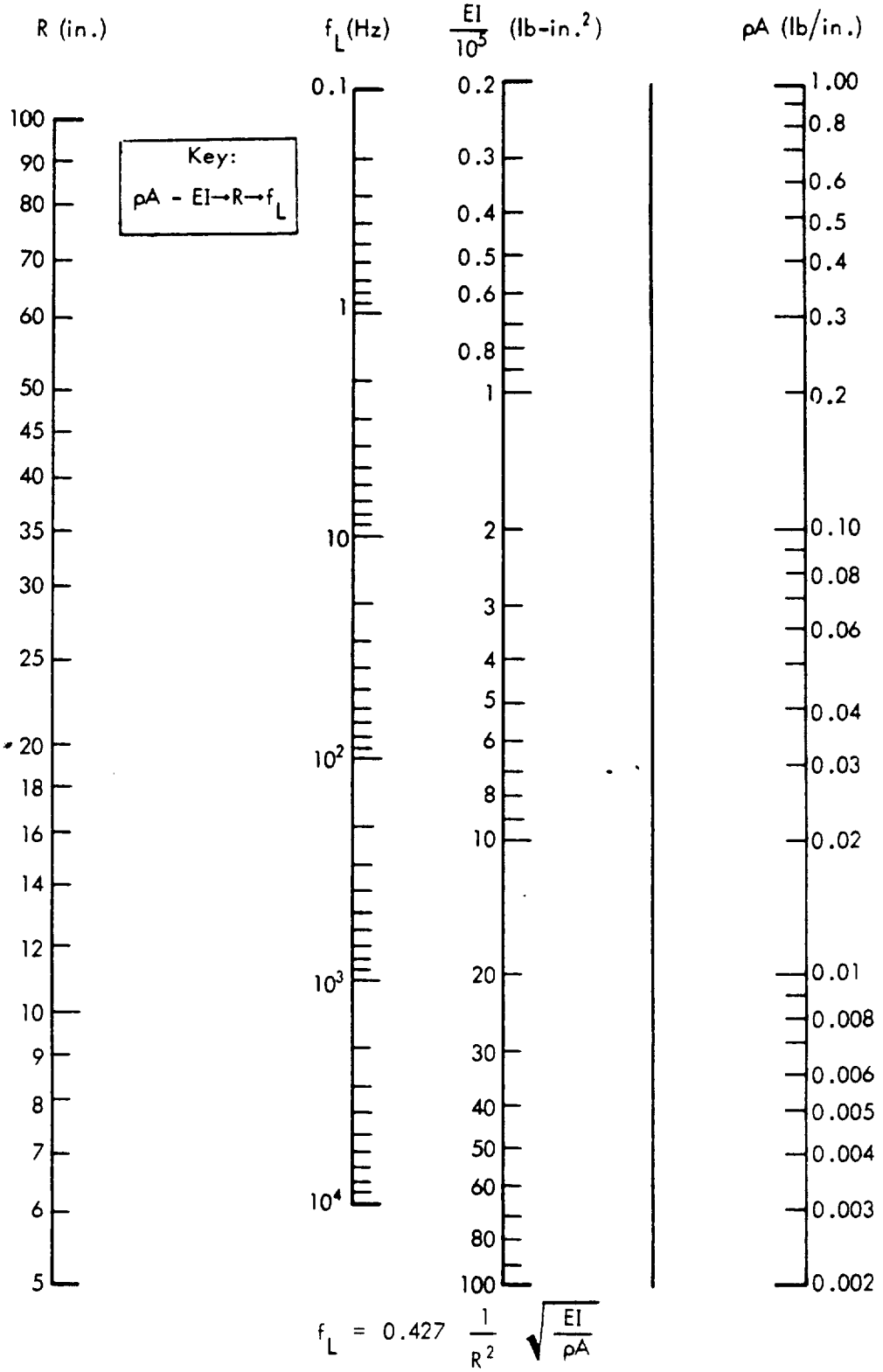

Figure 4.8. Alignment Chart for Determining the Lowest Fundamental Frequency of Rings

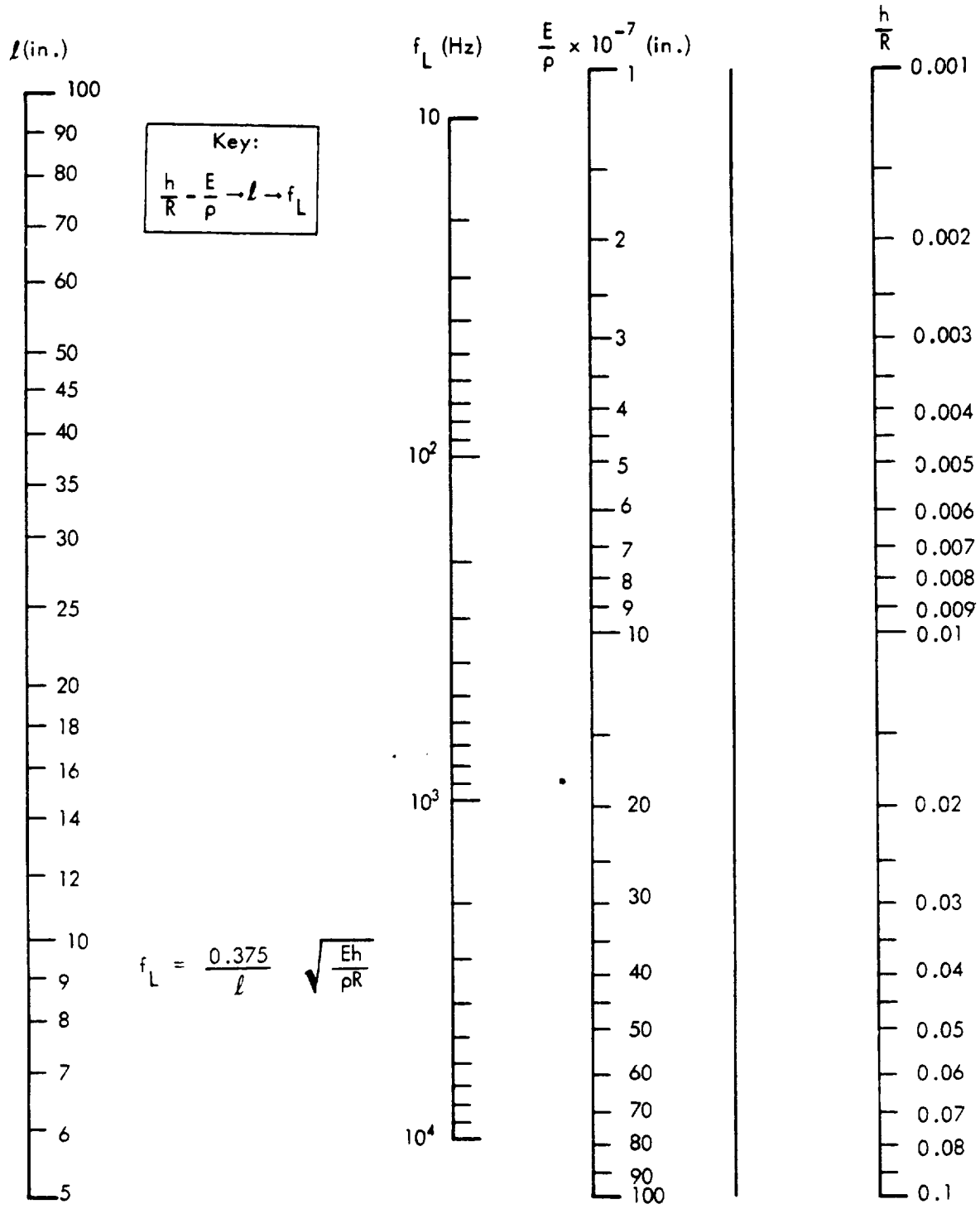

Figure 4.9. Alignment Chart for Determining the Lowest Fundamental Frequency of Unstiffened Cylinders

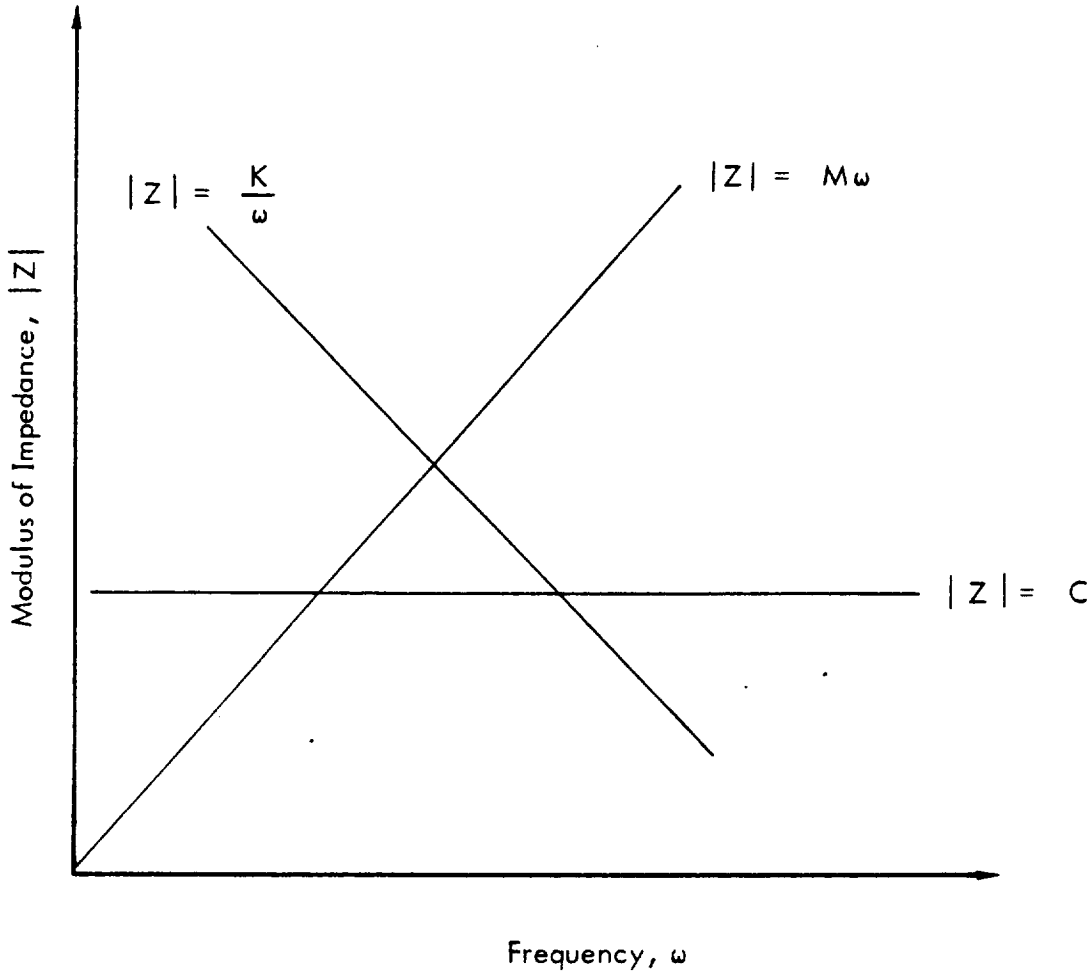

Figure 4.11. The Variation with Frequency of the Magnitude of the Impedance of an Ideal Damping, Spring and Mass Systems

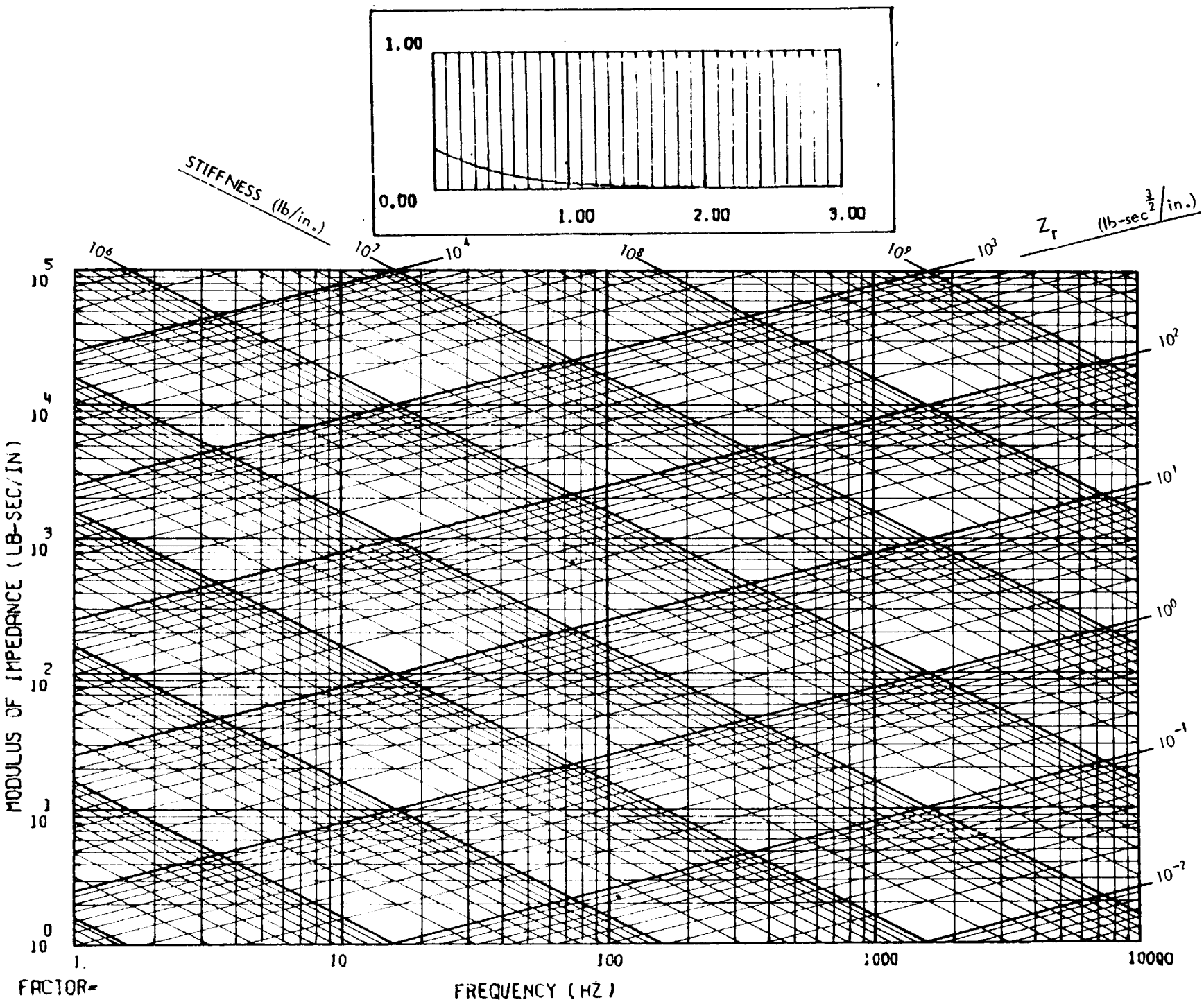

Figure 4.12. Impedance Chart for Stiffeners

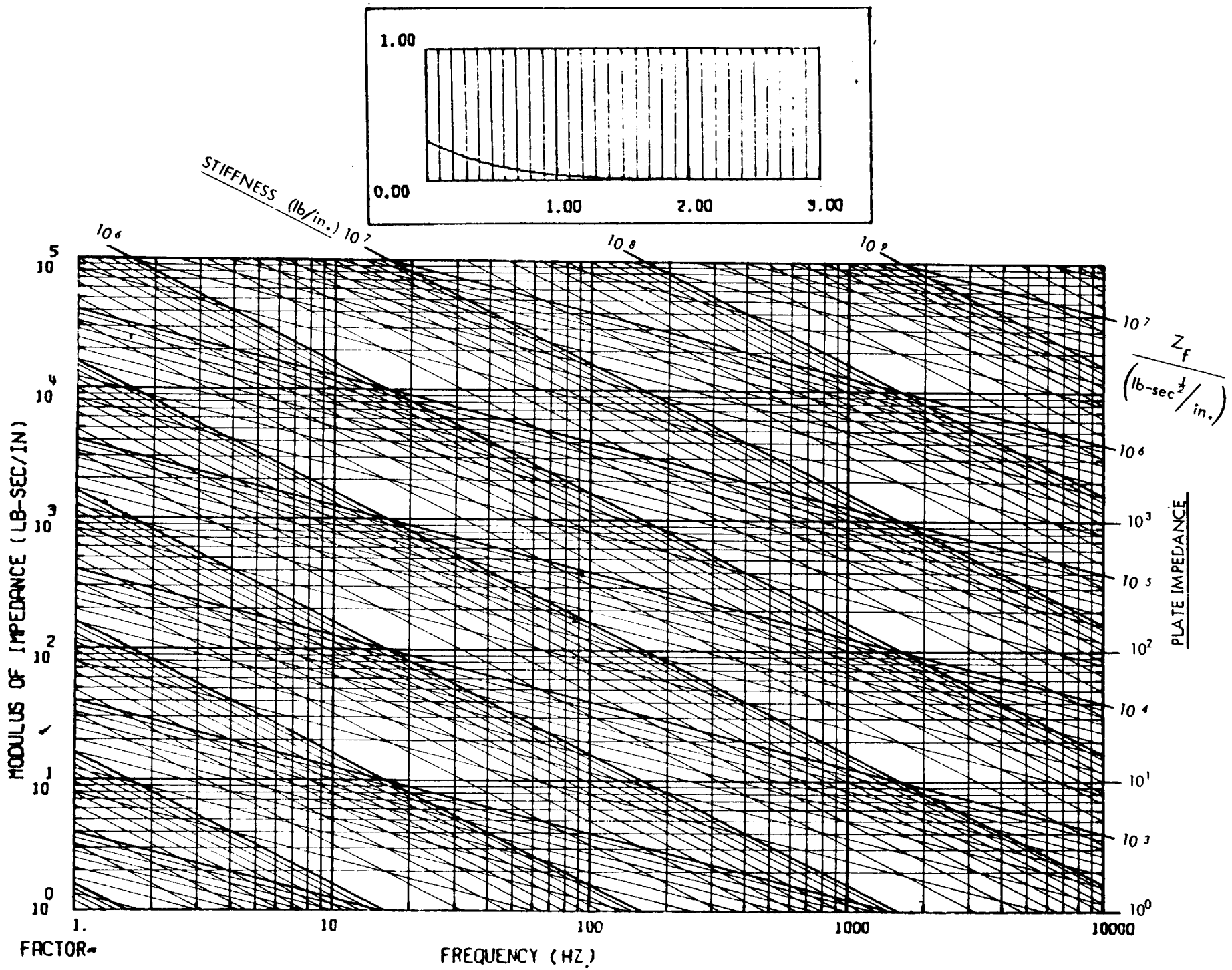

Figure 4.13. Impedance Chart for Cylindrical Shells

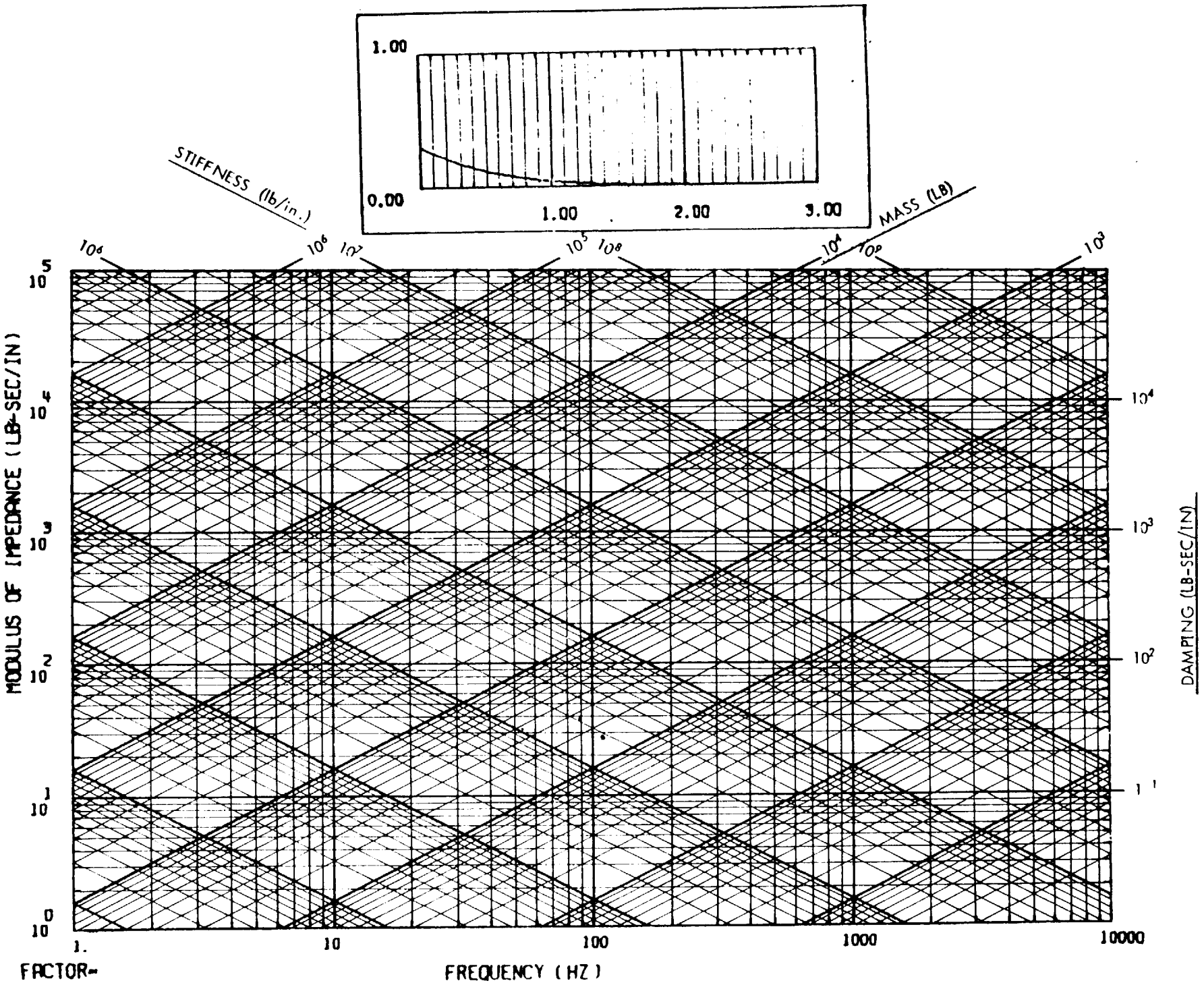

Figure 4.14. Impedance Chart for Component Packages

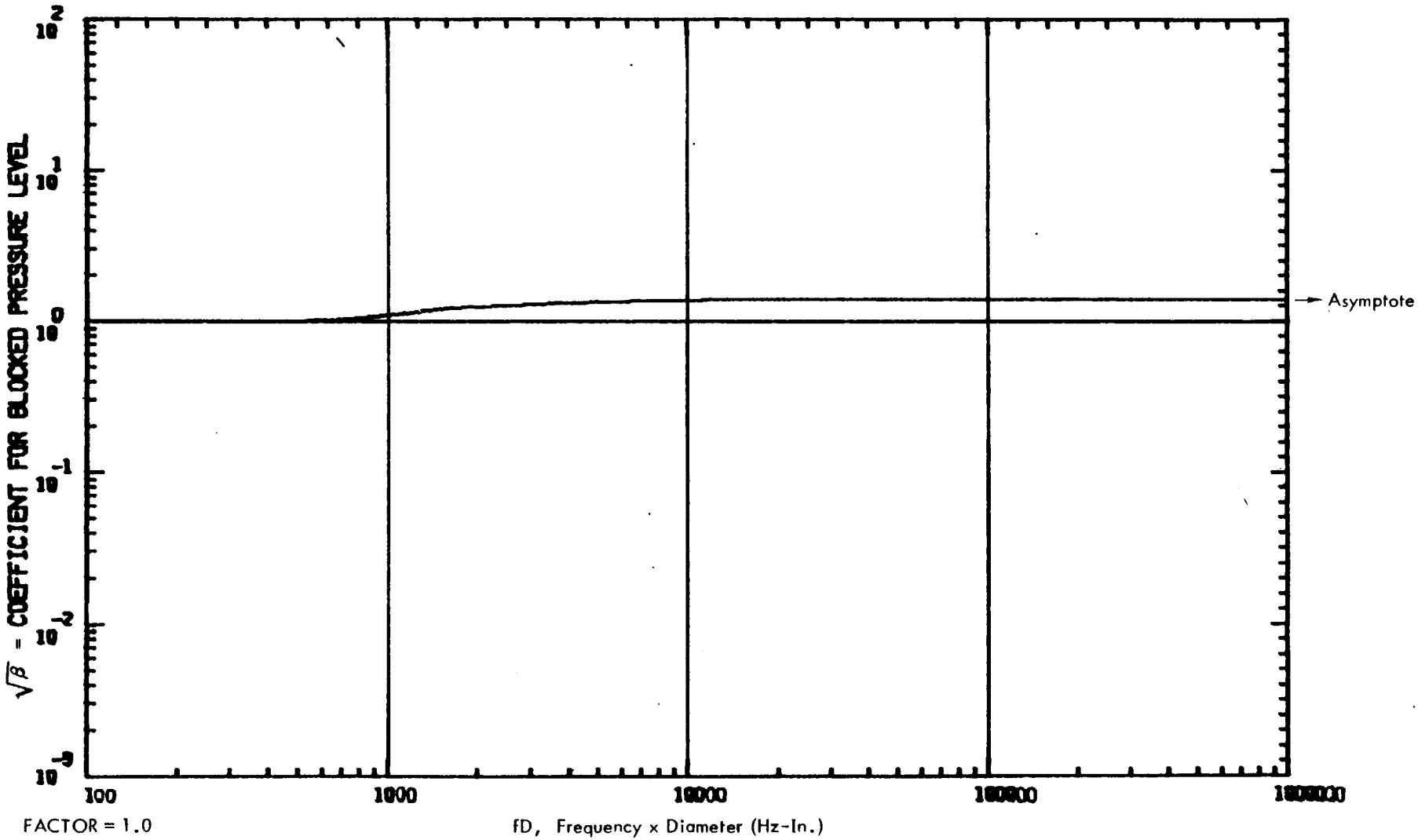

Figure 4.15. Theoretical $\sqrt{\beta}$ - Curve for Obtaining Blocked Pressure Level of a Cylinder in a Random Sound Field

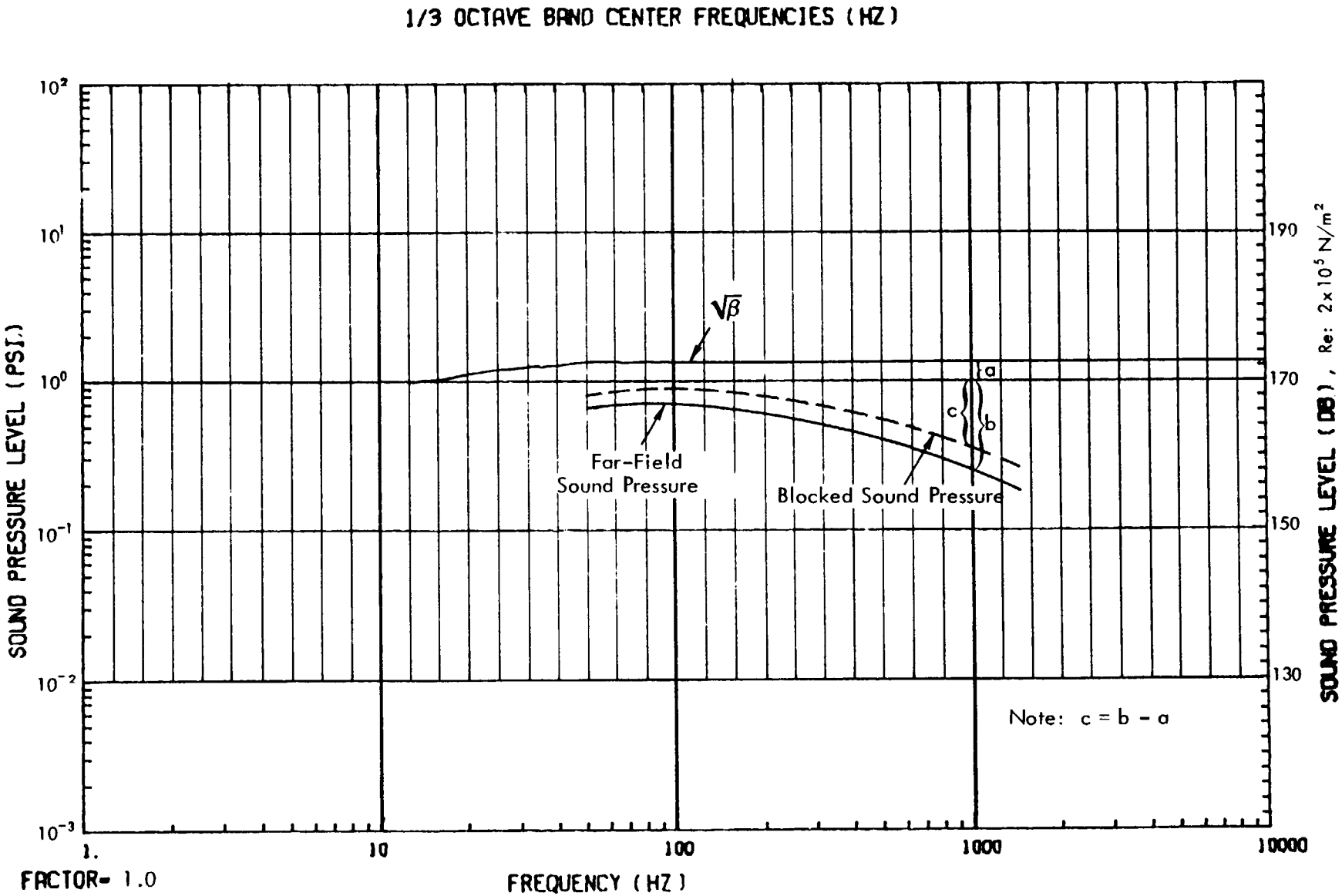

Figure 4.16. Determination of Blocked Pressure Spectrum

α = Acoustic mobility (in./sec/psi)

m = Surface density (weight) (lb/in.^{2})

D = Diameter (in.)

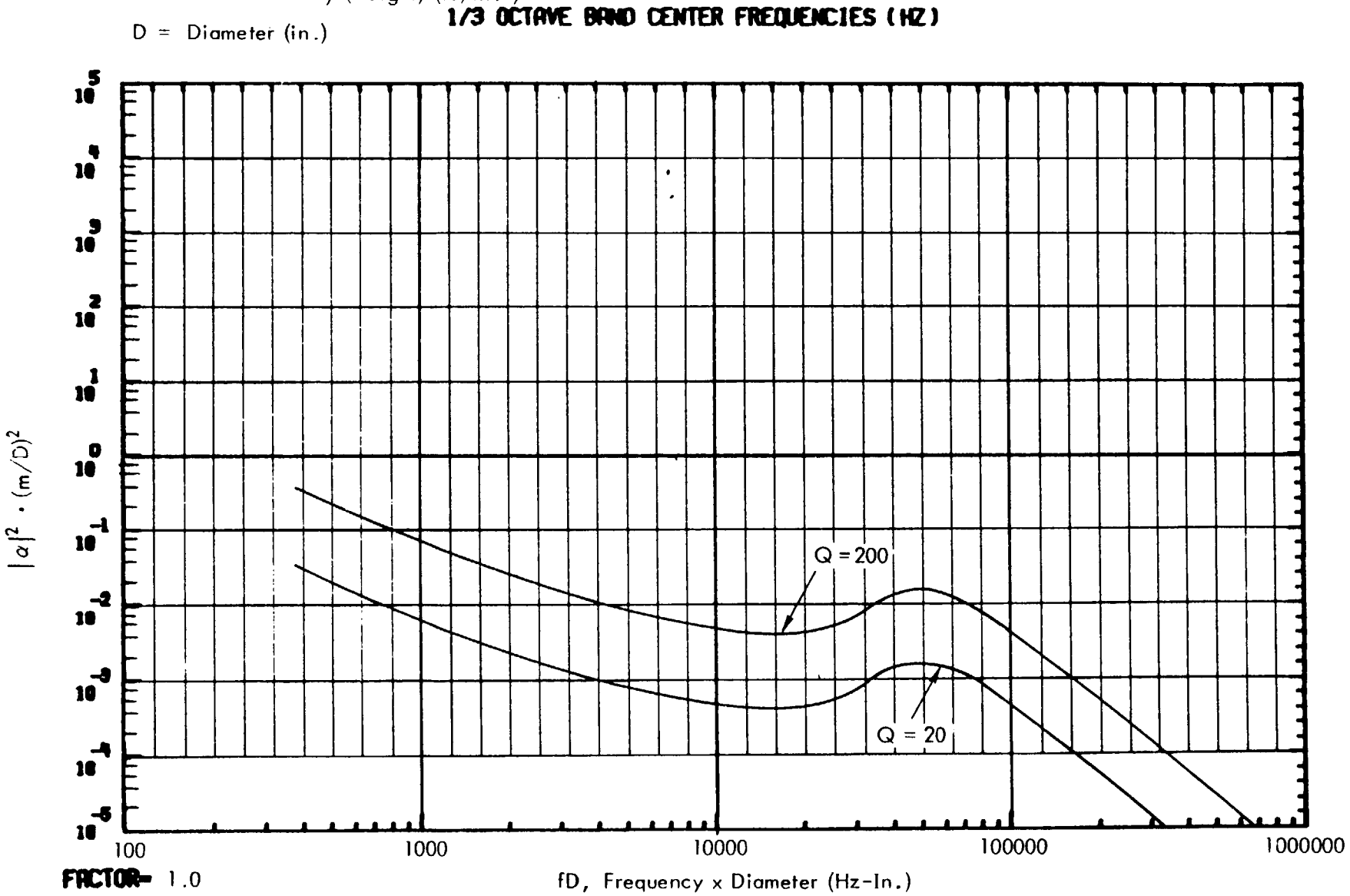

Figure 4.17. Velocity Acoustic Mobility Levels for Cylindrical Structures for Damping Q = 200

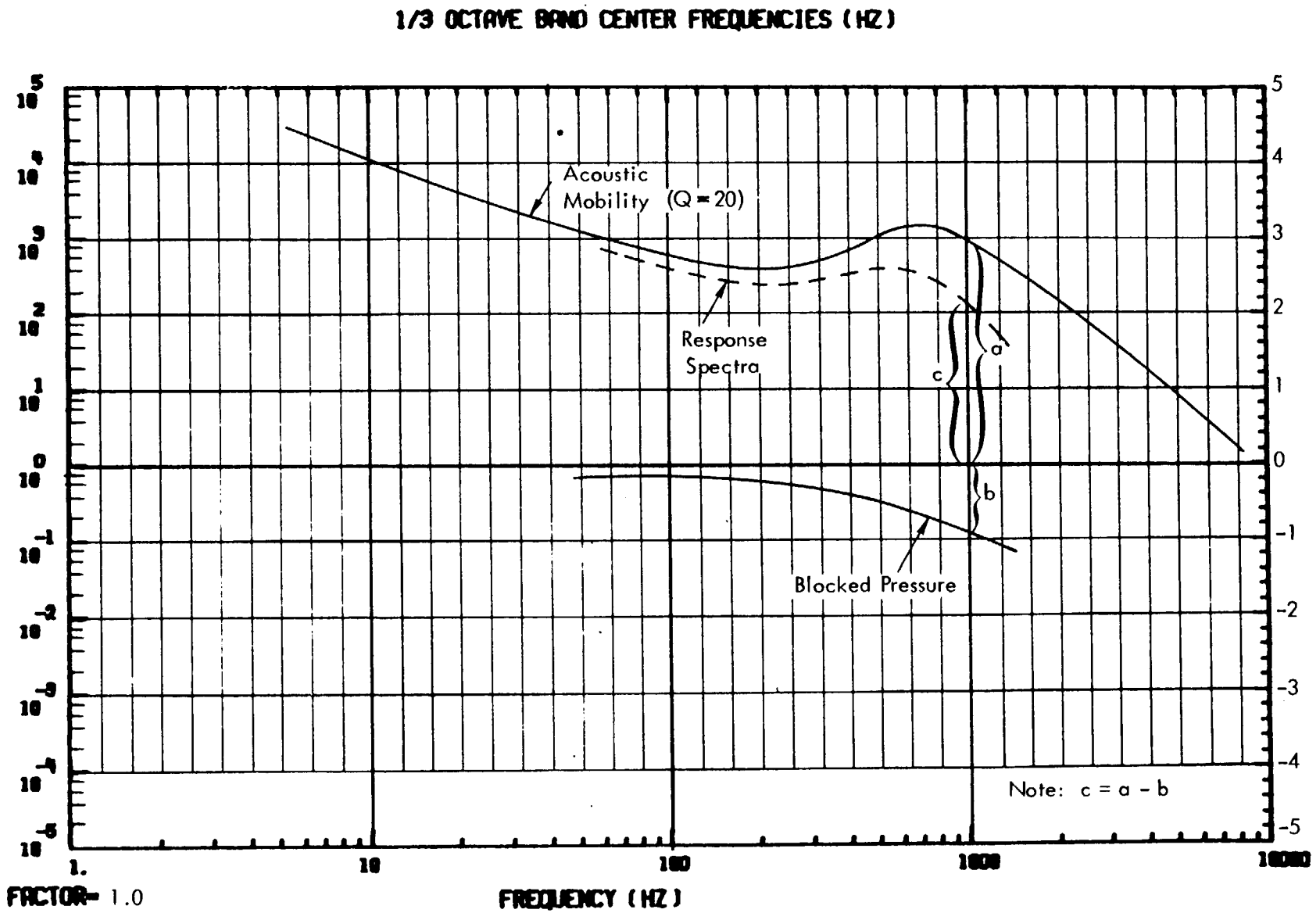

Figure 4.18. Determination of Structural Response Spectrum

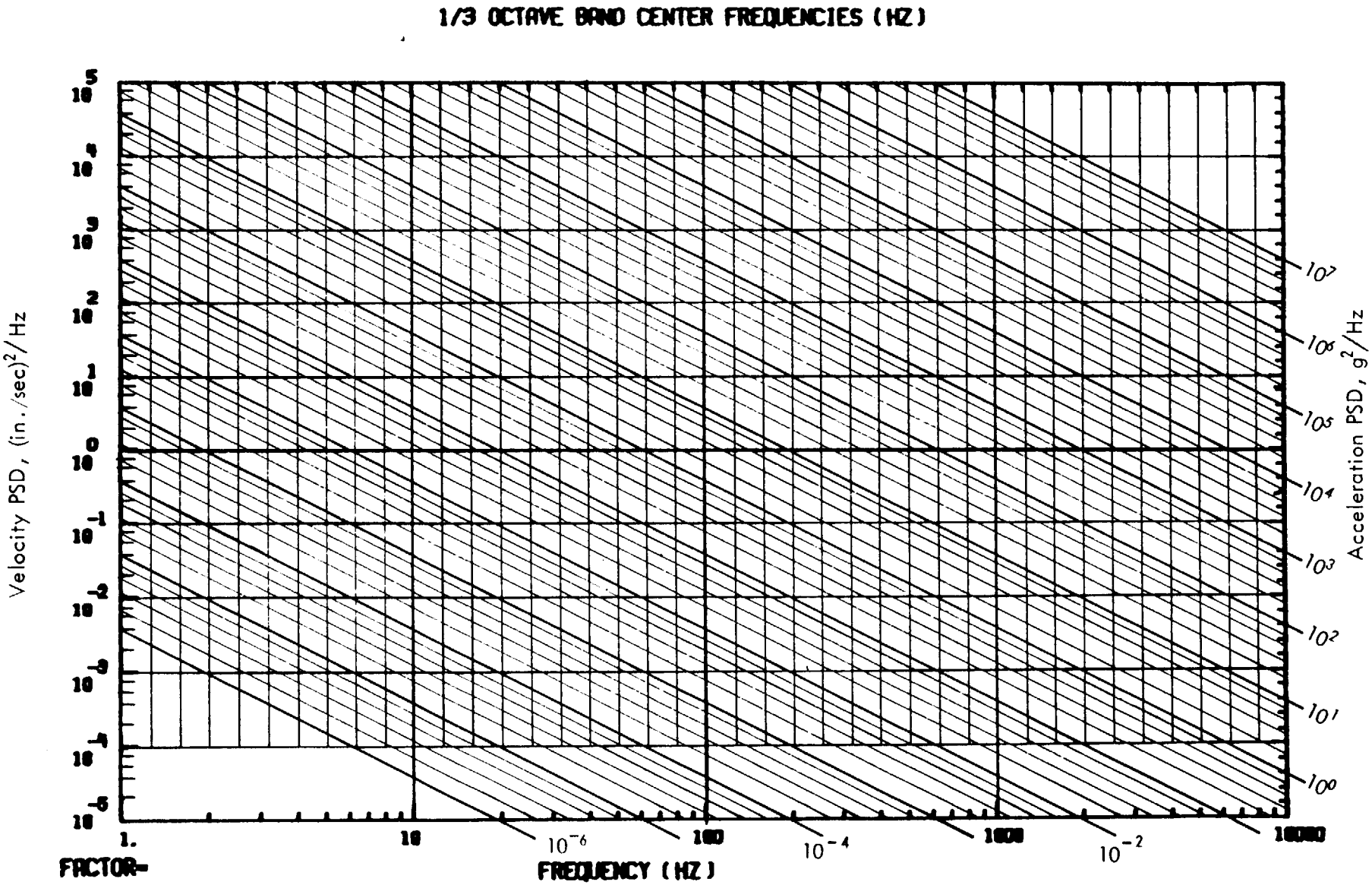

Figure 4.19. Velocity-Acceleration Response Conversion Chart

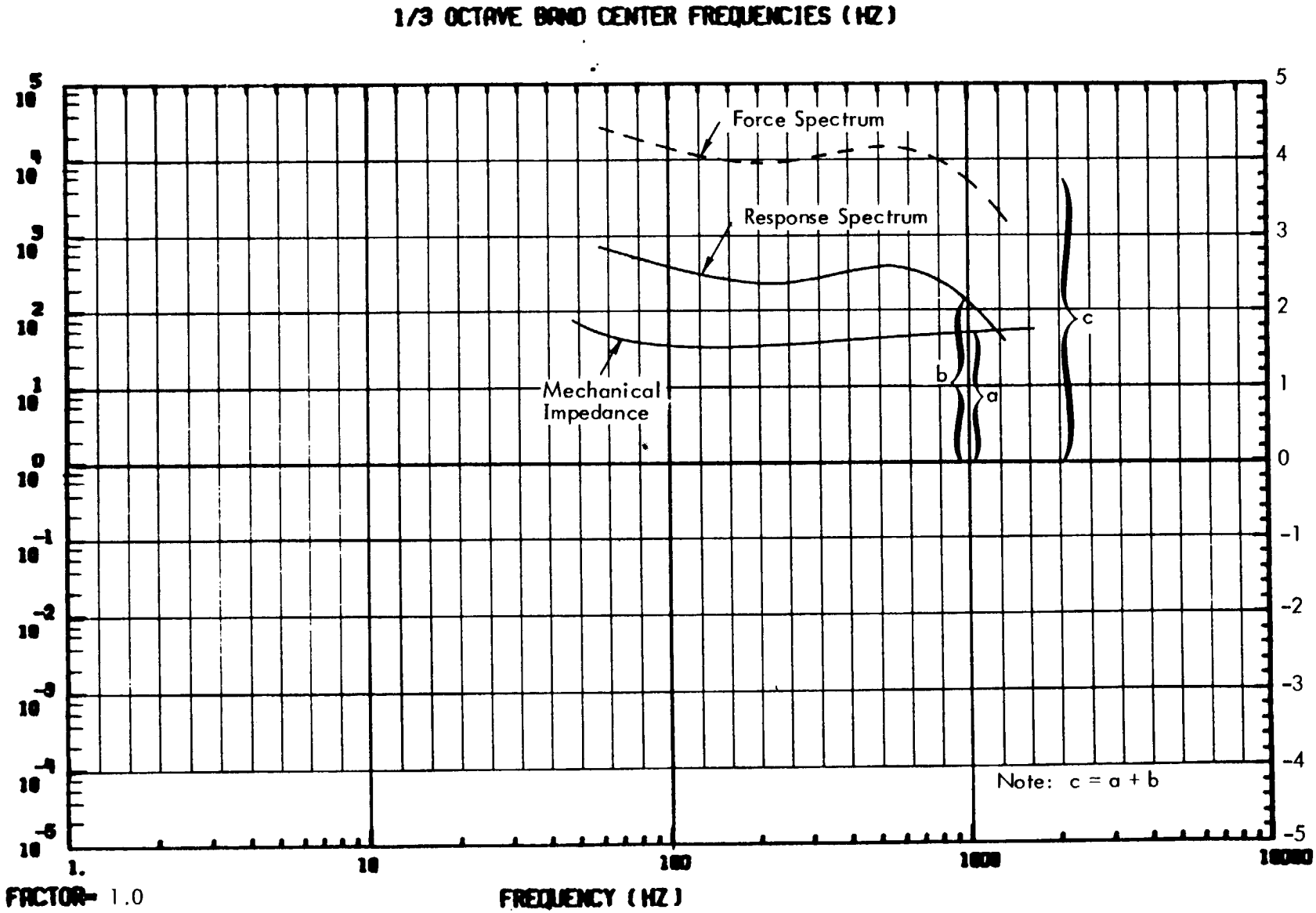

Figure 4.20. Force Spectrum Computation

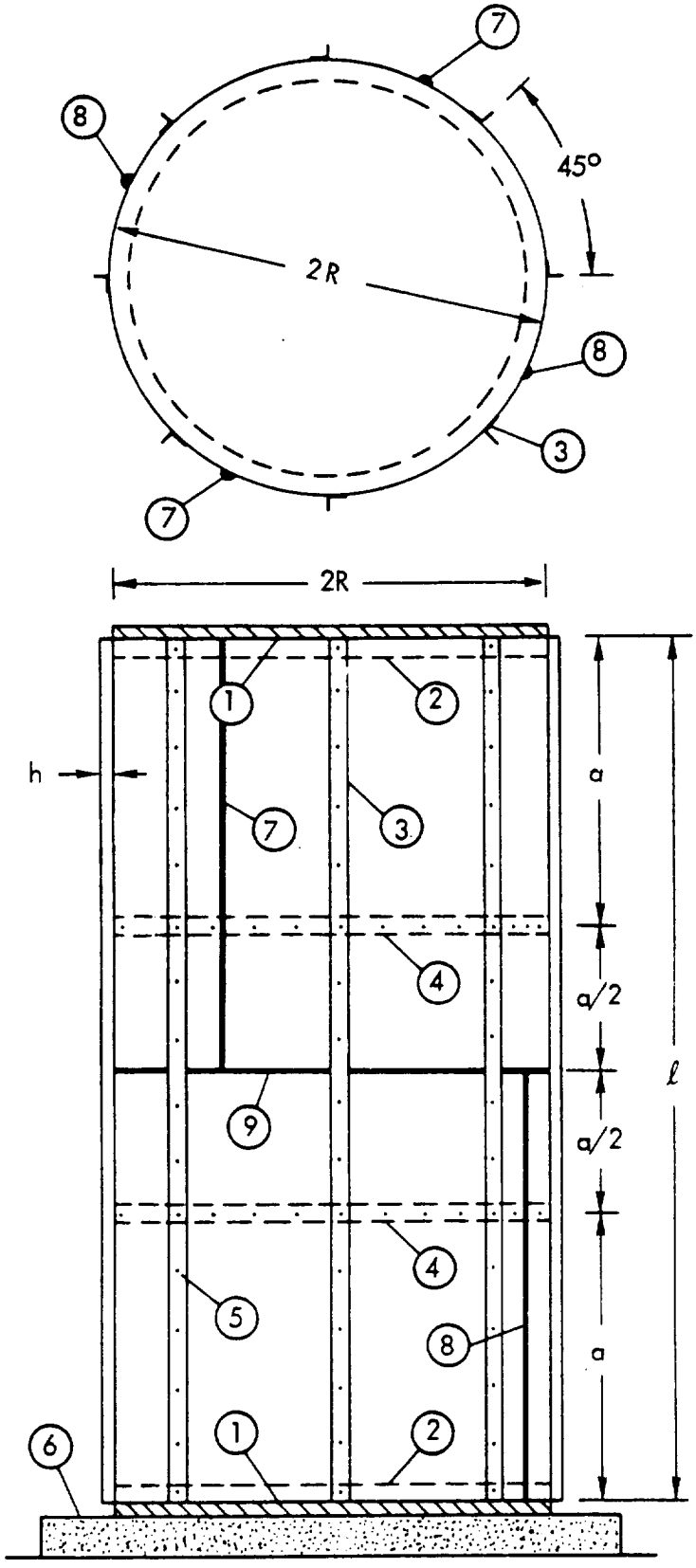

1. Two flat circular plywood bulkheads
2. Two angle section end rings
3. Eight angle section stringers
4. Two channel section ring frames
5. 176 pop rivets
6. Foam rubber support
7. Upper axial weld lines
8. Lower axial weld lines
9. Circumferential weld line

Figure 5.1. Geometry and Dimensions of Fully-Stiffened Configuration of Cylinder

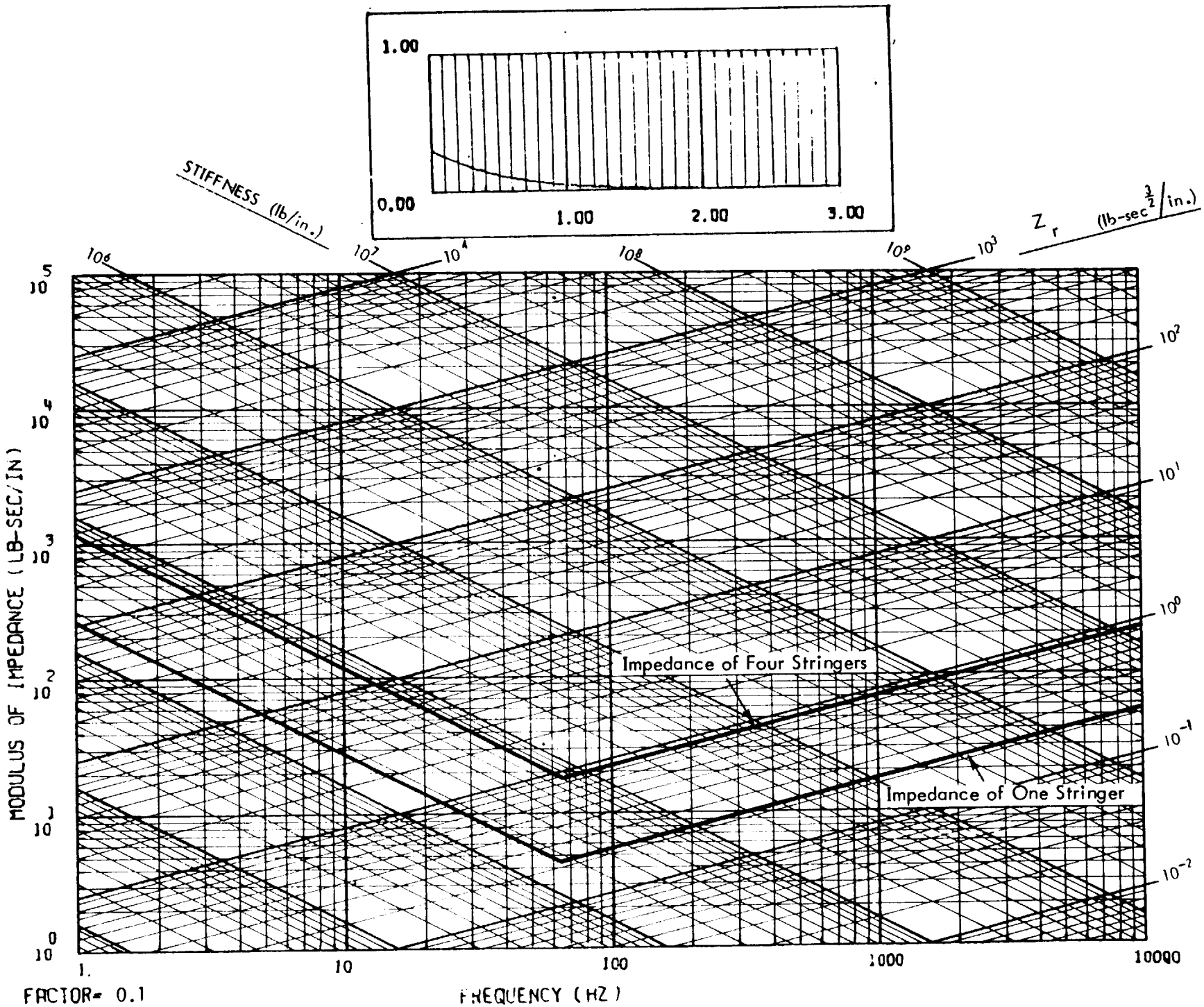

Figure 5.2. Impedances of Stringers

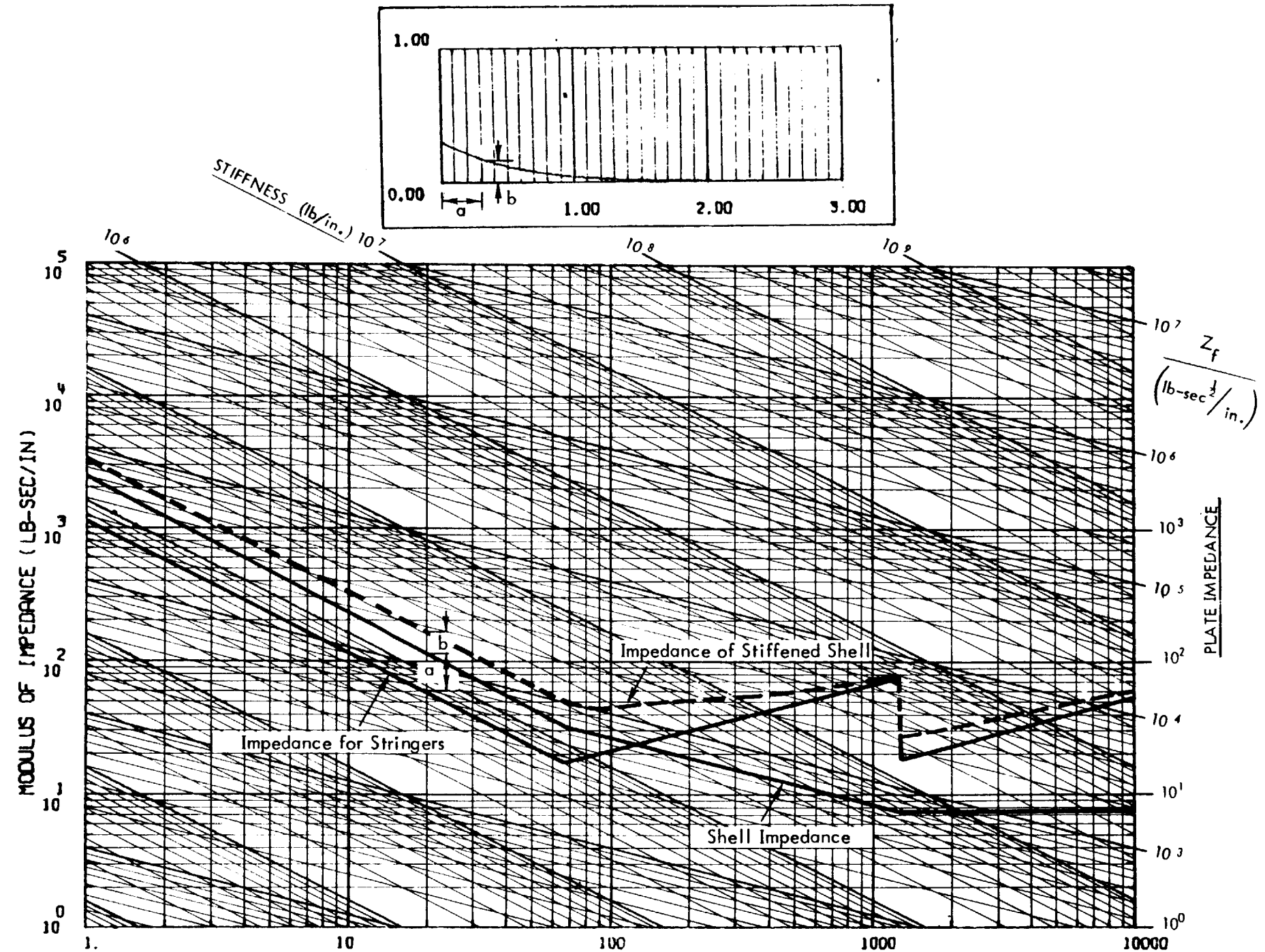

Figure 5.3. Impedance of Stiffened Shell

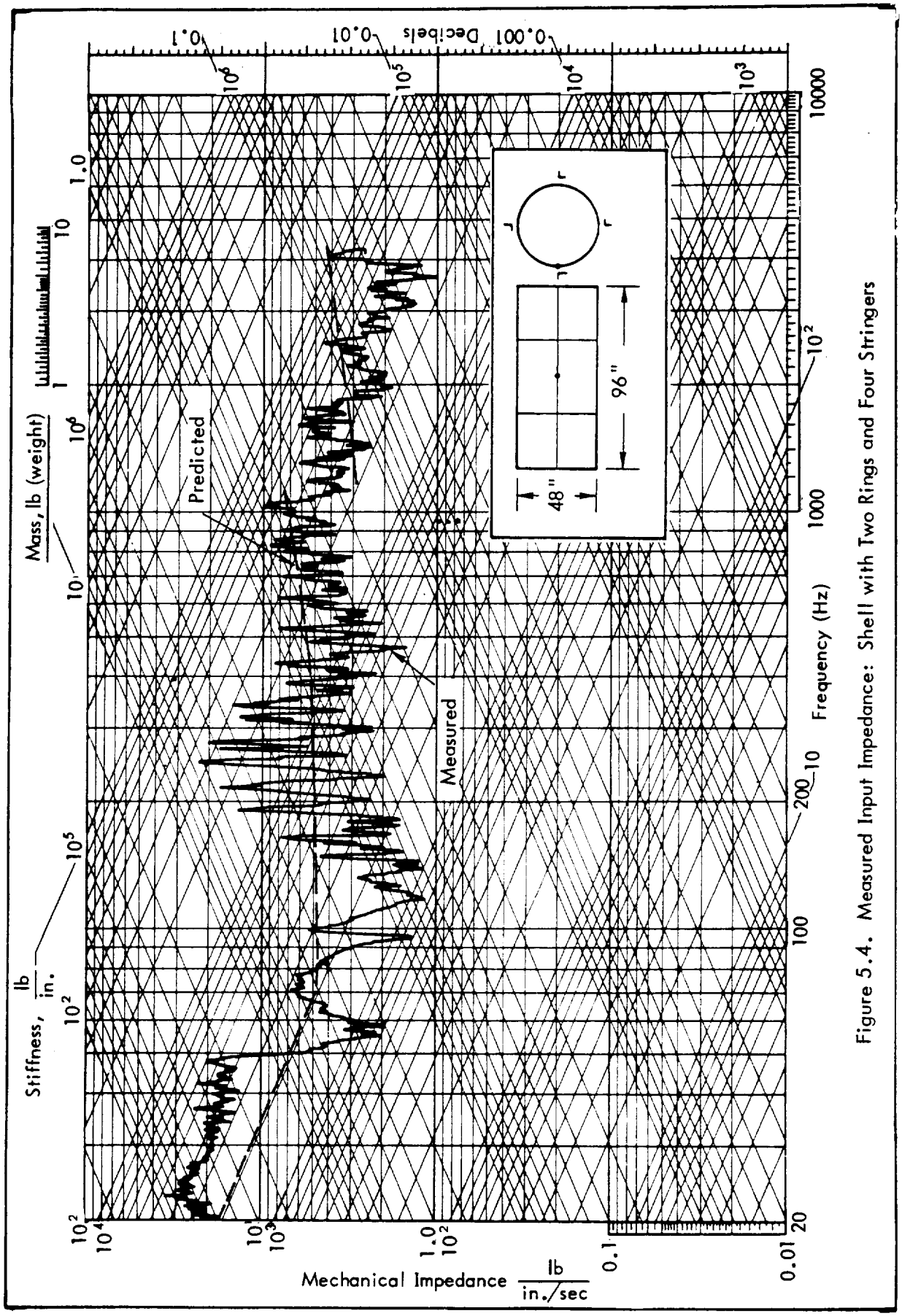

Figure 5.4. Measured Input Impedance: Shell with Two Rings and Four Stringers

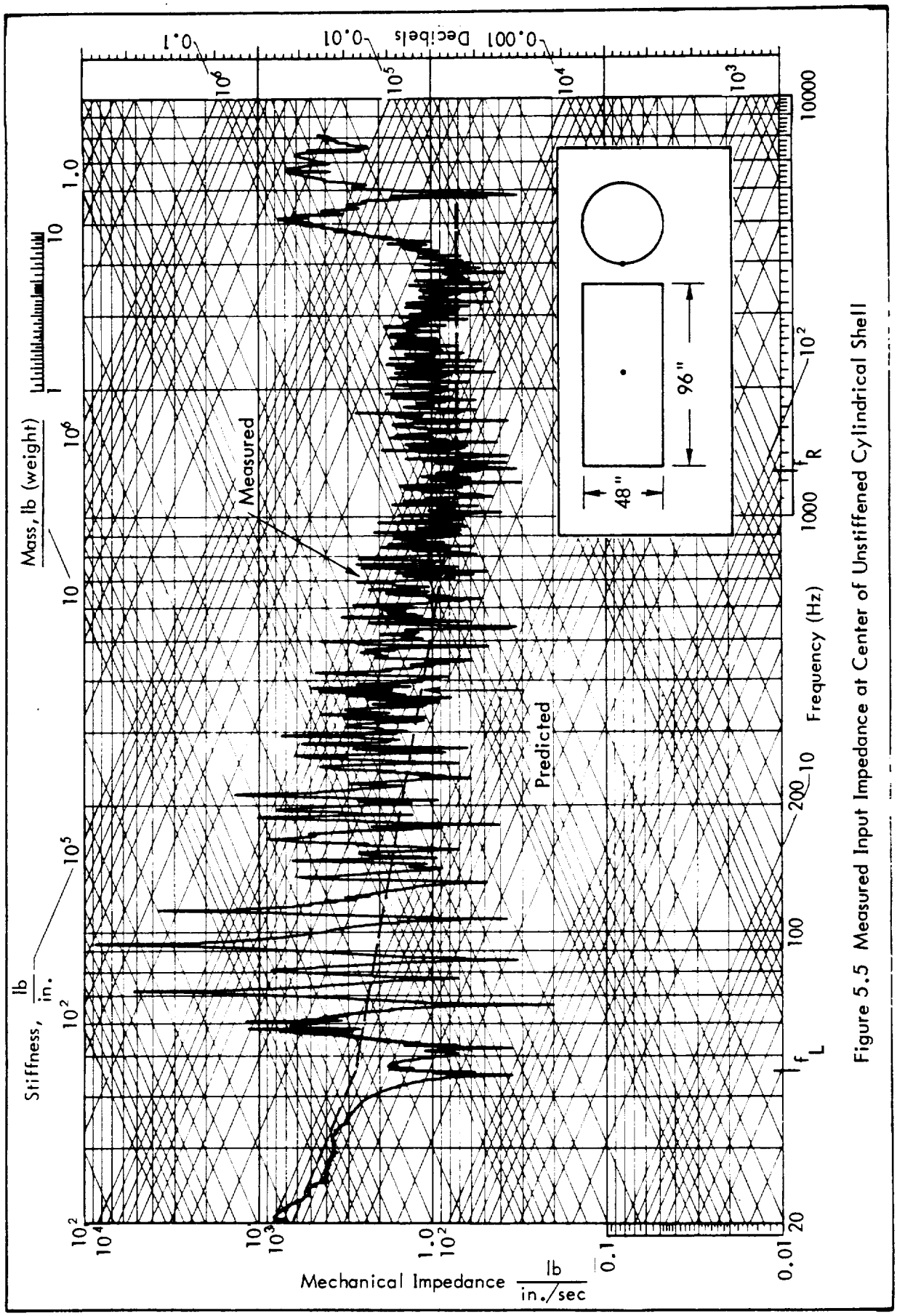

Figure 5.5 Measured Input Impedance at Center of Unstiffened Cylindrical Shell

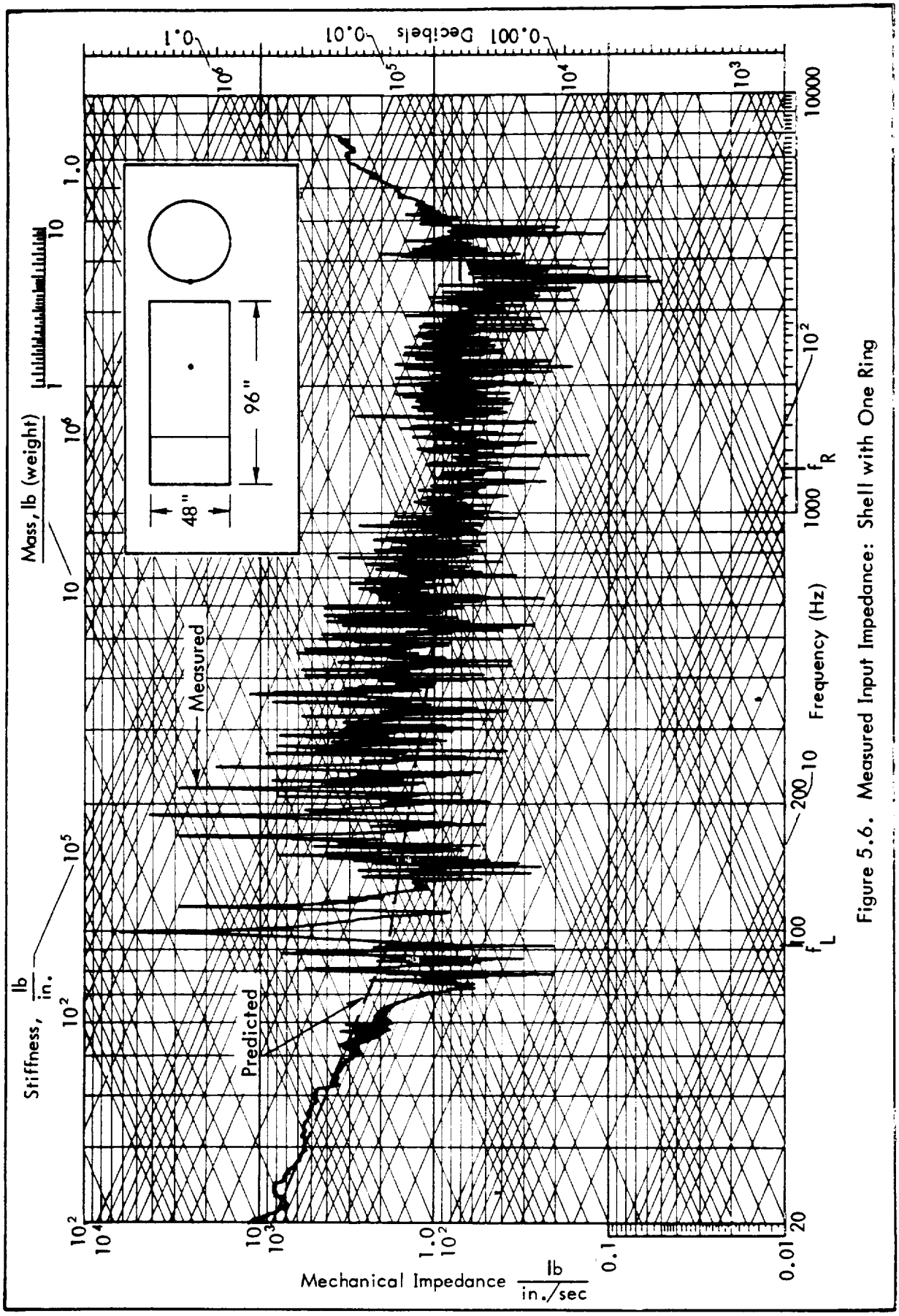

Figure 5.6. Measured Input Impedance: Shell with One Ring

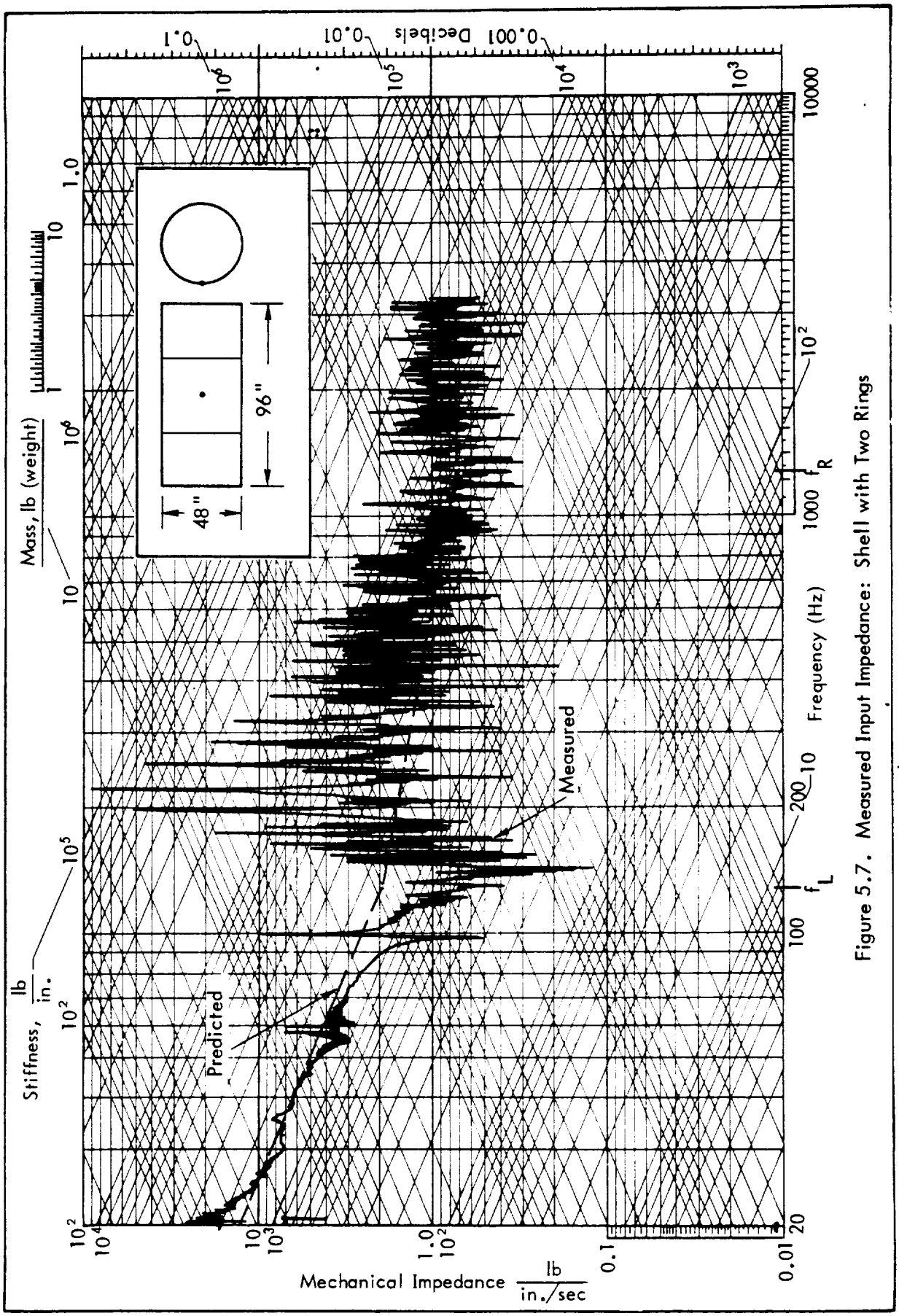

Figure 5.7. Measured Input Impedance: Shell with Two Rings

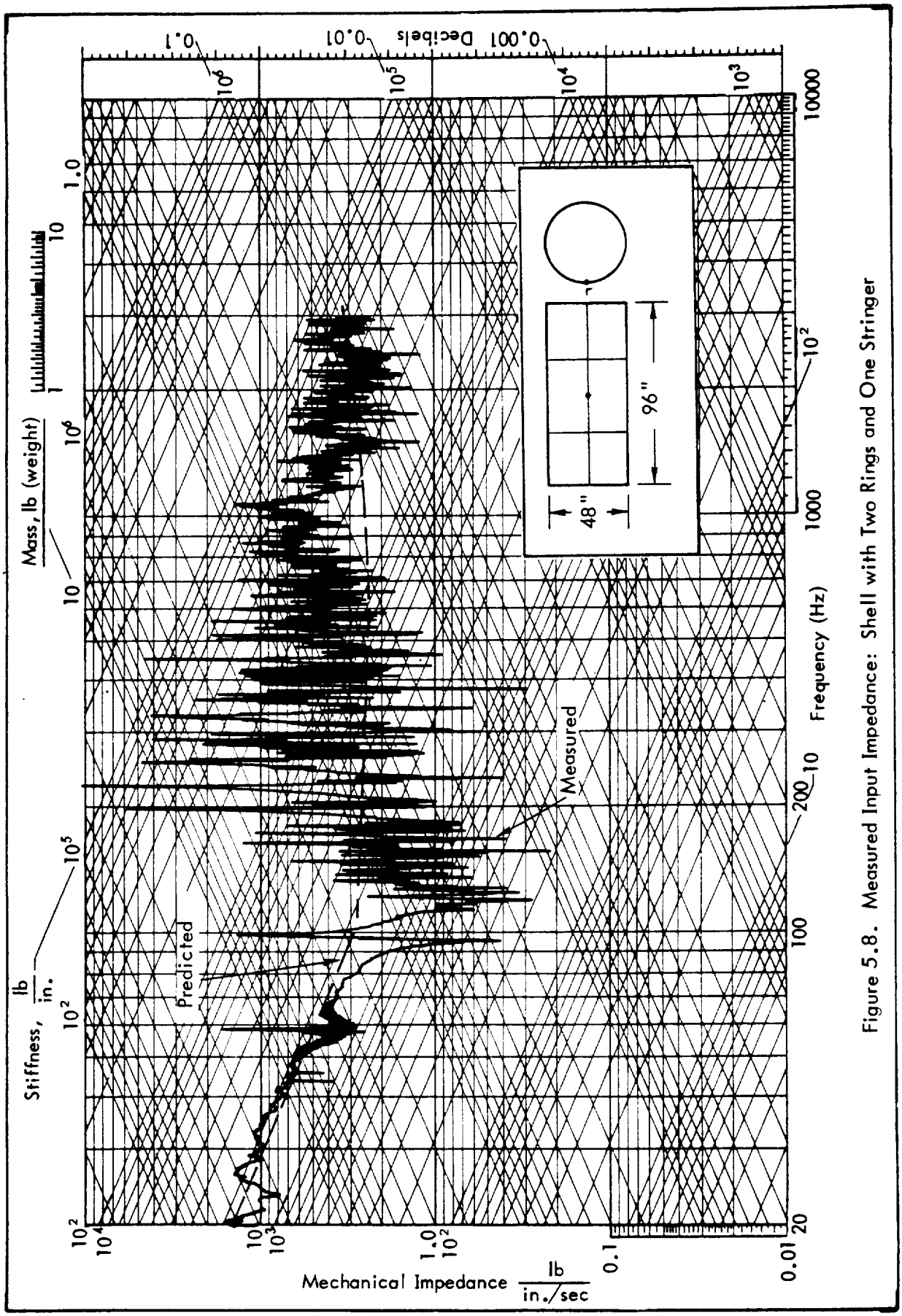

Figure 5.8. Measured Input Impedance: Shell with Two Rings and One Stringer

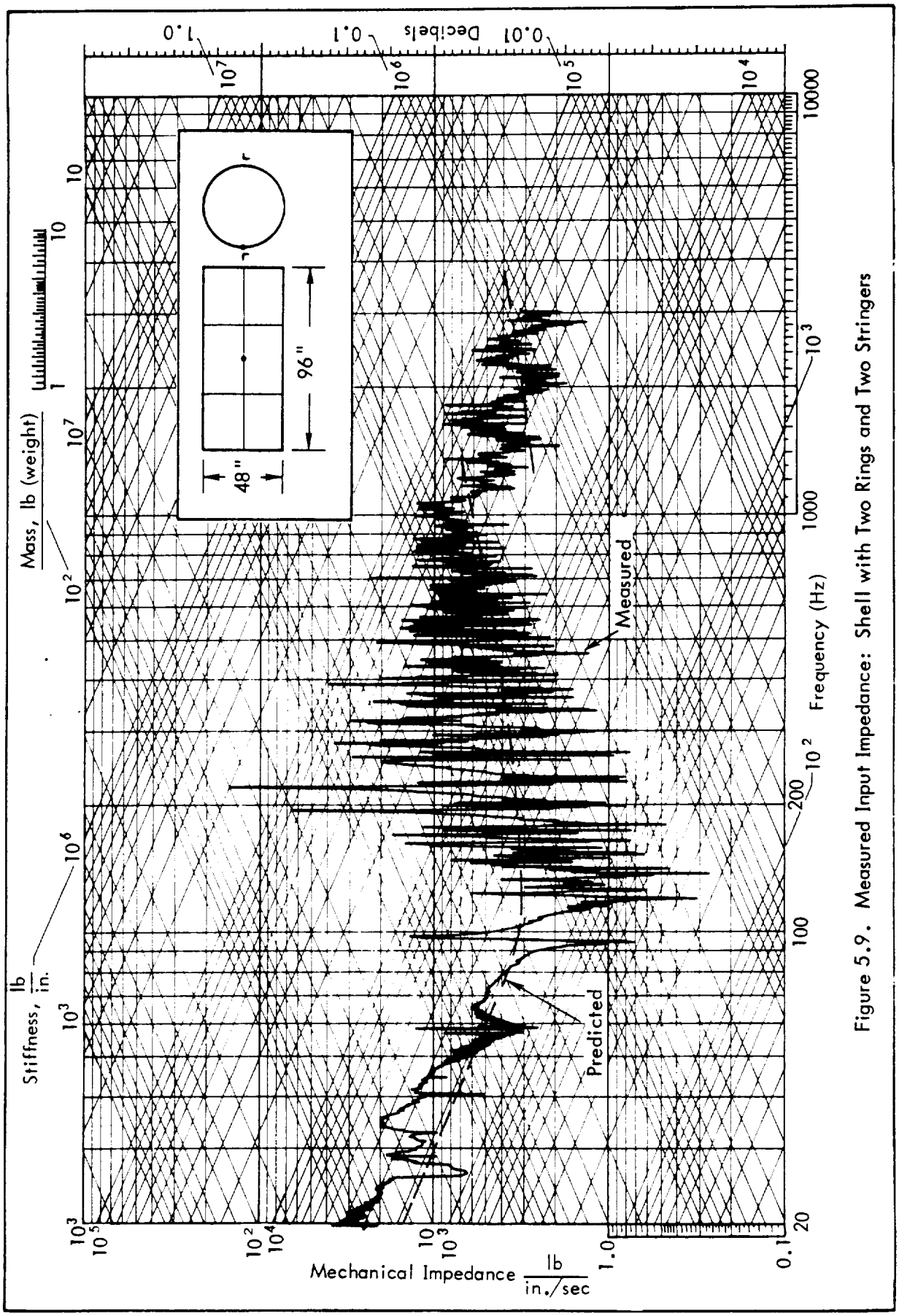

Figure 5.9. Measured Input Impedance: Shell with Two Rings and Two Stringers

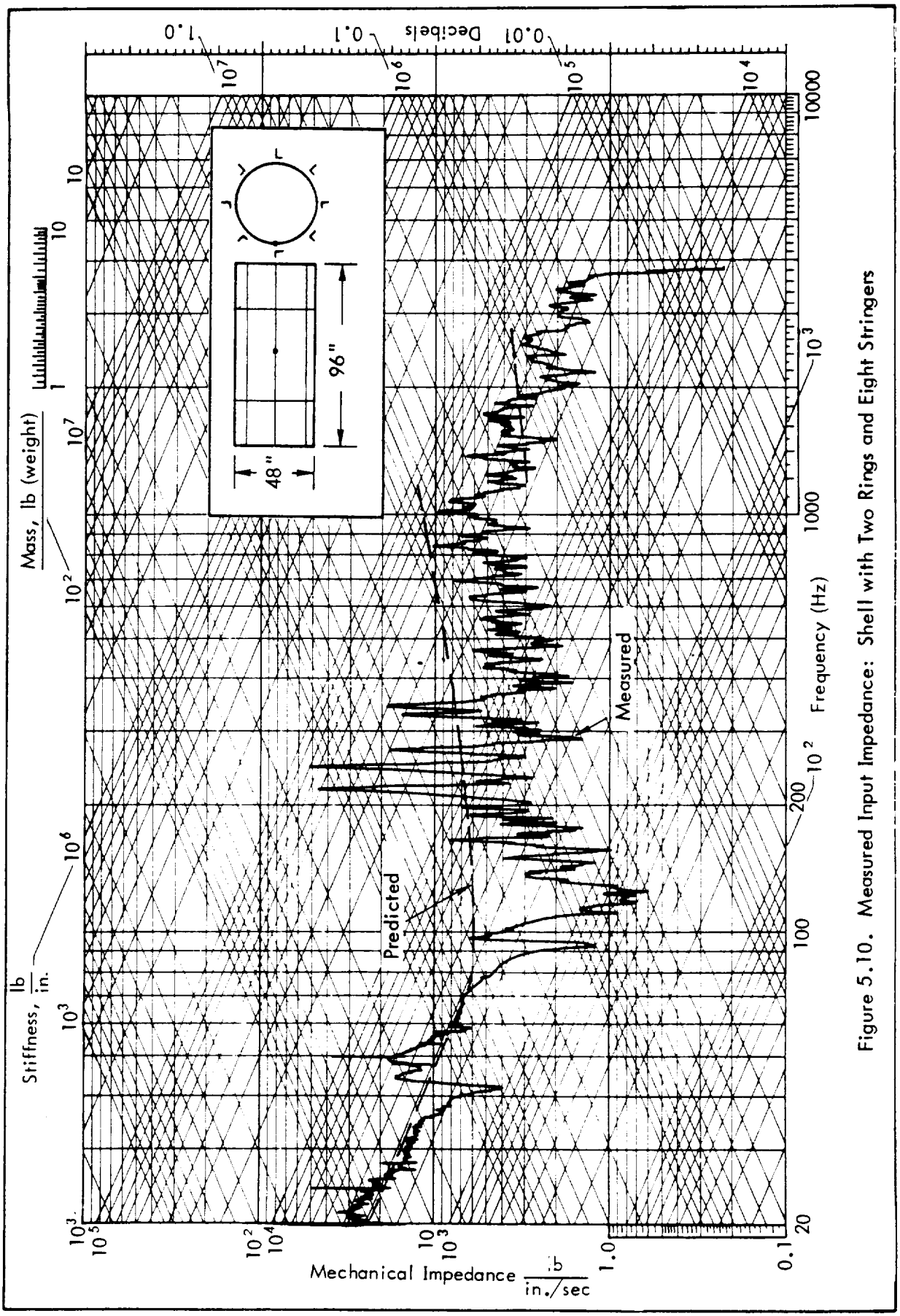

Figure 5.10. Measured Input Impedance: Shell with Two Rings and Eight Stringers

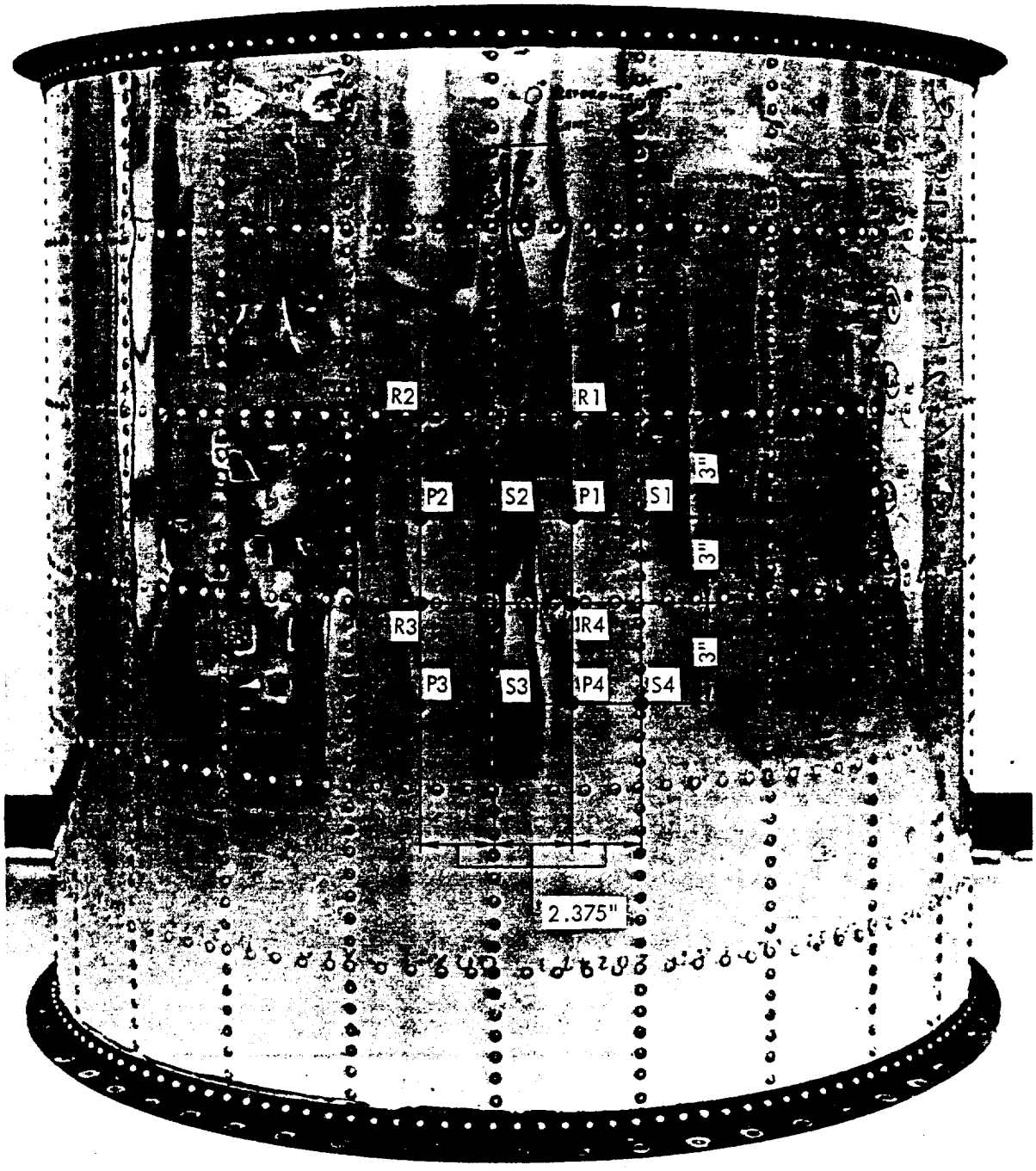

Figure 5.11. Stiffened Cylinder and Input Impedance Measurement Locations

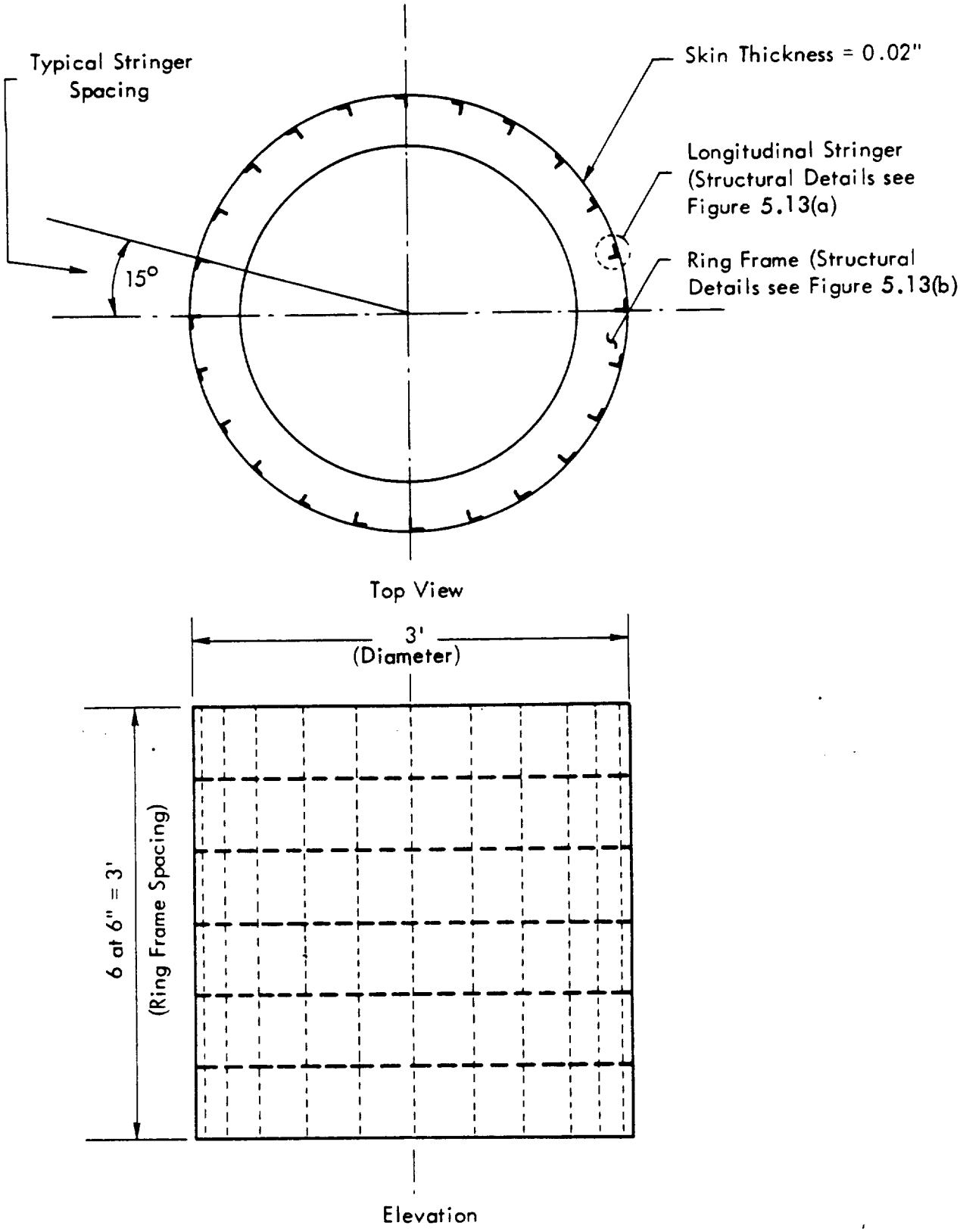

Figure 5.12. Structural Configuration of the Stiffened Aluminum Cylinder (End Rings and Bulkheads not shown)

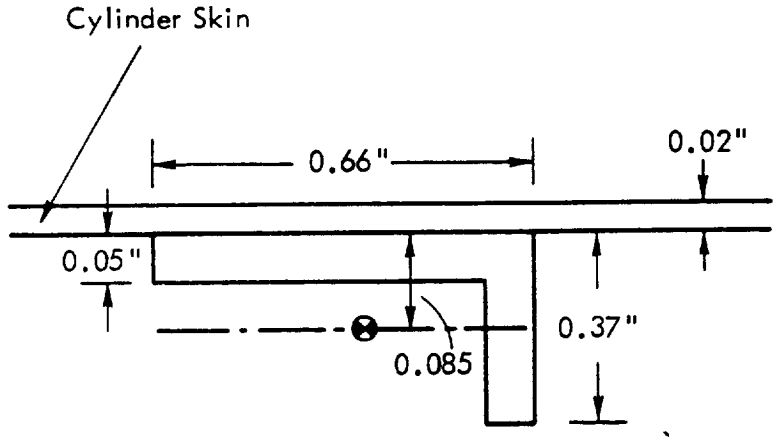

(a) Cross-Section of Longitudinal Stringer

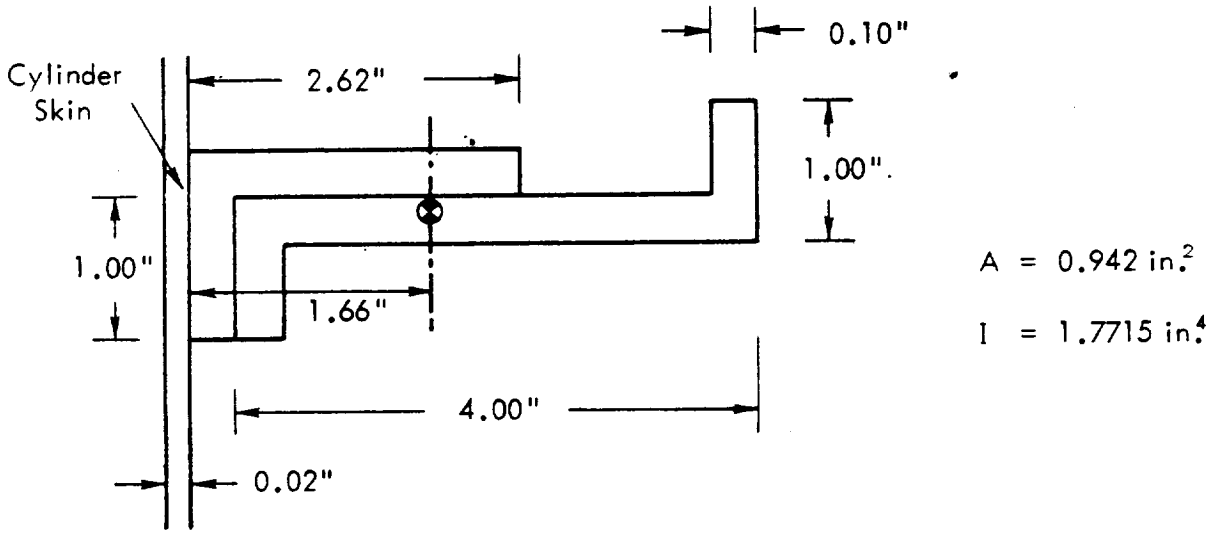

(b) Cross-Section of Circumferential Ring

Figure 5.13. Structural Details of Ring Frames and Stringers

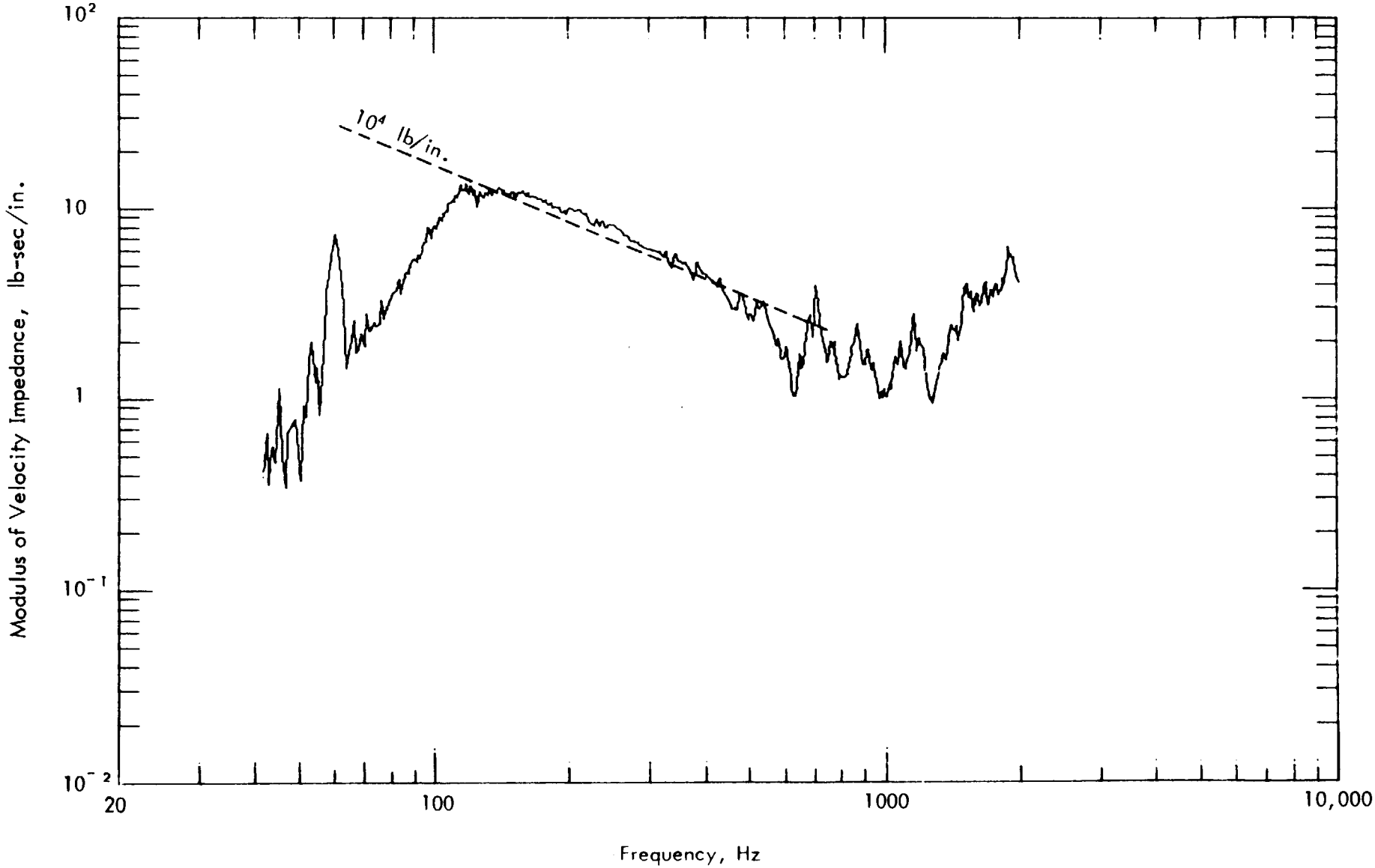

Figure 5.14. Measured Structural Impedance for Stiffened Cylinder

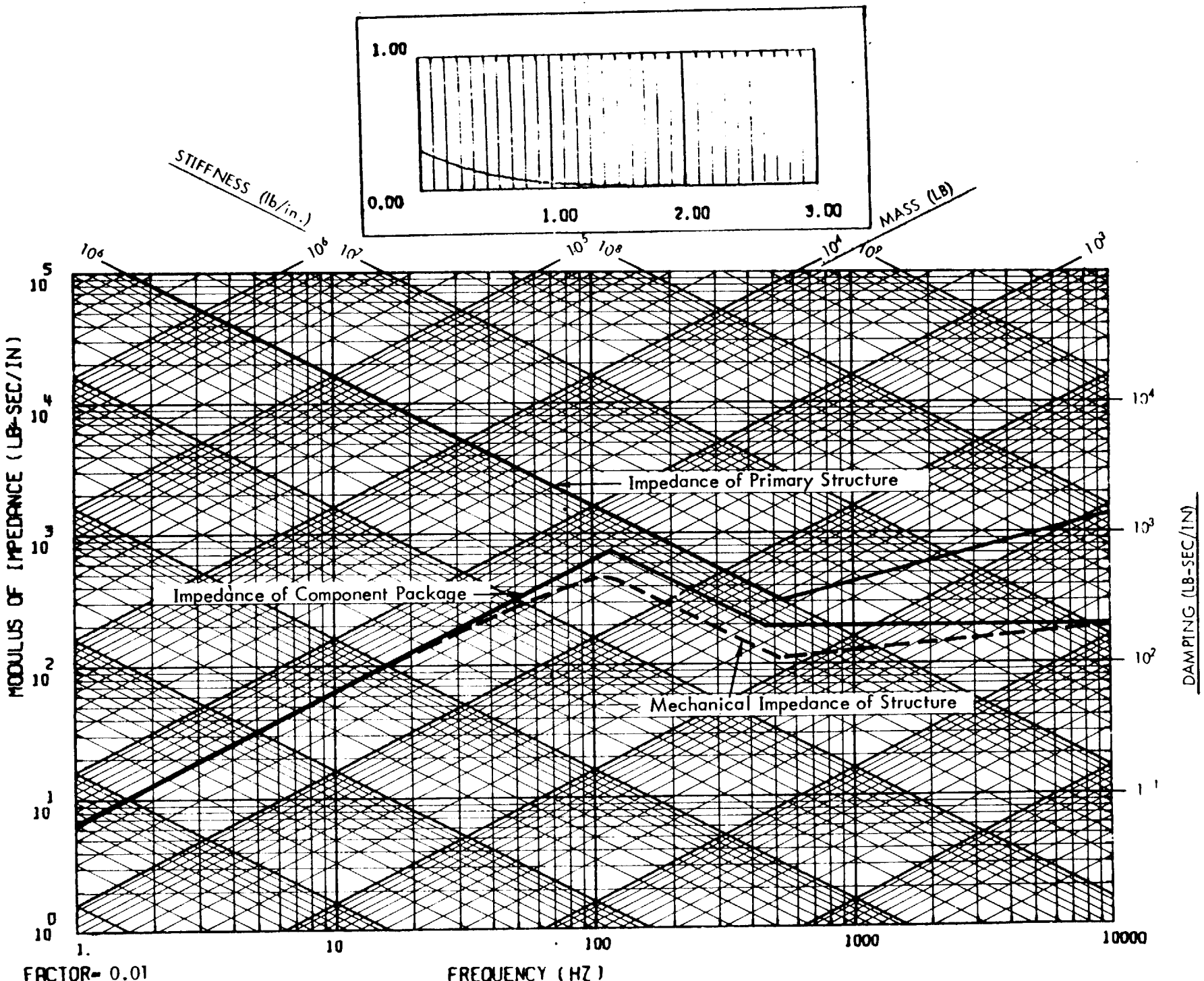

Figure 5.15. Determination of Structural Impedance

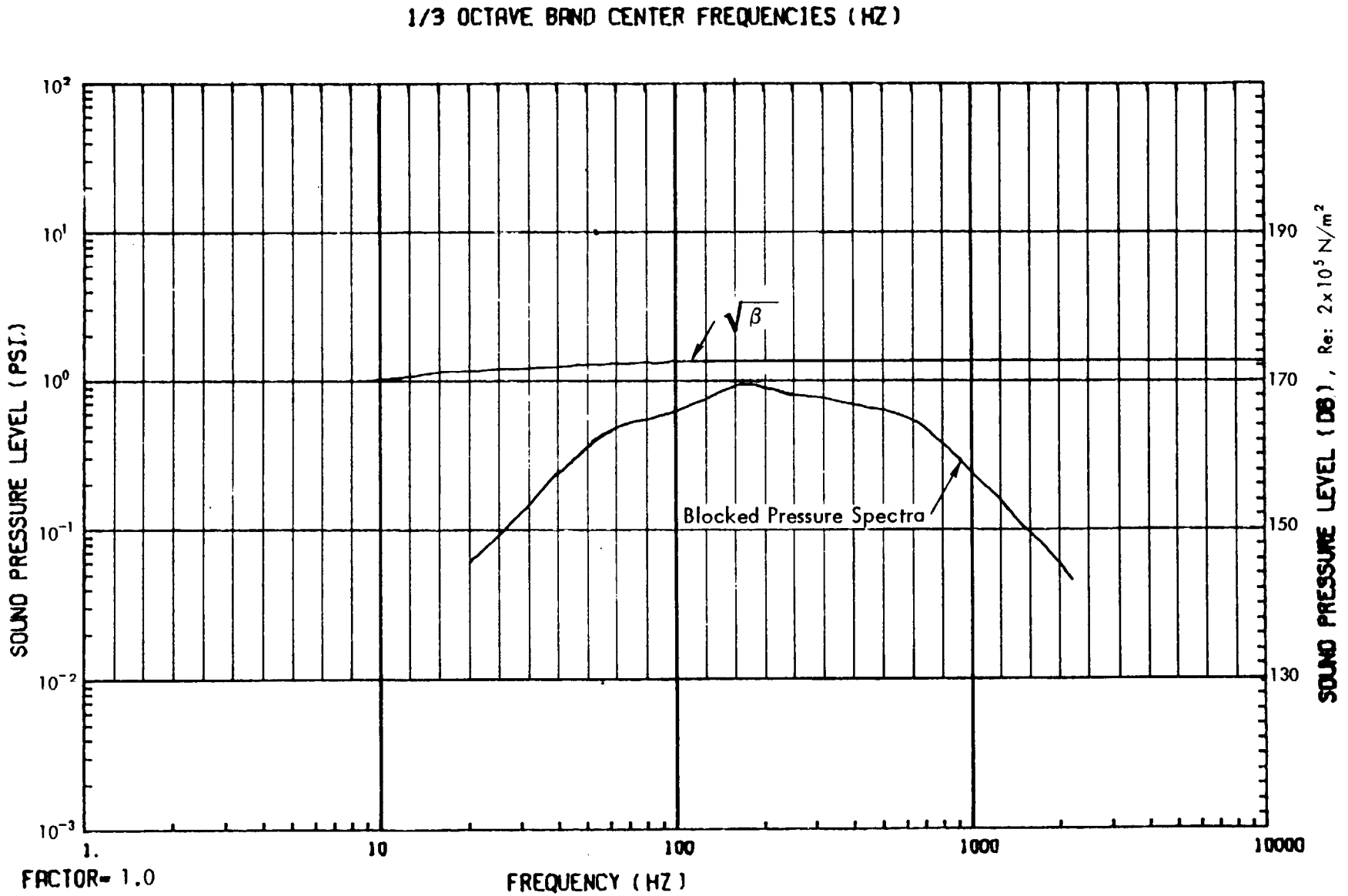

Figure 5.16. Determination of Blocked Pressure Spectra

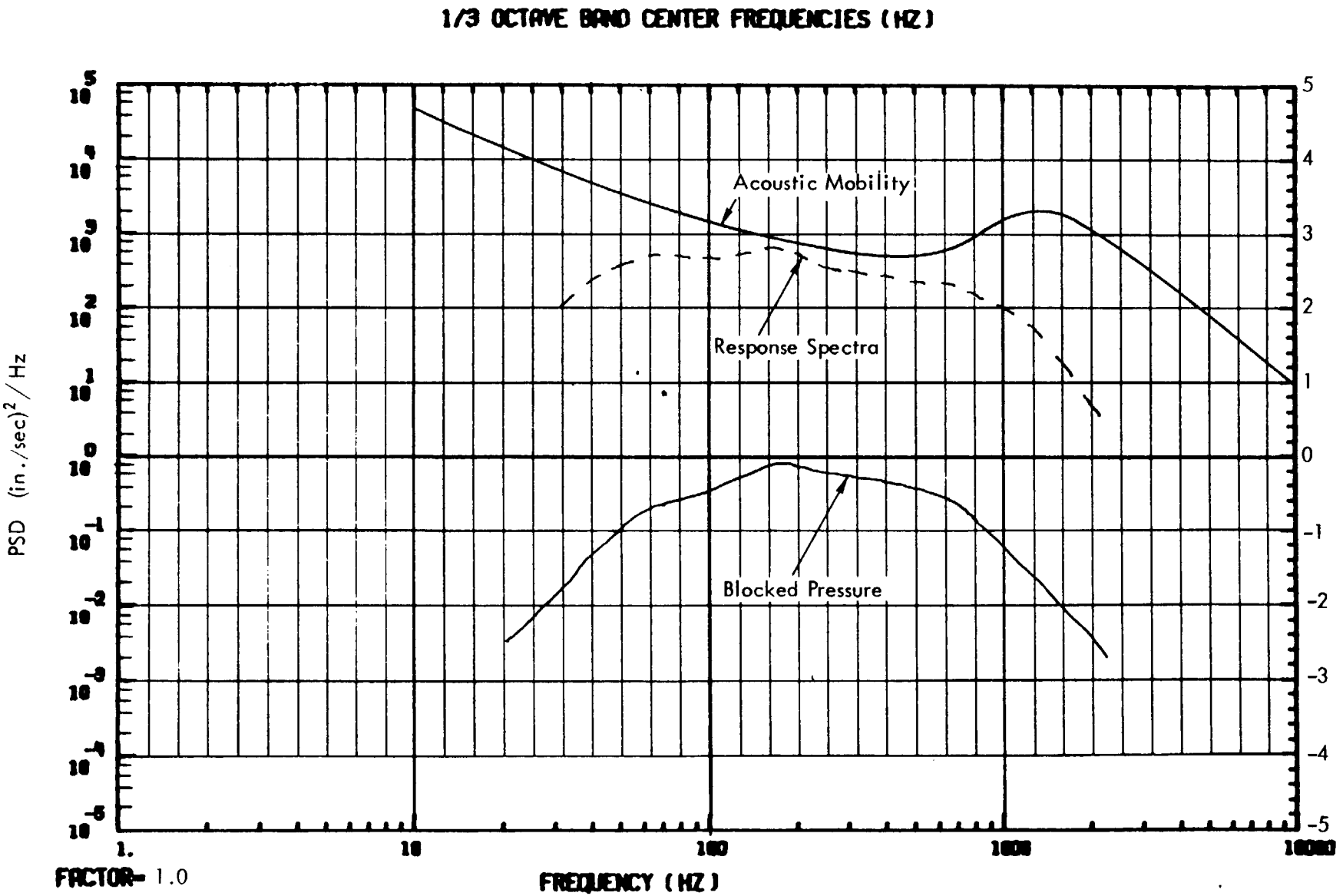

Figure 5.17. Determination of Structural Response Spectra

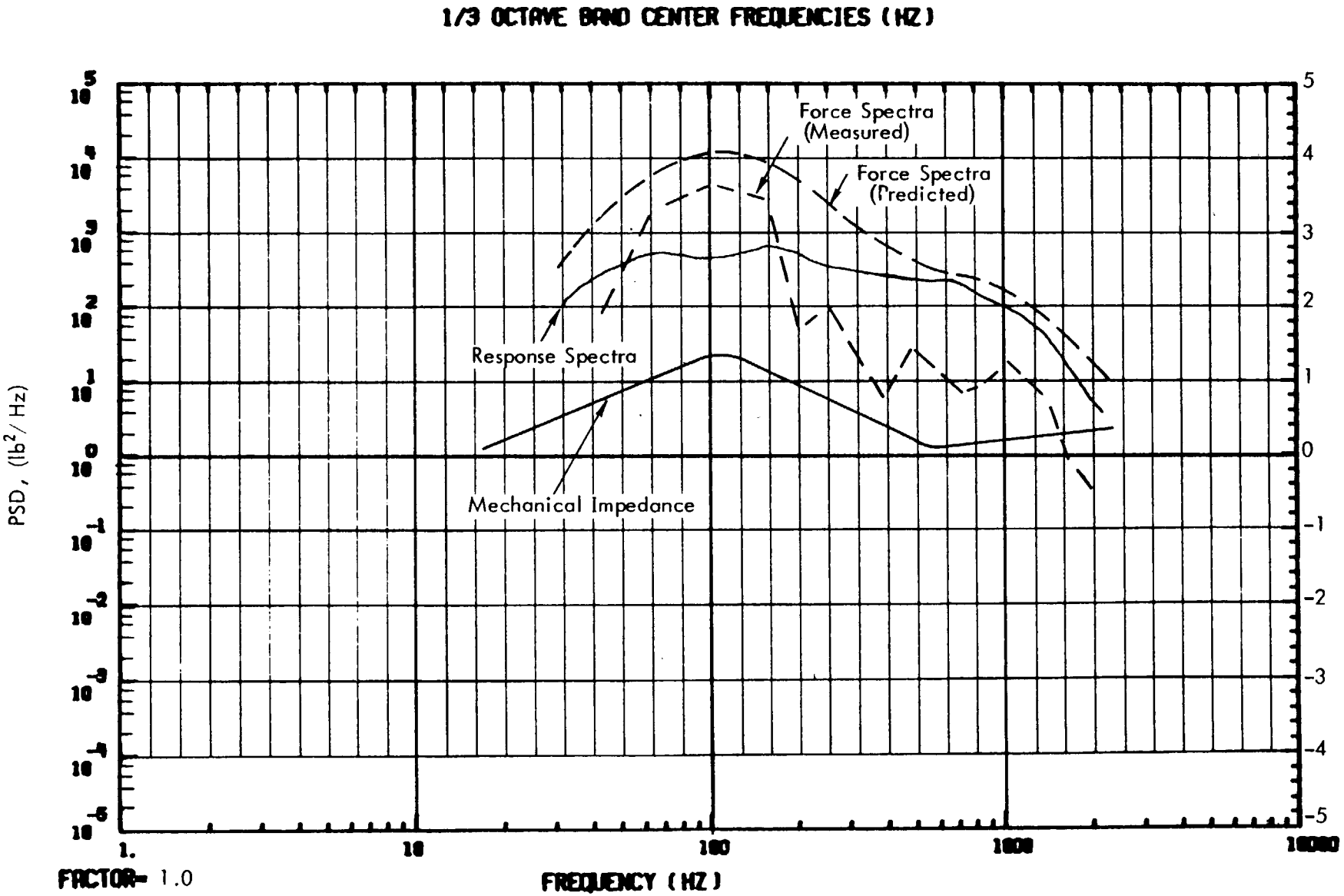

Figure 5.18. Computation and Comparison of Force Spectra

APPENDIX A

DERIVATION OF FORCE-SPECTRUM EQUATION

$$V_L(\omega) = \frac{F_0(\omega)}{Z_L(\omega) + Z_s(\omega)} \tag{2}$$

But the blocked force $F_0(\omega)$ is not a readily measurable quantity, therefore, it is necessary to find an equivalent term which is suitable for measurement.

By definition, the constant source velocity, $V_0(\omega)$, is the velocity at the attachment terminal with no loads attached. Thus, by setting $Z_L(\omega)$ in Equation (2) to zero, the source velocity is determined by the following equation:

$$V_0(\omega) = \frac{F_0(\omega)}{Z_s(\omega)} \tag{3}$$

or

$$F_0(\omega) = V_0(\omega) \cdot Z_s(\omega) \tag{4}$$

Substituting Equation (4) into Equation (1), and rearranging terms, the driving force $F_L(\omega)$ is obtained:

$$F_L(\omega) = V_0(\omega) \cdot \frac{Z_s Z_L}{Z_L + Z_s} \tag{5}$$

Equation (5) shows that the interaction force spectrum is equal to the velocity spectrum of the unloaded structure multiplied by the summation of the impedances of the support structure and the component packages, connected in series. All of the above quantities can be obtained through measurement techniques.

1.2 Structural Responses to Acoustic Excitations

Responses of structures to acoustic excitations, as shown in Figure A-4, can be expressed by the following equations (Reference 2):

$$\Phi_{\dot{x}}(\vec{r},\omega) = \sum_m \sum_m \frac{\Phi_m(\vec{r})\,\Phi_n(\vec{r}) \cdot A^2}{Z_m(\omega)\,Z_n(\omega)^*}\,\Phi_{p_0}(\omega)\,J_{mn}^2(\omega) \qquad (6)$$

where

$\Phi_{\dot{x}}(\vec{r},\omega)$ = Velocity power spectral density at point r

$\Phi_{p_0}(\omega)$ = Power spectral density of reference sound pressure which is assumed to be constant over the surface of component mounting locations

A = Surface area

$Z_m(\omega)$ = Modal impedance

$$= \frac{K_m}{i\omega}\left[1 - \left(\frac{\omega}{\omega_m}\right)^2 + \frac{i}{Q_m}\left(\frac{\omega}{\omega_m}\right)\right]$$

$Z_n(\omega)^*$ = Complex conjugate of $Z_n(\omega)$

$J_{mn}^2(\omega)$ = Joint acceptance function of the mn^{th} mode

$$= \int_s \int_{s'} \frac{\Phi_m(\vec{s})\,\Phi_n(\vec{s'})}{A^2}\,\frac{\Phi_p(\vec{s},\vec{s'},\omega)}{\Phi_{p_0}(\omega)}\,d\vec{s}\;d\vec{s'}$$

$d\vec{s},\ d\vec{s'}$ = Infinitesimal area vectors

$\Phi_p(\vec{s},\vec{s'},\omega)$ = Cross-power spectral density of the sound pressure field

$\Phi_m(\vec{r}),\ \Phi_m(\vec{s})$ = Normal mode at $\vec{r}$ and $\vec{s}$, respectively

K_m = Generalized stiffness

ω_m = m^{th} natural frequency = $\sqrt{K_m / M_m}$

M_m = Generalized mass = $\int_s \rho(\vec{s})\,\Phi_m^2(\vec{s})\,d\vec{s}$

Q_m = Generalized dynamic magnification factor

ρ = Surface mass density

By rearranging terms in Equation (6), the acoustic velocity mobility is obtained:

$$\left| \alpha_{\dot{x}} (\vec{r}, \omega) \right|^2 = \frac{\Phi_{\dot{x}}(\vec{r}, \omega)}{\Phi_{p_0}(\omega)} = \sum_m \sum_n \frac{\phi_m(\vec{r}) \phi_n(\vec{r}) \cdot A^2}{Z_m(\omega) Z_n(\omega)} J_{mn}^2(\omega) \tag{7}$$

In practice, velocity responses of a complex structure subjected to acoustic excitations may be expressed as follows:

$$\Phi_{\dot{x}}(\vec{r}, \omega) = \Phi_p(\vec{r}, \omega) \left| \alpha_{\dot{x}}(\vec{r}, \omega) \right|^2 \tag{8}$$

where $\Phi_p(\vec{r}, \omega)$ is the blocked sound pressure spectrum at $\vec{r}$.

To determine the acoustically induced driving force spectra $\Phi_L(\vec{r}, \omega)$ at attachment points, it is necessary to transform a vibro-acoustic system to an equivalent one-dimensional impedance model, so that Equation (5) can be applied directly to determine $\Phi_L(\vec{r}, \omega)$. Such a transformation is illustrated in Figure A-5 . The equivalent one-dimensional model is represented by a support structural impedance, $Z_s(\vec{r}, \omega)$, the component impedance, $Z_L(\vec{r}, \omega)$, and an equivalent blocked force spectrum, $\Phi_{BF}(\vec{r}, \omega)$. Applying Equations (4), (5) and (8) to the above system, the blocked force spectra equation is obtained:

$$\text{Blocked Force Spectra: } \Phi_{BF}(\vec{r}, \omega) = \Phi_{\dot{x}}(\vec{r}, \omega) \cdot \left| Z_s(\vec{r}, \omega) \right|^2 \tag{9}$$

and the component-structure interaction force spectra is presented as follows:

$$\Phi_L(\vec{r}, \omega) = \Phi_p(\vec{r}, \omega) \cdot \left| \alpha_{\dot{x}}(\vec{r}, \omega) \right|^2 \cdot \left| \frac{Z_s Z_L}{Z_s + Z_L} \right|^2 \tag{10}$$

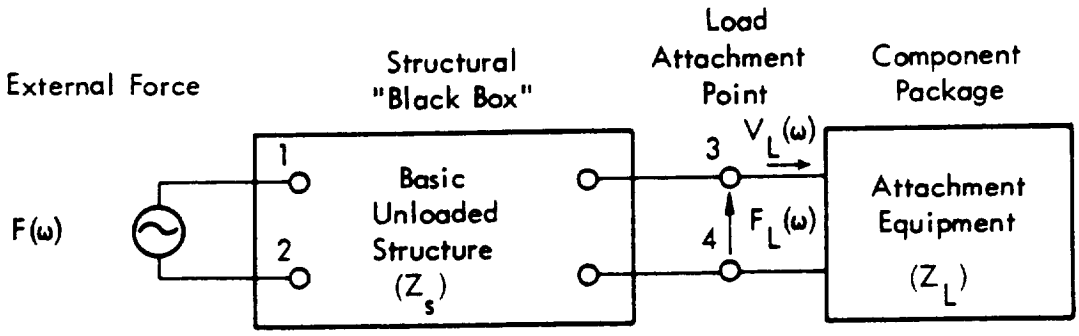

Figure A-1. One-Dimensional Impedance Model of a Structural System

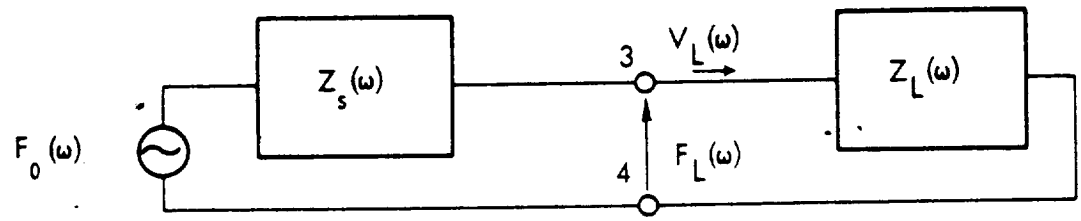

Figure A-2. Equivalent-Constant Force Model

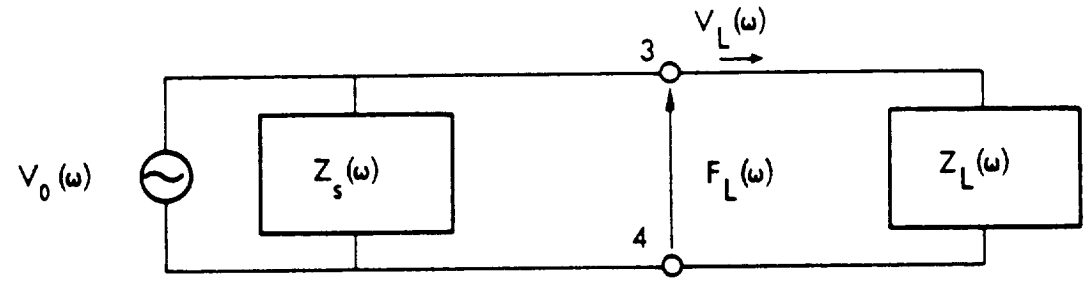

Figure A-3. Equivalent-Constant Velocity Model

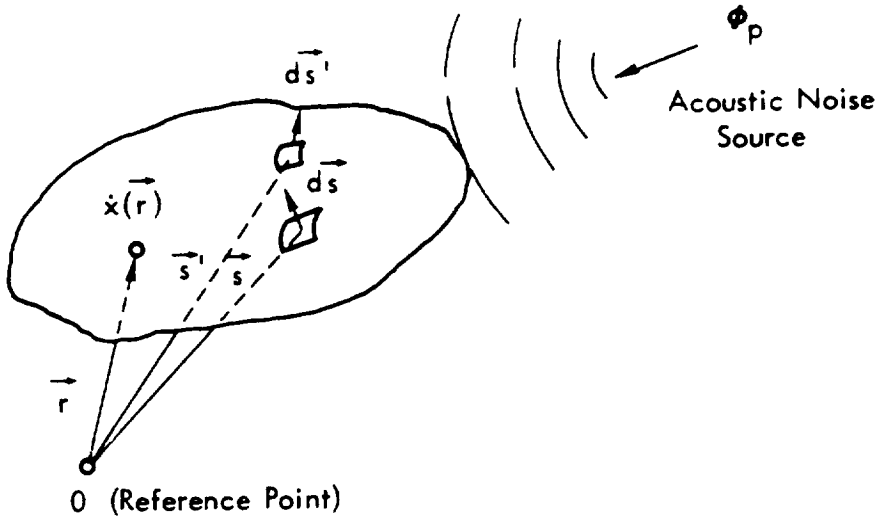

Figure A-4. Structure Response Subject to Acoustic Excitation

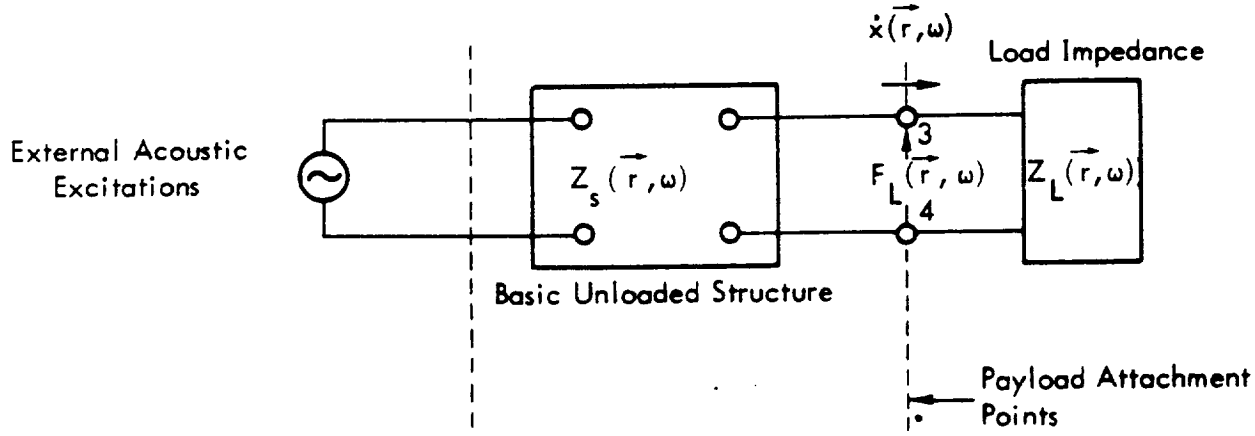

(a) A Typical Structure Subject to the Acoustic Excitations

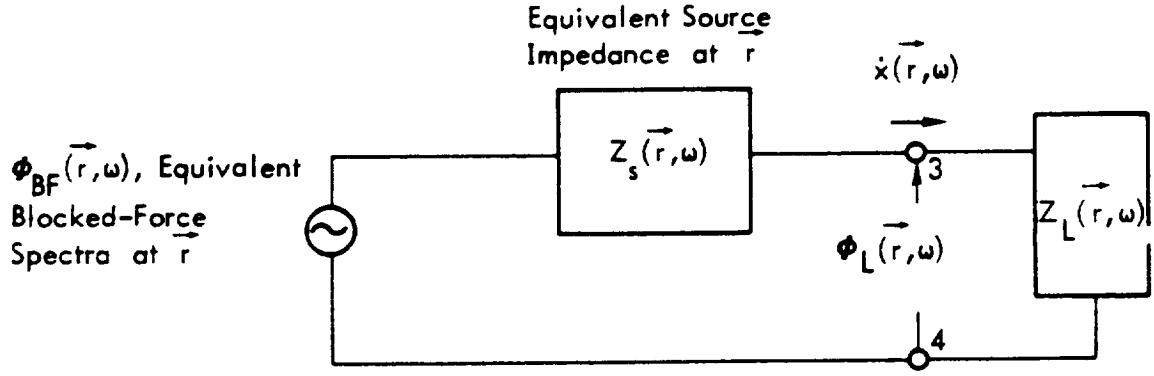

(b) An Equivalent One-Dimensional Impedance Model

Figure A-5. One-Dimensional Model of a Structural System Subject to Acoustic Excitations

REFERENCES

1. Tang, K.Y., Alternating-Current Circuits, International Textbook Company, Scranton, Pennsylvania, 1955.

2. Powell, A., "On the Response of Structures to Random Pressures and to Jet Noise in Particular," Random Vibration, Vol. I, Chapter 8, John Wiley and Sons, Inc., New York, 1958.

APPENDIX B

DERIVATION OF EQUATIONS RELATED TO DYNAMIC CHARACTERISTICS OF STRUCTURES

APPENDIX B

DERIVATION OF EQUATIONS RELATED TO DYNAMIC CHARACTERISTICS OF STRUCTURES

1.0 INTRODUCTION

Brief derivations of equations on input impedances, resonant frequencies and modal densities, as previously presented in Section 3.0, are given in this appendix. The structural elements considered in the derivation consist of the following categories:

- Beam (or stringer)
- Ring frame
- Unstiffened shell
- Stiffened shell

Several computer programs have been written to evaluate input-impedance equations. A complete description of these programs is presented in Appendix D. A listing of published papers relevant to the formulation of impedance equations is presented in the Bibliography.

2.0 EQUATIONS FOR BEAM (OR STRINGER)

The response of a beam which is excited by a point oscillating force of frequency ω acting perpendicular to the beam at point ℓ_0 can be calculated by solving the classical beam equation:

$$\frac{EI}{\rho A}\ \frac{d^4 w}{dx^4} - \omega^2 w = \frac{1}{\rho A}\ F\delta\left(x - \ell_0\right) \tag{1}$$

where:

w = Transverse displacements of the beam

δ = Dirac delta function

E = Young's modulus

I = Sectional modulus

ρ = Mass density

A = Area

Equation (1) is valid provided that the bending wavelength, λ, is much greater than the thickness of the beam, where λ is defined as:

$$\lambda = \frac{2\pi}{k} \tag{2}$$

and

$$k = \left[\frac{\rho A}{EI}\right]^{1/4} \sqrt{\omega} \tag{3}$$

Consider a finite beam of length ℓ. The displacement response of the beam can then be expressed in terms of the mode shapes, $\Phi_m(x)$, and the corresponding resonant frequencies, ω_m, as follows:

$$w_0 = \frac{1}{\rho A} \sum_{m=0}^{\infty} \frac{1}{\omega_m^2 - \omega^2}\ \frac{\Phi_m^2\left(\ell_0\right)}{\int_0^{\ell} \Phi_m^2(x)\, dx} \tag{4}$$

where:

$$i = \sqrt{-1}$$

The resonant frequencies of a simply supported beam can be shown as follows:

$$\omega_m^2 = \frac{EI}{\rho A} \frac{m^4 \pi^4}{\ell^4} \qquad \text{and} \qquad \Phi_m(x) = \sin \frac{m\pi x}{\ell} \tag{5}$$

Therefore, one obtains:

$$w_0 = \frac{2F}{\rho A \ell} \sum_{m=1}^{\infty} \frac{\Phi_m^2(\ell_0)}{\omega_m^2} \frac{1}{\left(1 - \omega^2/\omega_m^2\right)} \tag{6}$$

The series in Equation (6) converges very rapidly and by setting the excitation frequency, ω, equal to zero in the above series, it is possible to obtain the static deflection at the location ℓ_0 in the closed form as expressed by Equation (7) below:

$$K = \frac{F}{w_0} = 48 \frac{EI}{\ell^3} \tag{7}$$

By including the contribution of the damping effect, the input impedance, which is defined as the ratio of the excitating force to the response velocity at the location ℓ_0, can then be written as:

$$\frac{1}{Z} = i\omega \sum_{m=1}^{\infty} \frac{\Phi_m^2(\ell_0)}{\frac{\ell}{2} \rho A \omega_m^2} \frac{1 - \left(\frac{\omega}{\omega_m}\right)^2 + \frac{i}{Q_m}\left(\frac{\omega}{\omega_m}\right)}{\left[1 - \left(\frac{\omega}{\omega_m}\right)^2\right]^2 + \frac{1}{Q_m^2}\left(\frac{\omega}{\omega_m}\right)^2} \tag{8}$$

where Q_m is the dynamic magnification factor for the m^{th} mode.

In Reference 1, the mechanical power transmitted into the beam was investigated. The conclusion shows that the average power is independent of the length of the beam and the end conditions, and can easily be computed if the impedance of the corresponding infinite system is known. The impedance equation of an infinite beam has been obtained by Cremer (Reference 2) as follows:

$$Z_{\infty} = 2(1+i)\ \rho A \left[\frac{EI}{\rho A}\right]^{1/4} \sqrt{\omega} \qquad (9)$$

3.0 EQUATIONS FOR RING FRAME

The governed equation of the radial displacement, w, of a ring with radius, R, cross-section area, A, mass density, ρ, and flexural rigidity, EI, is given by (Reference 3):

$$k^4 \left(\frac{\partial^6 w}{\partial \theta^6} + 2 \frac{\partial^4 w}{\partial \theta^4} + \frac{\partial^2 w}{\partial \theta^2} \right) - \omega^2 \left(\frac{\partial^2 w}{\partial \theta^2} - w \right) = \frac{F}{\rho A} \frac{\partial^2 \delta(\theta)}{\partial \theta^2} \qquad (10)$$

where

$$k = \frac{1}{R} \left[\frac{EI}{\rho A} \right]^{1/4} \qquad (11)$$

In this equation, the ring is excited by a point driving force of frequency ω in the radial direction, and θ is the angle around the ring. Equation (10) is valid only when the thickness of the ring is much smaller than the radius a, and when $\omega < C_L/R$, where C_L is the longitudinal velocity in the ring material.

A rather straightforward method of solving Equation (10) under given sinusoidal input conditions is to expand the displacement in terms of the eigenfunctions, $\cos n\theta$. By applying this technique, the input impedance of the ring may be obtained:

$$\frac{1}{Z} = \frac{i\omega w}{F} = \sum_{n=1}^{\infty} \left(\pi R \, Z_n \right)^{-1} \qquad (12)$$

and the so-called "modal impedance" may be written as follows:

$$Z_n = i\omega\rho A \left(\frac{1+n^2}{n^2} \right) \left(1 - \frac{\omega_n^2}{\omega^2} \right) \qquad (13)$$

where

$$\omega_n^2 = k^4 \frac{n^2 (n^2-1)^2}{n^2+1} \quad , \quad n \geq 1$$

= angular resonant frequency of the n mode of ring

The above expression for the input impedance can be summarized analytically as follows:

$$Z^{-1} = \frac{\alpha}{4 i \rho A R \omega} \left[1 + \cot (\pi \alpha) \right] \qquad (14)$$

where:

$$\alpha = \sqrt{\omega} \Big/ k$$

Figure B-1 shows the modulus and phase angular of the input impedance obtained from the analytical prediction based on the above equation. Figure B-2 shows the measured impedance from the experimental testing results. Satisfactory agreement between these two plots can be observed.

4.0 EQUATIONS FOR UNSTIFFENED CYLINDRICAL SHELL

The partial differential equations governing the motion of a thin cylindrical shell of radius, R, and thickness, h, in the axial, circumferential and radial directions are given by:

$$L_1(u, v, w) = \rho h \frac{R^2}{D} \left(u_{\tau\tau} - P_1 \right)$$

$$L_2(u, v, w) = \rho h \frac{R^2}{D} \left(v_{\tau\tau} - P_2 \right) \qquad (15)$$

$$L_3(u, v, w) = \rho h \frac{R^2}{D} \left(w_{\tau\tau} + P_3 \right)$$

where the L_1, L_2 and L_3 are the space differential operators as derived in Reference 4. Subscript τ denotes differentiation with respect to dimensionless time parameter τ defended by:

$$\tau = \omega t \qquad (16)$$

where ω is the circular frequency of the steady forcing function. The quantity ρ is the mass density of shell material and:

$$D = Eh^3/12(1-\nu^2) \qquad (17)$$

is the flexural rigidity in which E and ν are the Young's modulus and Poisson's ratio of shell, respectively. Axial, circumferential and radial displacements are designated by u, v and w, respectively, and are expanded in Fourier series as:

$$u = \sum_{n=0}^{\infty} \sum_{m=0}^{\infty} U_{mn} \cos \frac{m\pi x}{\ell} \cos n\theta$$

$$v = \sum_{n=1}^{\infty} \sum_{m=1}^{\infty} V_{mn} \sin \frac{m\pi x}{\ell} \sin n\theta \qquad (18)$$

$$w = \sum_{n=0}^{\infty}\sum_{m=1}^{\infty} W_{mn} \sin \frac{m\pi x}{\ell} \cos n\theta$$

Substituting the above expression into these equations of motion, after some manipulation, and utilizing the orthogonality relations of the sine and cosine function, a set of simultaneous equation for the Fourier modal amplitude factors U_{mn}, V_{mn} and W_{mn} can be reduced. The eigenvalues of these homogeneous matrix equations, which satisfy the boundary conditions of a simply supported, circular cylindrical shell, are the angular frequency parameters which correspond to the (m,n) mode of the shell. The resonance frequencies of a simply supported finite cylinder of length are found to be as follows (Reference 5):

$$\Omega_{mn}^2 = (1-\nu^2)k^4 \Big/ (k^2+n^2)^2 + \beta^2 \left\{ (k^2+n^2)^2 - \frac{1}{2}\left[n^2(4-\nu) - 2 - \nu \right] \Big/ (1-\nu) \right\} \qquad (19)$$

where:

$$\Omega_{mn} = \frac{\omega_{mn} R}{C_L} \qquad (20)$$

and $$C_L = \sqrt{\frac{E}{\rho(1-\nu^2)}}$$

C_L = longitudinal speed of sound in shell material

ω_{mn} = angular resonant frequency of the (m,n) mode

$k = m\pi R/\ell$

$\beta = h \Big/ 2\sqrt{3}\, R$

In the above expressions the end conditions were derived from simply supported cylinders. However, the equations can be applied to cylinders with other boundary conditions. This is so because the resonance frequencies of a cylinder with any nondissipative boundary conditions are identical to the resonant frequencies of a supported cylinder whose length is equal to the distance between the modal lines that are closest to the ends.

Consider now that a radial point force, which is harmonic at frequency ω with an amplitude F act on the shell at point $(x_0, 0)$. This exciting force can be expanded as:

$$F\delta(x-x_0)\,\delta(\theta-0) = \frac{2F}{\pi a \ell} \sum_{n=0}^{\infty} \sum_{m=1}^{\infty} F_{mn} \sin \frac{m\pi x_0}{\ell} \sin \frac{m\pi x}{\ell} \cos n\theta \qquad (21)$$

By utilizing the nonhomogeneous matrix equations, the amplitude of radial displacement of the shell at location of point force can be represented by the summation of the following classical modal expansion:

$$w = \sum_{n=0}^{\infty} \sum_{m=1}^{\infty} \Phi_{mn}(x_0) \frac{F_{mn}}{K_{mn}} Y_{mn}(\omega) \qquad (22)$$

where:

$\Phi_{mn}(x_0) = \sin \frac{m\pi x_0}{\ell}$

= radial mode shape of shell at location of point force

$F_{mn} = F\,\Phi_{mn}(x_0)$

= generalized force for the (m,n) mode

$K_{mn} = M_{mn}\,\omega_{mn}^2$

= generalized stiffness of the (m,n) mode

$M_{mn} = \zeta_{mn} M_0$

= generalized mass of the (m,n) mode

$M_0 = 2\pi R \ell h \rho$

= total mass of shell

$$\zeta_{mn} \simeq 0.5 \qquad \text{for } n = 0$$

$$\simeq 0.25 \left(1 + \frac{1}{n^2} \right) \qquad \text{for } n \geq 1 \tag{23}$$

$$Y_{mn}(\omega) = H_{mn}(\omega) \cdot e^{-iQ_{mn}(\omega)}$$

$$= \text{dynamic magnification factor for the } (m,n) \text{ mode vibrating at frequency } \omega \tag{24}$$

and

$$H_{mn}(\omega) = \left\{ \left[1 - \left(\frac{\omega}{\omega_{mn}} \right)^2 \right]^2 + \frac{1}{Q_{mn}^2} \left(\frac{\omega}{\omega_{mn}} \right)^2 \right\}^{1/2} \tag{25}$$

$$\theta_{mn}(\omega) = \tan^{-1} \left[\frac{1}{Q_{mn}} \left(\frac{\omega}{\omega_{mn}} \right) \Big/ \left[1 - \left(\frac{\omega}{\omega_{mn}} \right)^2 \right] \right] \tag{26}$$

$$Q_{mn} = \text{dynamic magnification factor for the } (m,n) \text{ mode}$$

By setting the excitation frequency, ω, equal to zero in the above series, it is possible to determine the static deflection of the shell to the statically applied point force as follows:

$$w(0) = \sum_{m=0}^{\infty} \sum_{m=1}^{\infty} \frac{\Phi_m^2 (x_0) F}{M_0 \zeta_{mn} \omega_{mn}^2} \tag{27}$$

It appears that we have here a fairly general solution for the problem of thin shell vibrations, at least for a certain useful set of boundary conditions. From a mathematical point of view, this is certainly true, but for practical applications it is not sufficient that a series like that will converge eventually. It is required that the series must converge so well that it may be obtained within a certain accuracy from a rather limited number of terms.

The above series may be slowly convergent for the following two cases: 1) resonant frequencies, ω_{mn}, increase slowly with the increase of m and n; and 2) spatial distributions of loading for which $\left| \phi_{mn}^2(x_0) \Big/ \zeta_{mn} \right|$ does not exhibit a rapid decrease with n — e.g., localized and point-type forces. Slow convergence in the above series for w(0), leads, of course, to slow convergence in the series for w as given in Equation (22). For such cases, a more rapidly converging modal series is needed to represent the solution and has been considered by several investigators. One method which could be applied in the present problem is the so-called modified (or Willian's) modal representation (Reference 6). In this method, the elastic response of shells is decomposed into two parts: an instantaneous static response under the applied force, and a dynamic portion consisting of a modal expansion which converges faster than would a purely modal representative of the response.

An application of this to the case of input impedance is as follows:

$$\frac{1}{Z} = \frac{\dot{w}}{F} = \frac{i\omega w}{F}$$

$$= i\omega \left[\frac{w}{F} - \frac{w(0)}{F} + \frac{w(0)}{F} \right]$$

$$= \frac{i\omega}{M_0} \left[\sum_{n=0}^{\infty} \sum_{m=1}^{\infty} \frac{\phi_m^2(x_0)}{\zeta_{mn}\,\omega_{mn}^2} \left(Y_{mn} - 1 \right) + \frac{M_0}{K} \right] \quad . \quad (28)$$

where: $K = F/w(0)$ is the static input stiffness of a cylindrical shell.

In the above expression, the term inside the bracket is:

$$I_{mn}(\omega) = Y_{mn}(\omega) - 1$$

$$= \frac{\left(\frac{\omega}{\omega_{mn}}\right)^2 \left[1 - \left(\frac{\omega}{\omega_{mn}}\right)^2 - \frac{1}{Q_{mn}^2} \right] - \frac{i}{Q_{mn}} \left(\frac{\omega}{\omega_{mn}}\right)}{\left[1 - \left(\frac{\omega}{\omega_{mn}}\right)^2 \right]^2 + \frac{1}{Q_{mn}^2} \left(\frac{\omega}{\omega_{mn}}\right)^2} \quad (29)$$

For $\omega_{mn} > \omega$, $I_{mn}(\omega) \longrightarrow 0$, while $Y_{mn}(\omega) \longrightarrow 1$. Thus the modified modal series, given in Equation (28), exhibits much faster convergence than the classic modal series.

For the cases of interest, the modal series representation for $w(0)$, given in Equation (27), is slowly convergent but it only requires one computation, which is independent of ω. Also, one can derive an alternate expression in a closed form by a process of direct integration for the static response stiffness for many structures which require considerably less computation.

A comparison of the above two methods for evaluating the driving point impedance of thin cylindrical shells was made and the results are summarized in Table B-1. Calculations were performed based on a thin aluminum cylinder with the following materials constants and thickness parameter.

$$\begin{aligned} h &= 0.08 \text{ in.} \\ R &= 24 \text{ in.} \\ \ell &= 96 \text{ in.} \\ E &= 1 \times 10^7 \text{ lb/in.}^2 \\ \rho &= 0.1 \text{ lb/in.}^3 \\ \nu &= 0.36 \end{aligned} \tag{30}$$

The results clearly demonstrate much faster convergence of the modified modal method.

Equation (28) was numerically evaluated for $x_0 = \ell/2$ and $Q_{mn} = 15$ for the same cylinder. The frequency range considered in this computation was between 1.0 Hz and 10,000 Hz. The computation was made for 25 frequency points for each frequency decade. The analytical prediction of the shell impedance, including amplitude and phase, is shown in Figure B-3. Also, the comparison is made on the amplitudes between the measured data (Figure B-3) and the analytical (Figure B-4) for a thin cylindrical shell with the same dimensions. These two plots show an excellent agreement between the average of the experimental data and the analytical predictions.

5.0 EQUATIONS FOR STIFFENED CYLINDRICAL SHELL

Consider a uniform, thin, cylindrical shell which has a single ring frame around the circumference. The purpose of this analysis is to derive an expression for the radial input impedance at the ring frame. The following assumptions are used in the formulation:

- The shell and ring frame have no material damping
- The neutral axes of the shell and ring frame are coincident

As derived in Section 3.0 of this appendix, the input impedance of rings can be written as:

$$\frac{1}{Z_r} = \sum_{n=1}^{\infty} \left(Z_{rn} \right)^{-1} \tag{31}$$

in which the modal impedance is:

$$Z_{rn} = i\omega\pi R\rho A \left(\frac{1+n^2}{n^2} \right) \left(1 - \frac{\omega_n^2}{\omega^2} \right) \tag{32}$$

Similarly, the input impedance of unstiffened shells is:

$$\frac{1}{Z_s} = \sum_{n=0}^{\infty} \left(Z_{sn} \right)^{-1} \tag{33}$$

$$Z_{sn} = 2\pi R\rho h\ell \Big/ i\omega \sum_{m=1}^{\infty} \frac{Y_{mn}}{\zeta_{mn}\omega_{mn}^2}$$

The n^{th} mode of the shell is dynamically coupled with the n^{th} mode of the ring frame since the shell and ring frame have the same mode shape, $\Phi_n(\theta) = \cos n\theta$. Because of the orthogonality of the set of mode shapes, $\Phi_n(\theta)$, the n^{th} mode of the system is dynamically uncoupled from all other circumferential modes. Thus, to determine the dynamic response of the system to any external loading, it is sufficient to determine the response of any n^{th} mode of the system, and then sum these modal response overall of the n^{th} modes. These harmonic responses of the structure can be readily obtained by expanding in the following series:

$$w(\theta) = \sum_{n=0}^{\infty} \overline{W}_n \, \phi_n(\theta) \tag{34}$$

where $\overline{W}_n$ = maximum amplitude of the n^{th} mode. The input-point impedance, Z, of the structural system is:

$$Z = \frac{F}{\dot{w}(0)} = \frac{F}{i\omega w(0)} = \frac{F}{i\omega} \left[\sum_{n=0}^{\infty} \overline{W}_n \right]^{-1} \tag{35}$$

The modal driving point impedance is defined as:

$$Z_n = \frac{F}{i\omega \overline{W}_n} = \frac{F_r}{i\omega \overline{W}_n} + \frac{F_s}{i\omega \overline{W}_n} \tag{36}$$

where:

F_r = force component applied to the ring frame

F_s = force component on the shell

Since the displacement, $\overline{W}_n$, is the same for both the shell and ring frames, it follows that:

$$Z_n = \frac{F_r}{i\omega \overline{W}_{rn}} + \frac{F_s}{i\omega \overline{W}_{sn}} = Z_{rn} + Z_{sn} \tag{37}$$

Thus, the point-input impedance of the coupled shell and ring frame is given by the expression:

$$Z = \sum_{n=0}^{\infty} \left[Z_{rn} + Z_{sn} \right]^{-1} \tag{38}$$

Similar derivation can be applied to the case of a uniform cylindrical shell which is stiffened by a stringer along the longitudinal direction. The result is given by:

$$Z = \sum_{m=1}^{\infty} \left[Z_{Bm} + Z_{sm} \right]^{-1} \tag{39}$$

In this equation, the modal impedances have been obtained in Sections 2.0 and 4.0 of this appendix, and are written as follows:

$$Z_{Bm} = \frac{1}{i\omega} \frac{\ell}{2} \rho A \omega_m^2 \left(1 - \frac{\omega^2}{\omega_m^2} \right) \tag{40}$$

$$Z_{sm} = 2\pi R \rho h \ell \Big/ i\omega \sum_{n=0}^{\infty} \frac{Y_{mn}}{\zeta_{mn} \omega_{mn}^2} \tag{41}$$

REFERENCES

1. Heckl, M.A., "Compendium of Impedance Formulas," BBN Report No. 774, May 1961.

2. Cremer, L., "The Propagation of Structure-Born Sound," Dept. of Science and Industry Research, Report No. 1, Series B.

3. Love, A.E.H., A Treatise on the Mathematical Theory of Elasticity, Dover, New York, p. 452.

4. Flugge, W., Stresses in Shells, Springer-Verlag, Inc., New York, p. 219, Equation (13), 1967.

5. Heckl, M.A., "Vibration of Point-Driving Cylindrical Shells," JASA, Vol. 34, No. 10, October 1962.

6. Sheng, James, "The Response of a Thin Cylindrical Shell to Transient Surface Loading," AIAA Journal, Vol. 3, No. 4, pp. 701-709, April 1965.

APPENDIX B — BIBLIOGRAPHY

1. Jones, R.C., "The Driving-Point Impedance of an Infinite Solid Plate," JASA, Vol. 17, No. 4, pp. 334-336, April 1946.

2. Thomas, D. A., "Mechanical Impedances of Thin Plates," JASA, Vol. 32, No. 10, pp. 1302-1304, October 1960.

3. Heckl, M.A., "Compendium of Impedance Formulas," BBN Report, No. 774, May 1961.

4. Love, A.E.H., A Treatise on the Mathematical Theory of Elasticity, Dover Publications, New York, p. 452.

5. Cremer, L., "The Propagation of Structure-Born Sound," Dept. of Science and Industry Research, Report No. 1, Series B, 1948.

6. Franken, P.A., "Input Impedance of Simple Cylindrical Structures," JASA, Vol. 32, No. 4, pp. 473-477, April 1960.

7. Smith, P.W., Jr., "Phase Velocities and Displacement Characteristics of Free Waves in a Thin Cylindrical Shell," JASA, Vol. 27, No. 6, pp. 1065-1072, November 1955.

8. Smith, P.W., Jr., "Minimum Axial Phase Velocity in Shells," JASA, Vol. 30, No. 2, pp. 140-141, February 1958.

9. Heckl, M.A., "Vibrations of Point-Driven Cylindrical Shells," JASA, Vol. 34, No. 10, pp. 1553-1557, October 1962.

10. Feit, D., "High-Frequency Response of a Point-Excited Cylindrical Shell," JASA, Vol. 49, No. 5 (Part 2), pp. 1499-1504, 1971.

11. Sheng, James, "The Response of a Thin Cylindrical Shell to Transient Surface Loading," AIAA Journal, Vol. 3, No. 4, pp. 701-709, April 1965.

12. Bushnell, D., "Dynamic Response of Two-Layered Cylindrical Shells to Time-Dependent Loads," AIAA Journal, Vol. 3, No. 2, pp. 1698-1703, 1965.

13. Smith, R.D., "Modified, More Rapidly Converging Modal Series Representation for Mechanical Admittance," JASA, Vol. 44, No. 1, pp. 99-103, 1968.

14. Palladina, J.L., Neubert, V.H., "Mobility of a Long Cylindrical Shell," JASA, Vol. 42, No. 2, pp. 403-411, 1967.

15. Lu, Y.P., Douglas, B.E. and Thomas, V.E., "Mechanical Impedance of Damped Three-Layered Sandwich Rings," AIAA Journal, Vol. 11, No. 3, Sp. 333-334, 1973.

16. Flügge, W., Stresses in Shells, Springer-Verlag, Inc., New York, p. 219, Equation (13), 1967.

17. Snowdon, J.C., Vibration and Shock in Damped Mechanical Systems, John Wiley and Sons, Inc., New York, 1968.

18. Skudrzyk, E., Simple and Complex Vibratory Systems, Pennsylvania State University Press, 1968.

TABLE B-1. COMPARISON OF CLASSICAL AND MODIFIED MODAL METHODS FOR MECHANICAL IMPEDANCE EVALUATION

Frequency (Hz)	Classical Modal Method (Terms)		Modified (William's) Modal Method (Terms)	
	M	N	M	N
1	151	51	77	24
10	151	51	77	20
100	139	45	73	16
1000	213	84	71	35
10000	339	168	119	56
Total Computer Time for 5 Frequency Points (XDS Sigma 5)	1.080 Minutes		0.167 Minutes	

NOTE: M and N are the maximum values of m and n required to have the sum of all $m = 1, 2, \ldots, M$ and all $n = 1, 2, \ldots, N$ terms be greater than 1000 times the next term in the series.

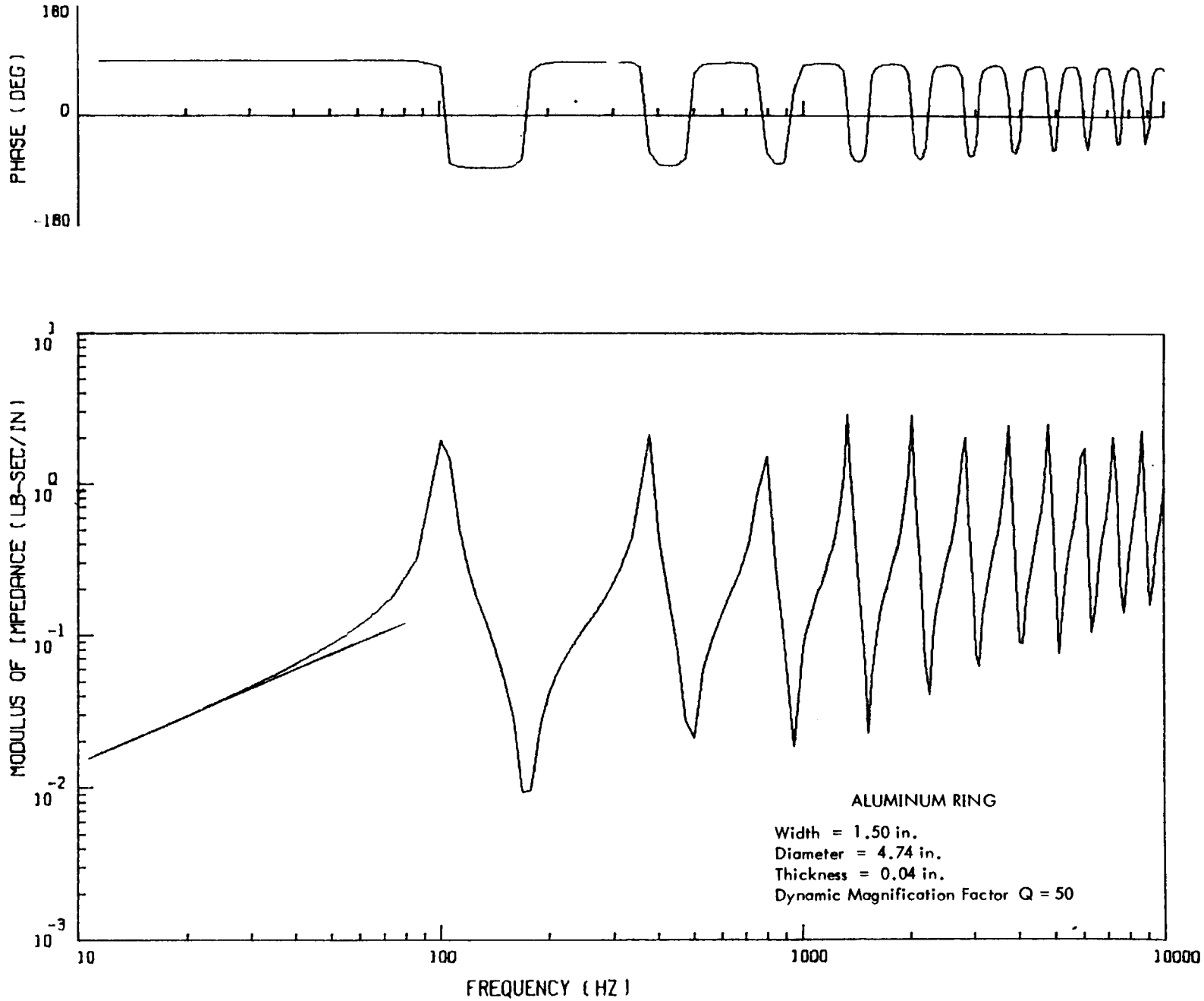

Figure B-1. Theoretical Input Impedance of a Ring

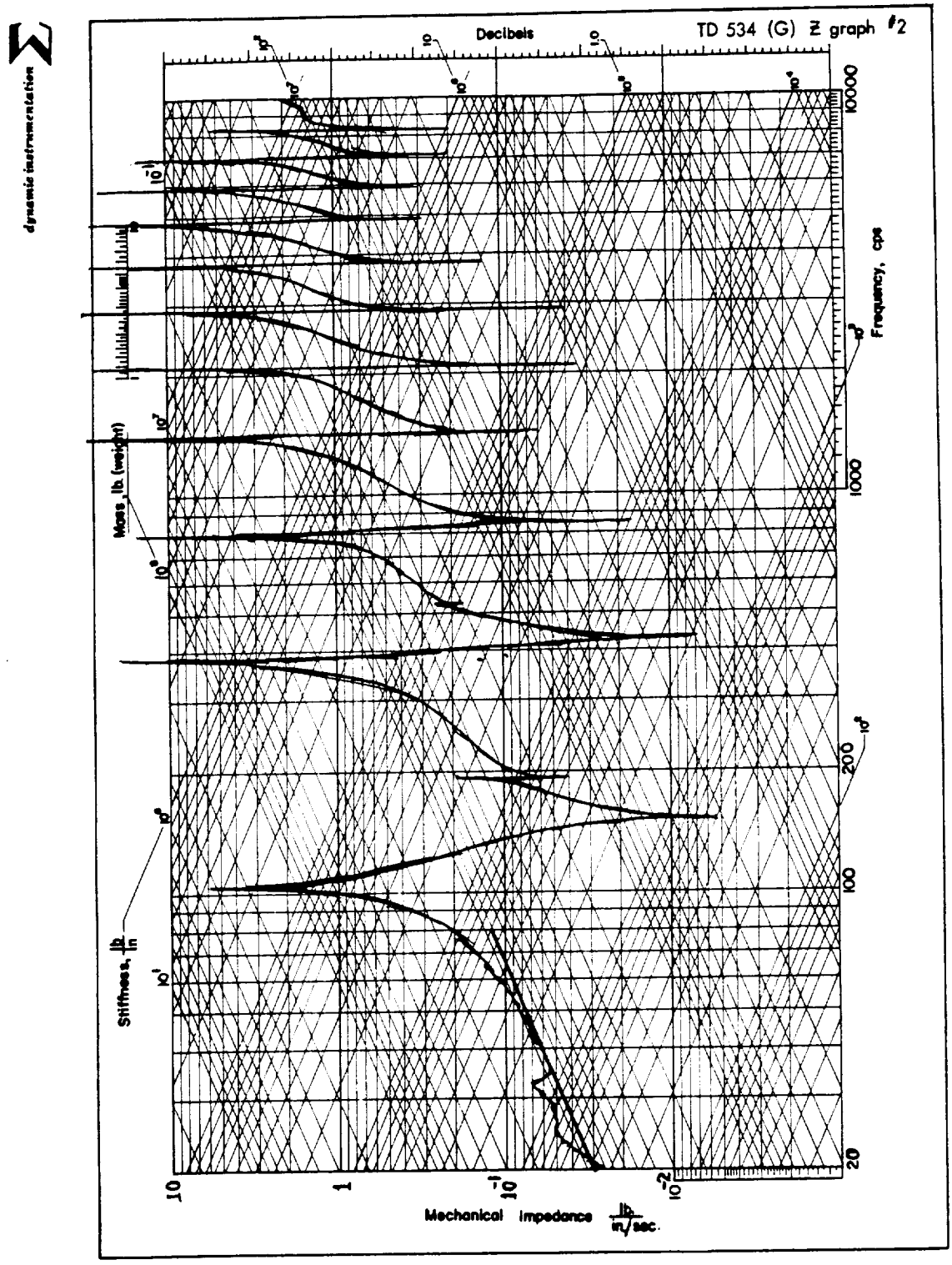

Figure B-2. Measured Input Impedance of a Circular Ring

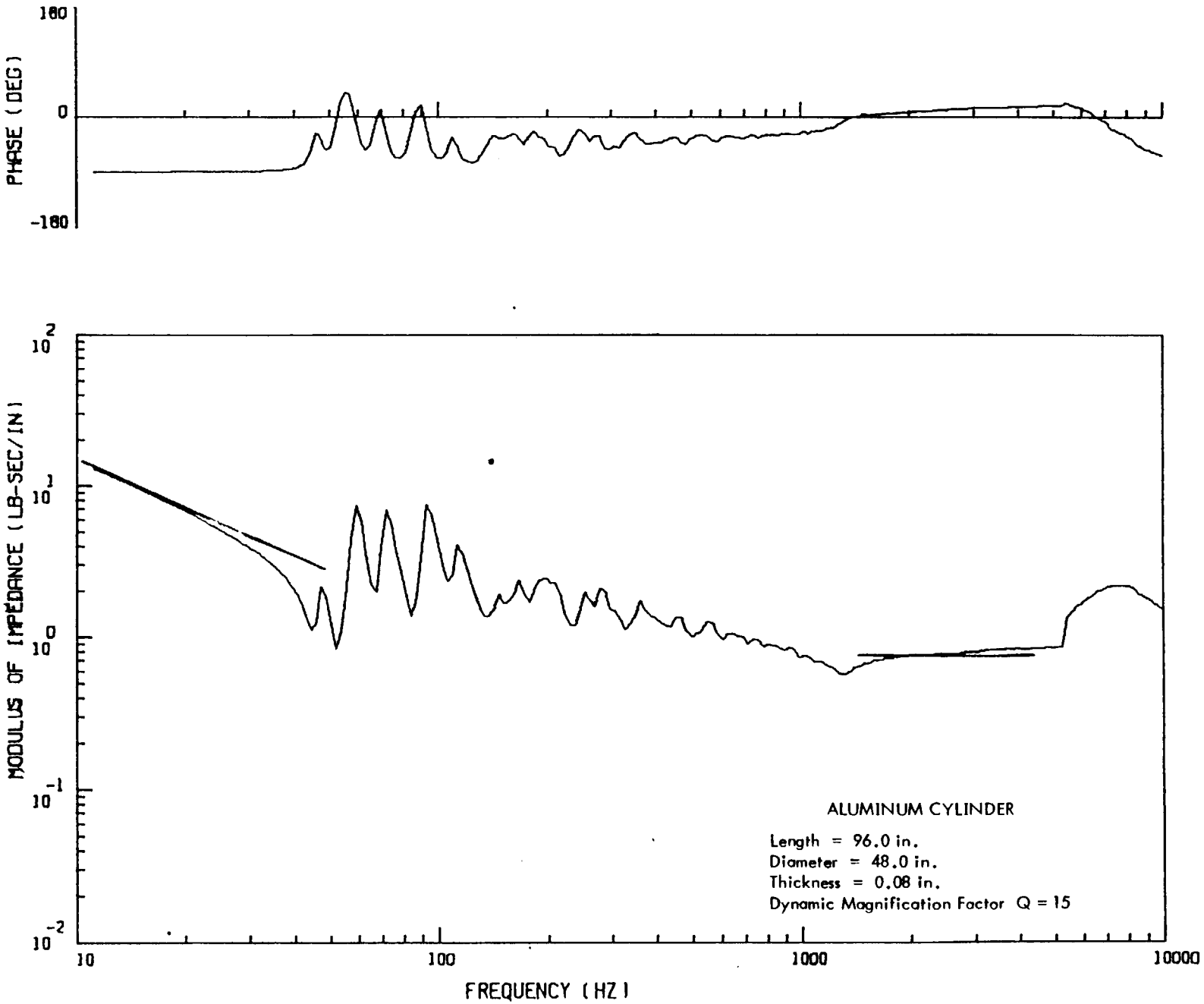

Figure B-3. Theoretical Input Impedance of a Finite Cylinder

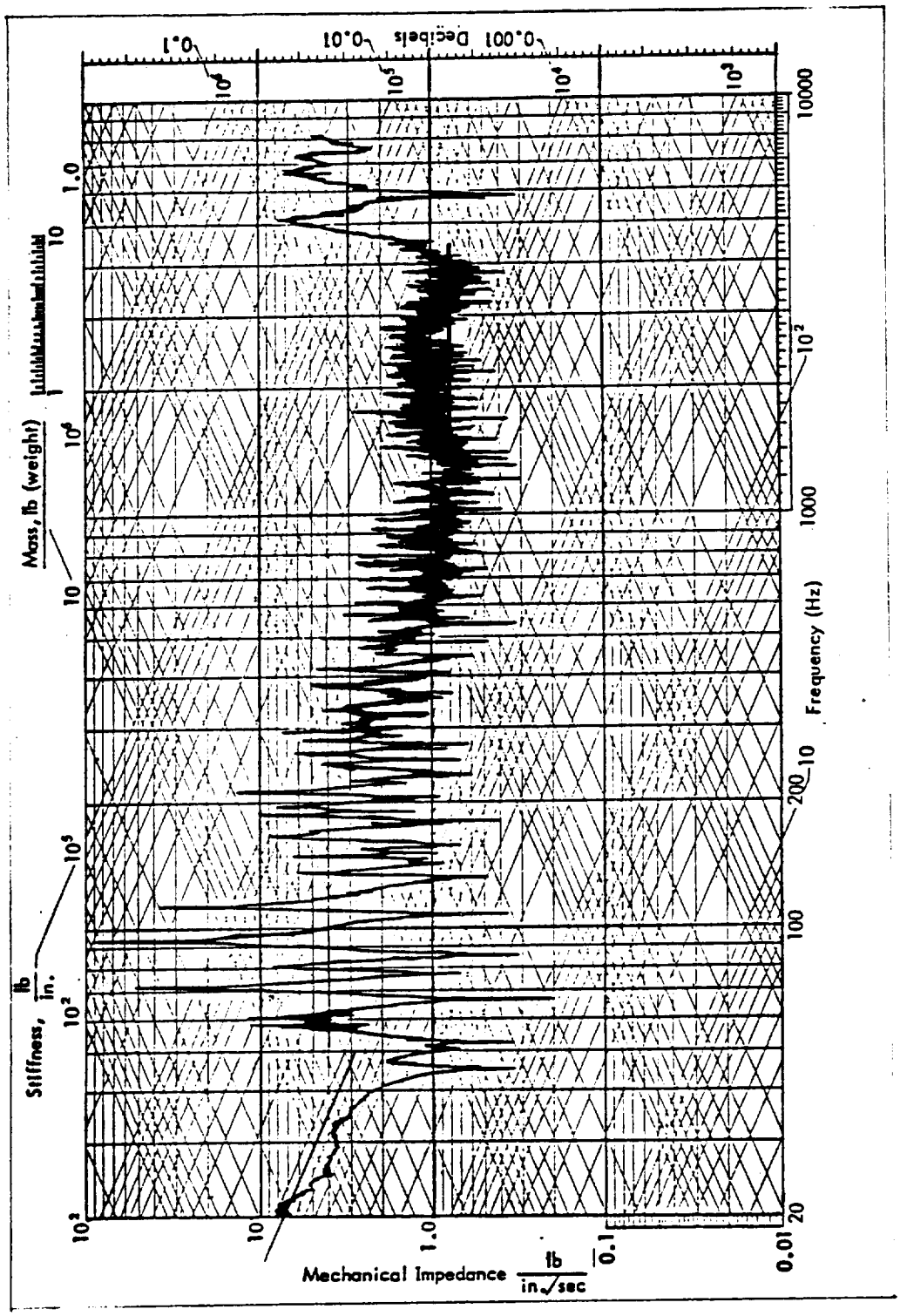

Figure B-4. Measured Input Impedance at Mid-length of an Unstiffened Cylindrical Shell

APPENDIX C

THEORETICAL AND EMPIRICAL METHODS FOR PREDICTING STRUCTURAL RESPONSE

APPENDIX C

THEORETICAL AND EMPIRICAL METHODS FOR PREDICTING STRUCTURAL RESPONSE

1.0 INTRODUCTION

Prediction of the vibration response of plate and shell structures exposed to random pressure fields is generally achieved by using one of the following three approaches:

1) Classical Modal Analysis

2) Statistical Energy Analysis

3) Empirical Analysis and/or Extrapolation

The development of modal analysis and statistical energy analysis is well documented in the literature (References 1-3 and 4-6, respectively). In general, modal analysis is most useful at low frequencies where the modal density of the structure is low, whereas the statistical energy analysis is most useful at frequencies where the modal density is high. For a cylinder, a sufficiently high modal density would be reached approximately two octaves below the ring frequency. Recent studies (Reference 7) have been conducted to evaluate the accuracy of these two analytical methods in conjunction with carefully controlled vibro-acoustic experiments. These studies have shown that both methods result in satisfactory accuracy provided that realistic values of damping are assumed for the computations.

The most significant disadvantage of these analytical approaches is the complexity of the calculations, since they require a digital computer in order to achieve response results over a broad enough frequency range. Another significant disadvantage is the fact that it is necessary to specify accurate values of damping for the structure. In the case of modal analysis the damping must be specified for each mode, whereas in the case of statistical energy analysis, the damping must be specified for each octave band or third octave band. The values of damping assumed for a given structure have a marked effect upon the final response spectrum.

Because of the complexities inherent in these analytical methods, considerable efforts have been made to develop empirical techniques for the prediction of vibration response (References 8-11). Initial developments concentrated upon the normalized response of Titan and Jupiter space vehicles (Reference 8) as shown in Figure C-1. Subsequent developments (References 10 and 11) have been limited to Saturn V type structure, and response information has been summarized in the form of data banks. The most significant disadvantage of these empirical approaches is the fact that response data are presented for very few types of structures and no attempt has been made to review all of the vibration data with a view to deriving a generalized response prediction curve.

Therefore, the objective of the present study was to examine vibration response data from a wide range of sources in an attempt to derive a single empirical response curve for cylindrical type structures. In Sections 2.0 and 3.0, the essential elements of modal analysis and statistical energy analysis are presented. This is followed in Section 4.0 by a description of empirical techniques for predicting vibration response, and relevant conclusions are presented in Section 5.0.

2.0 MODAL ANALYSIS

2.1 General Theory

In predicting vibration response by superposition of the response of the normal modes, it is implicitly assumed that the mean-square response amplitude of each mode can be obtained independently, and that the summation of these mean-square responses is insensitive to coupling between modes. In fact, the total mean-square response of a structure at any point depends upon the summation of the mean square modal responses and upon the summation of the cross-correlations between pairs of modes. The latter cross terms are in some cases significant; however, each term in this summation becomes equal to zero if the space average of the mean square response is obtained. The cancellation of modal cross-correlations for space average response is due to orthogonality between the modes. The analysis of structural response to random pressure fields by modal superposition was initially formulated by Powell (References 1, 2 and 3); detailed results were derived for the response of structures to plane acoustic waves and to a two-dimensional reverberant acoustic field. The theory was extended to predict the response of panels to turbulent boundary layer pressure fluctuations by Wilby (Reference 12), and to a three-dimensional reverberant acoustic field by Crocker and White (Reference 13). More recently, this work has been extended by Bozich and White (Reference 14) to predict the responses of cylindrical shells to attached boundary layers, and by Cockburn (Reference 15) to predict responses to simultaneously applied fluctuating pressure fields such as separated flows and oscillating shocks.

It can be shown that Powell's final result for the space-averaged radial acceleration of a cylindrical shell is given by:

$$\frac{S_{\ddot{u}}(\omega)}{S_p(\omega)} = \frac{1}{(\mu g)^2} \sum_{\substack{m=1 \\ n=0}}^{\infty} \beta_{mn} H^2 \left(\frac{\omega_{mn}}{\omega} \right) \cdot j_{mn}^2(\omega) \qquad (1)$$

where $S_{\ddot{u}}(\omega)$ is the acceleration mean-square (power) spectral density in g^2/Hz, $S_p(\omega)$ is the pressure mean-square (power) spectral density in $(psi)^2/Hz$, μ is the mass per unit area of the shell surface in lb sec^2/in^3., j_{mn}^2 is the joint acceptance of the (mn) shroud mode, and g is gravitational acceleration in $in./s^2$. The remaining dimensionless terms, β_{mn} (introduced by the space averaging), and $H\left(\omega_{mn}/\omega\right)$ (the magnification factor of the (mn) mode at frequency ω) are defined as follows:

$$\beta_{mn} = 2, \quad , \quad m = 1, 2, \ldots . ; \quad n = 0$$

$$= \frac{4n^4}{(1+n^2)^2} \quad , \quad m = 1, 2, \ldots . ; \quad n = 1, 2, 3 \ldots .$$

$$H\left(\frac{\omega_{mn}}{\omega}\right) = \left[\left\{ \left(\frac{\omega_{mn}}{\omega}\right)^2 - 1 \right\}^2 + \frac{1}{Q_{mn}^2} \left(\frac{\omega_{mn}}{\omega}\right)^2 \right]^{-1/2}$$

where Q_{mn} is the magnification factor at resonance, ω_{mn}, of the (mn) shell mode, and the subscripts m and n refer to the number of axial half waves and the number of full circumferential waves, respectively. The joint acceptance term, $j_{mn}^2(\omega)$, has a maximum value of unity, and refers to the direct joint acceptance of the (mn) mode of the shell. Physically, it is a measure of the coupling between the fluctuating pressure environment and the structure, and is generally assumed to be separable into m(axial) and n(circumferential) components, such that $j_{mn}^2(\omega) = j_m^2(\omega) \cdot j_n^2(\omega)$, as follows:

$$j_m^2(\omega) = \frac{1}{L_x^2} \int_{x=0}^{L_x} \int_{x'=0}^{L_x} C(\xi, \omega) \cdot \Phi_m(x) \cdot \Phi_m(x') \, dx \, dx' \qquad (2)$$

$$j_n^2(\omega) = \frac{1}{L_y^2} \int_{y=0}^{L_y} \int_{y'=0}^{L_y} C(\eta, \omega) \cdot \Phi_n(y) \cdot \Phi_n(y') \, dy \, dy' \qquad (3)$$

In the above relations, $\Phi_m(x)$ and $\Phi_m(x')$ represent the axial components of the mode shapes at points x and x' on the shroud, while $\Phi_n(y)$ and $\Phi_n(y')$ represent the circumferential components at points y and y' on the shroud. The quantities L_x and L_y denote the axial and circumferential lengths of the shell, respectively, and the terms $C(\xi, \omega)$ and $C(\eta, \omega)$ represent the axial and circumferential narrow band space-correlation coefficients of the particular fluctuating pressure environment. Axial separation distances $(x - x')$ are denoted by ξ, and circumferential separation distances $(y - y')$ by η.

Since the acceleration power spectral density, defined by Equation (1), has been normalized by the pressure power spectral density, the problem of predicting the vibration response essentially reduces to the determination of the joint acceptances, $j_{mn}^2(\omega)$, for each fluctuating pressure environment. Computation of the response on this basis therefore provides a convenient means of comparing the effects of different pressure correlation characteristics upon vibration response. For conversion to absolute vibration response levels, the normalized response given by Equation (1) is simply multiplied by the power spectral density of the fluctuating pressure field. For a particular structure and fluctuating pressure field, the joint acceptances are evaluated by substituting the axial and circumferential mode shapes and narrow band correlation coefficients into Equations (2) and (3). Closed-form expressions for the joint acceptances of cylindrical structures to a number of random pressure fields have been published by several investigators (References 14, 15 and 16). For cylindrical structures subjected to localized random pressure fields, Bozich and White (Reference 14) derived joint-acceptances for attached turbulent boundary layers, a reverberant acoustic field and a progressive wave acoustic field. Joint acceptances for rocket noise at lift-off, separated flow and shock wave oscillation have been derived by Cockburn (Reference 15).

It can be seen from Equations (2) and (3) that for a given structure the joint acceptances are determined by the functional form of the narrow band space correlation coefficients.

2.2 Joint Acceptances

The complete closed-form expressions for the joint acceptances are not presented here, since they are quite lengthy and may be found in References 7 and 12-16. However, for the purposes of hand-computing the responses of individual modes, approximate joint acceptances are presented in this section. These approximations were presented in Reference 7 for hand-computation of structural response to reverberant acoustic fields, grazing incidence and normal incidence acoustic waves, rocket noise and attached turbulent boundary layers. These expressions were derived by dividing the frequency range of the excitation into three distinct regions, as follows: frequencies well below coincidence, frequencies well above coincidence, and frequencies which are coincident. The condition of coincidence is defined by wavelength matching of the elastic wave in the structure and the pressure wave which is forcing the structure, i.e., $\lambda_e = \lambda$ at coincidence. From this definition, $2L_x/m = \lambda$, and thus:

$$\frac{2L_x}{\lambda} = m \qquad \text{at coincidence}$$

In the circumferential direction, $\lambda_e = L_y/n$ and hence:

$$\frac{L_y}{\lambda} = n \qquad \text{at coincidence.}$$

Now, at coincidence the structural response becomes a maximum, with axial and circumferential joint acceptances displaying peak values at $2L_x/\lambda = m$ and $L_y/\lambda = n$, respectively.

For a reverberant acoustic field, it may be shown that the joint acceptances are as follows:

$$\left.\begin{aligned} j_m^2(\omega) &\approx \frac{1}{3}\left(\frac{2L_x}{m\lambda}\right)^2 \quad \text{for } m = \text{even} \\ &\approx \frac{4}{(m\pi)^2} \quad \text{for } m = \text{odd} \\ j_n^2(\omega) &\approx \frac{1}{3}\left(\frac{L_y}{n\lambda}\right)^2 \end{aligned}\right\} \; f \ll f_{\text{coincidence}} \tag{4}$$

$$\left.\begin{aligned} j_m^2(\omega) &\approx \frac{1}{4m} \\ j_n^2(\omega) &\approx \frac{1}{4n} \end{aligned}\right\} \; f = f_{\text{coincidence}} \tag{5}$$

$$\left.\begin{aligned} j_m^2(\omega) &\approx \frac{\lambda}{4L_x} \\ j_n^2(\omega) &\approx \frac{\lambda}{2L_y} \end{aligned}\right\} \; f \gg f_{\text{coincidence}} \tag{6}$$

For excitation by turbulent boundary layer pressure fluctuations, it may be shown that the joint acceptances are as follows:

$$j_m^2(\omega) \doteq \frac{2}{(m\pi)^2}\left[\frac{1}{\Delta} + \frac{\delta_x}{2\sqrt{\Delta}}\right] \; ; \; f \ll f_{\text{coincidence}} \tag{7}$$

$$j_m^2(\omega) \doteq \frac{1}{2\delta_x} \; ; \; f = f_{\text{coincidence}} \tag{8}$$

$$j_m^2(\omega) \doteqdot \frac{\delta_x}{\gamma_x^2} \qquad f \gg f_{coincidence} \tag{9}$$

$$j_n^2(\omega) \doteqdot \frac{2\delta_y}{\left[\left(2\pi n\right)^2 + \delta_y^2\right]} \tag{10}$$

In the above expressions:

$$\Delta \doteqdot \left[1 + \left(\frac{\delta_x}{m\pi}\right)^2\right]^2$$

$$\delta_x = 0.10\,\frac{L_x\omega}{U_c} + 0.27\,\frac{L_x}{\delta_b}$$

$$\delta_y = 0.72\,\frac{L_y\omega}{U_c} + 1.95\,\frac{L_y}{\delta_b} \tag{11}$$

$$\gamma_x = \frac{L_x\omega}{U_c}$$

U_c = Convection velocity

δ_b = Boundary layer thickness

3.0 STATISTICAL ENERGY ANALYSIS

3.1 General Theory

Statistical energy analysis has been used extensively to predict the response and noise reduction of complex structures excited by random pressure fields (References 4, 5, 6 and 7). This method of analysis is based upon the basic principle that the time average power flow between two simple oscillators, linearly coupled and excited by a wide-band excitation, is proportional to the difference in their time-average total energy, the power flow being always from the oscillator of higher energy to that of lower energy.

When a multi-modal system is excited in a band of frequencies, its modes can be divided into resonant and non-resonant modes within the band. The energy transmission between non-resonant modes and between resonant and non-resonant modes cannot be predicted by the statistical energy analysis and, usually, it is calculated by using classical vibrational analysis. However, for energy transmission between resonant modes, the following power balance equation is valid (Reference 7):

$$P_{AB} = \omega \eta_{AB} n_A \left[\frac{E_A}{n_A} - \frac{E_B}{n_B} \right] \tag{12}$$

where

ω = center frequency of the excitation band

$\eta_{AB} = \Phi_{AB} N_B / \omega$ = coupling loss factor

n_A = average modal density of system A over a band of frequency Δ; it is defined as:

$$n_A = \frac{N_A (f + \Delta/2) - N_A (f - \Delta/2)}{\Delta}$$

$N_A(f)$ = average number of modes with resonance frequencies below f

n_B = average modal density of system B.

Formulas for modal densities of some of the most commonly used structural elements are as follows:

- Simply Supported Beam

$$n_b(\omega) = \frac{\ell}{2\pi} \quad \frac{1}{\sqrt{\omega K C_\ell}} \tag{13}$$

where

$n_b(\omega)$ = modal density, number of resonance frequencies per radian per second

ω = frequency in rad/sec

ℓ = length of beam

K = radius of gyration

C_ℓ = longitudinal wavespeed in beam material

- Simply Supported Rectangular Plate

$$n_p(\omega) = \frac{\ell_1 \ell_2}{2\pi} \quad \frac{\sqrt{3}}{h C_\ell} \tag{14}$$

where

$n_p(\omega)$ = modal density of plate

ℓ_1, ℓ_2 = dimensions of plate

h = thickness of plate

- Free Ring

$$n_r(\omega) = \frac{R}{2\sqrt{\omega}} \quad \left[\frac{\mu}{EJ}\right]^{1/4} \tag{15}$$

where

$n_r(\omega)$ = modal density of ring

R = radius of ring

μ = mass per unit length

E = Young's modulus

J = moment of inertia of cross-section area

- Clamped Circular Plate

$$n_{cp}(\omega) = \frac{R^2 \sqrt{12}}{\pi^2 h C_\ell} \tag{16}$$

where

$n_{cp(\omega)}$ = modal density of circular plate

R = radius of plate

h = thickness of plate

C_ℓ = longitudinal wavespeed of material

- Simply Supported Cylindrical Shell (Reference 17)

$$n_{Cyl}(\omega) = \frac{\ell \sqrt{3}}{\pi h} \int_0^{\theta_0} \frac{d\theta}{\sqrt{1 - \frac{1}{\nu^2} \sin^4 \theta}} \tag{17}$$

where

$$\theta_0 = \begin{cases} \sin^{-1} \sqrt{\nu} & \text{for} \quad \nu < 1 \\ \pi/2 & \text{for} \quad \nu \geq 1 \end{cases}$$

$n_{Cyl}(\omega)$ = modal density of cylinder

h = thickness of shell wall

ℓ = length of cylinder

ν = f/f_r

f = frequency

f_r = ring frequency = $2\pi R/C_\ell$

R = radius of cylinder

C_ℓ = longitudinal wavespeed in shell material

The integral of Equation (17) can be evaluated numerically with the aid of a digital computer. However, for practical purposes, the curve presented in Figure C-2 can be used for hand computations of modal densities of cylinders.

For more complex structures a good estimate of the modal density can be obtained by adding the modal densities of the various elements composing the structure.

- Acoustic Space

$$n_a(f) = \frac{4 f^2 V}{c_0^3} \qquad (18)$$

where

f = frequency in Hz

V = volume of acoustic space

c_0 = speed of sound in acoustic medium

The coupling loss factors, η_{AB}, depend upon the type of structure being considered and upon the environment exciting this structure. These factors are treated subsequently.

Many complex aerospace structures can be considered as being built up from elementary structural elements such as those considered above. A typical example is a shroud and payload assembly. A study which shows the application of the statistical energy analysis to predict the response of this type of assembly to a reverberant field is presented in Reference 18. For the purpose of simplicity and because the principle expressed by Equation (12) can be applied to any two vibrating systems, the subsequent discussion and presentation of formulae for the structural response and noise reduction will be limited to panels and shells.

3.2 Response to Random Pressure Fields

3.2.1 Reverberant Acoustic Field — In the case of a cylinder excited by a reverberant acoustic field, the following expression can be derived to predict the response:

$$\frac{S_{a_2}}{S_{p1}} = \frac{\pi c_0}{A \rho_s \rho_0} \left[\frac{\eta_{2AF,1}\, \eta_{2AF}}{2\eta_{2AF,1} + \eta_{2AF}} + \frac{\eta_{2AS,1}\, \eta_{2AS}}{2\eta_{2AS,1} + \eta_{2AS}} \right] \cdot$$

$$\cdot \left[1 + \frac{S_{p3}}{S_{p1}} \right] \left(\frac{g^2}{psi^2} \right) \qquad (19)$$

where

S_{a_2} = acceleration spectral density

S_{p1} = external sound pressure spectral density

S_{p3} = internal sound pressure spectral density

The Noise Reduction is simply:

$$\frac{S_{p1}}{S_{p3}} = \frac{\eta_{2AS,1}\, \eta_{2AS} + \eta_{1AF,1}\, \eta_{2AF} + \eta_3\, \eta_3}{\frac{\eta_{2AS,1}\, \eta_{2AS}}{2\eta_{2AS,1} + \eta_{2AS}} + \frac{\eta^2_{2AF,1}\, \eta_{2AF}}{2\eta_{2AF,1} + \eta_{2AF}}} - 1 \qquad (20)$$

where

c_0 = speed of sound in acoustic medium

ρ_0 = mass density of acoustic medium

A = surface area of cylinder

ρ_s = surface mass density of cylinder

g = gravitational acceleration

n_{2AF} = modal density of resonant acoustically fast (AF) modal group

n_{2AS} = modal density of resonant acoustically slow (AS) modal group

n_3 = modal density of resonant interior space modes (Equation (18))

$\eta_{2AF,1}$ = coupling loss factor between the acoustic field and the resonant AF mode group

$\eta_{2AS,1}$ = coupling loss factor between the acoustic field and the resonant AS mode group

η_{2AF} = dissipating loss factor of the resonant AF modal group

η_{2AS} = dissipating loss factor of the resonant AS modal group

η_3 = dissipating loss factor of the interior space modal group

The modal density of the acoustically fast modes is given by:

$$n_{2AF}(\nu) = \begin{cases} \dfrac{\partial}{\partial \nu}\left[\dfrac{2\ell}{\pi R\beta}\displaystyle\int_0^{\theta_0}\left[\dfrac{\nu_c}{2} - \dfrac{\nu_c}{2}\left(1 - \dfrac{4\sin^4\theta}{\nu_c^2}\right)^{1/2}\right]d\theta\right] & \text{for } \nu < 1 \quad \text{if } \nu_c > 1 \\ 0 \quad \text{for } 1 < \nu < \nu_c \quad \text{if } \nu_c > 1 & \\ n_{Cyl}(\nu) \quad \text{(i.e., Equation (17))} \quad \text{for } \nu > \nu_c & \end{cases} \tag{21}$$

where

ℓ = length of shell

θ_0 = $\sin^{-1}\sqrt{\nu}$

R = radius of shell

$$\beta = \frac{h}{R\sqrt{12}}$$

$$\nu_c = f_c / f_r$$

f_c = acoustic critical frequency ≡ frequency at which the free-bending wave speed in the panel is equal to the speed of sound. Therefore, the critical frequency is found from

$$c_b = \sqrt{\omega_c} \left[\frac{D}{\mu} \right]^{1/4} = c_0$$

or

$$f_c = \frac{c_0^2}{2\pi} \sqrt{\frac{\mu}{D}}$$

where

c_b = bending wave speed

D = flexural rigidity

μ = surface mass density

c_0 = speed of sound in air.

For hand computations, the curve of Figure C-2 can be used to determine η_{2AF}.

The modal density of the AS modal group is given by the difference between the total modal density and the AF modal density.

The coupling factor between the acoustic field and the acoustically fast modes is given by (symbols are listed after Equation (20)):

$$\eta_{2AF,1} = \frac{\rho_0 c_0}{2\pi f \rho_s} \tag{22}$$

The coupling factor for the AS group (for $f > f_r$ and when the cylinder dimensions are greater than an acoustic wavelength) is (Reference 4):

$$\eta_{2AS,1} = \frac{\rho_0 c_0^2}{2\pi f f_c \rho_s A} \left[2\lambda_0 g_1\left(f/f_c\right)^2 + P_r g_2\left(f/f_c\right) \right] \tag{23}$$

where

λ_0 = acoustic wavelength

P_r = radiating perimeter = $4\pi R$

$$g_1\left(f/f_c\right) = \begin{cases} \left(4/\pi^4\right)\left(1 - 2f/f_c\right) \Big/ \sqrt{f/f_c\left(1 - f/f_c\right)} & f < 0.5\, f_c \\ 0 & f \geq 0.5\, f_c \end{cases}$$

$$g_2\left(f/f_c\right) = \left\{ \left(1 - f/f_c\right) \mathrm{Ln}\left[\left(1 + \sqrt{f/f_c}\right) \Big/ \left(1 - \sqrt{f/f_c}\right) \right] + 2\sqrt{f/f_c} \right\} \Big/ 4\pi^2 \left(1 - f/f_c\right)^{3/2}$$

For hand computation, the graphs shown in Figure C-3 can be used to evaluate the g_1 and g_2 functions.

When the cylinder dimensions are smaller than an acoustic wavelength, and for $f < f_r$, the following coupling factor is used:

$$\eta_{2AS,1} = \frac{\rho_0 c_0^2}{2\pi f f_c \rho_s A} \left(\frac{4}{\pi^4} P_r \sqrt{f/f_c} \right) \tag{24}$$

The structural loss factors are given by:

$$\eta_{2AF} = \eta_{2AS} = \frac{1}{Q} \tag{25}$$

where Q is the dynamic magnification factor at resonance.

The loss factor of the inside acoustic volume can be expressed in terms of the average absorption coefficient α as:

$$\eta_3 = \frac{c_0 \alpha}{4\pi f R} \tag{26}$$

In the case of a plate excited by a reverberant acoustic field, Equation (19) may be used to predict the plate response, if the proper values for the modal densities and the noise reduction, S_{p1}/S_{p3}, are used. The expression for computing the modal density of a simply supported plate is given by Equation (14). In computing the ratio S_{p1}/S_{p3}, two different cases must be taken into consideration, firstly, the case in which the plate is fully immersed in the field and therefore excited on both sides, and secondly, the case in which only one side of the plate is exposed to the acoustic field, such as the case of a panel mounted on the wall of a rigid enclosure. For the case of the two-sided excitation, there is, of course, no noise reduction through the panel, and the ratio S_{p3}/S_{p1} in Equation (19) is equal to unity. For the other case, no substantial differences exist between the expressions for predicting the response of plates and cylindrical shells.

3.2.2 Boundary Layer Turbulence — The procedure for obtaining an expression to predict the response of plates and shells to attached boundary layer turbulence is similar to the reverberant field case. For a cylindrical shell, three vibrating systems are considered, namely, the turbulence environment, the resonant modes of the shell and the acoustic field inside the cylinder. Power balance equations, similar to Equation (12), can be written for these systems. These equations can be solved for the energy content of those modal systems, and by introducing the following expressions;

$$S_p(f) = \frac{\rho_0 c_0^2 E}{V \Delta} \tag{27}$$

$$S_a(f) = \frac{\omega^2 E}{M \Delta} \tag{28}$$

It may be shown that the acceleration response spectrum is given by the relation:

$$\frac{S_{a_2}}{S_{p1}} = \frac{\omega P_{1,2}}{\rho_s} \left(\frac{1}{\eta_2 + \eta_{2,3}} \right) \tag{29}$$

Equation (27) gives the sound pressure spectral density $S_p(f)$ in terms of the average energy, E, within a band of frequency, Δ, the density of the medium, ρ_0, the speed of sound, c_0, and the volume, V. Equation (28) gives the acceleration spectral density of a structural system $S_a(f)$, in terms of the average energy, E, the mass, M, the band center frequency, ω, and the band of frequency, Δ.

The terms in Equation (29) are defined as follows:

S_{a_2} = Acceleration spectral density of shell

S_{p_1} = "Fixed" microphone (PSD) of the environment

ρ_s = Mass surface density of shell wall

η = Dissipating loss factor of shell = $1/Q$

$\eta_{2,3}$ = Coupling factor between the acoustic field and the structure

$P_{1,2}$ = Power which is transferred by one unit of S_{p_1} to a unit area of the shell; $in.^3/(lb\text{-}sec)$

A more complete treatment of the response to turbulent boundary layer pressure fluctuations, including the derivation of the power term $P_{1,2}$, may be found in Reference 7.

4.0 EMPIRICAL ANALYSIS

4.1 Review of Empirical Techniques

Empirical methods for predicting structural response to random pressure fields were formulated initially by Mahaffey and Smith (Reference 19). Following the publication of their method, empirical techniques were proposed by Eldred, et al. (Reference 20), Franken (Reference 8), Condos and Butler (Reference 21), Barrett (Reference 22), Curtis (Reference 23), Brust and Himelblau (Reference 24) and Winter (Reference 25).

Of the above methods, the Franken method has generally been considered to be the most suitable for space vehicle vibration prediction. The majority of the other methods are based upon aircraft vibration data, whereas Franken's method is based solely on Titan and Jupiter space vehicle data. Specifically, Franken found that acceleration measurements plotted in the form of:

$$\frac{S_{\ddot{u}}(f)}{S_p(f)} \quad (\mu g)^2 \quad \text{Versus} \quad (fD)$$

gave a general curve as shown in Figure B-1. The symbols listed above are defined as follows:

$S_{\ddot{u}}(f)$ = the mean-square (power) spectral density of the acceleration (g^2/Hz)

$S_p(f)$ = the mean-square (power) spectral density of the fluctuating pressures $((psi)^2/Hz)$

μg = the surface density of the structure $(lb/in.^2)$

f = the frequency (Hz)

D = the vehicle diameter (ft)

More recently, empirical methods have taken the form of data banks for Saturn V-type structures (References 10 and 11), wherein acceleration power spectral densities divided by the corresponding pressure power spectral densities are given for various stations along the length of the vehicle at lift-off, transonic and maximum dynamic pressure. Obviously this type of approach to space vehicle vibration prediction imposes severe constraints when attempting to predict the behavior of structures other than Saturn V-type hardware.

Therefore, the objective of the present study was to investigate the validity of Franken's empirical method when applied to other experimental data obtained from typical cylindrical structures. Initially a literature survey was conducted in order to obtain useful vibration data for a range of acoustic environments. In many cases, although satisfactory acoustic and vibration data were available, no information was available concerning skin thicknesses and surface densities. As a result of the literature survey, the following sources of vibration data were selected for evaluation:

- The external MARL shroud (Reference 26)
- The Spacecraft Lunar Module Adapter, SLA (Reference 27)
- Wyle Cylinder No. 2 (Reference 7)
- Saturn V Skin-Stringer Structure (Reference 11)
- A BBN model shroud (Reference 4)
- Titan I first-stage structure (Reference 28)
- Republic Cylinder No. 7 (Reference 29)
- Wyle Cylinder No. 1 (Reference 7).

Complete details of the above structures are summarized in Table C-1.

4.2 Development of an Empirical Prediction Method

Initially the vibro-acoustic data were plotted in the form suggested by Franken, i.e., $S_{\ddot{u}}(f) \cdot (\mu g)^2 / S_p(f)$ Versus $f \cdot D$. These results are shown in Figure C-4, together with Franken's original curve from Reference 8.

It is immediately observed that considerable scatter exists between the various experimental measurements. More surprising is the fact that the Titan I data from Reference 28 do not lie on Franken's suggested curve, even though the curve has been suggested as being typical for Titan I structure. There are two probable causes for the scatter evident in Figure C-4. Firstly, the acoustic environments include static firings, near-plane waves in a free field, launch acoustic environments, and reverberant acoustic fields. Consequently, the environment-to-structure coupling efficiencies (or joint acceptances) will be different. Secondly, the damping properties of the various structures vary significantly; typically, the damping will cover the range from $Q = 10$ for skin-stringer-ring frame structure to about $Q = 150$ for thin homogeneous sheet structure.

The possibility of a better collapse of the experimental data was investigated in the following manner. It was stated in Section 2.0 that Powell's result (References 1, 2 and 3) for acceleration response may be shown to be given by the relation:

$$\frac{S_{\ddot{u}}(\omega)}{S_p(\omega)} = \frac{1}{(\mu g)^2} \sum_{\substack{m=1 \\ n=0}}^{\infty} \beta_{mn} H^2\left(\frac{\omega_{mn}}{\omega}\right) \cdot j_{mn}^2(\omega) \qquad (30)$$

TABLE C-1. DETAILS OF STRUCTURES ANALYZED

Structure	Diameter D-ft	Skin Thickness h-in.	Surface Weight (μg)-in^2	Length -in.	Acoustic Excitation	Typical Q
MARL (Reference 26)	21.7	1.0	0.0078	300.0	Far-Field Rocket Noise (Static Firing)	50
SLA (Reference 27)	20.6*	1.7	0.0139	81.2*	Rocket Noise (Lift-Off)	50
Wyle Cylinder No. 2 (Reference 7)	2.0	0.04	0.0043	48.0	Reverberant Field	100-200 (Measured)
Saturn V Skin-Stringer Structure (Reference 11)	33.0	0.071	0.01955	27.0*	Rocket Noise (Lift-Off)	5-10
BBN Model Shroud (Reference 4)	2.66	0.087	0.00538	78.5	Reverberant Field	80 (Measured)
TITAN I First Stage (Reference 28)	10.0	0.1	0.01	36.0*	Rocket Noise (Static Firing)	5-10
REPUBLIC Cylinder (Reference 29)	3.0	0.018	0.00509	36.0	Reverberant Field	100
Wyle Clinder No. 1 (Reference 7)	4.0	0.08	0.0087	96.0	Reverberant Field	100-200 (Measured)

* NOTE: These dimensions are "effective" values since the available vibro-acoustic data were collected from local regions of the overall structure. For the remaining structures, the available vibro-acoustic data represent space-averages for the entire structure.

Now when the modal density is relatively high and the frequency separation between modes is low, the modal response bandwidths may increase so that they overlap. In this case the number of modes N having resonant frequencies within the bandwidth Δf centered at frequency f is:

$$N = \Delta f \cdot n(f)$$

$$= \frac{f\, n(f)}{Q}$$

where $n(f)$ = modal density.

If all N modes have approximately the same response level, then the <u>total</u> mean-square response is approximately N times the response of any one mode.

Now since all N modes are resonating within the bandwidth Δf, it may be assumed that:

$$H^2\left(\frac{\omega_{mn}}{\omega}\right) \doteq Q^2$$

and it may also be assumed that $\mathcal{J}_{mn}$, $j_m^2(\omega)$ and $j_n^2(\omega)$ are approximately the same for all N modes. Thus Equation (30) may be approximated by:

$$\frac{S_{\ddot{u}}}{S_p} = \frac{\mathcal{J}_{mn} \cdot Q^2 \cdot j_{mn}^2(\omega)}{(\mu g)^2} \cdot N$$

$$= \frac{\mathcal{J}_{mn} \cdot Q \cdot f \cdot n(f) \cdot j_{mn}^2(\omega)}{(\mu g)^2} \qquad (31)$$

Now from Figure C-2, it may be observed that in any frequency band, n(f) for a cylindrical shell is equal to some constant C_1 (proportional to frequency) multiplied by $\ell/h\, f_r$ where ℓ is the length of the cylinder, h is the skin thickness and f_r is the ring frequency. Thus, Equation (31) may be approximated further to:

$$\frac{S_{\ddot{u}}}{S_p} \cdot (\mu g)^2 \cdot \frac{h}{\ell} = \mathcal{J}_{mn} \cdot Q \cdot \frac{f}{f_r} \cdot j_{mn}^2(\omega) \cdot C_1 \qquad (32)$$

Since f_r is proportional to 1/D, this suggests that if the following parameters are plotted,

$\frac{S_{\ddot{u}}}{S_p} \cdot (\mu g)^2 \cdot \frac{h}{\ell}$ Versus (fD), the experimental data should show some degree of collapse.

The vibro-acoustic data were re-plotted according to this relationship and are shown in Figure C-5. While a slightly better collapse of the data is evident, the scatter is still quite large and therefore there seems little advantage in plotting the data in this manner. It was therefore decided that Franken's original response parameter, $S_{\ddot{u}}/S_p \cdot (\mu g)^2$, should be retained.

In fact the large scatter in the data shown in Figure C-4 is considered to be due primarily to the variation in damping or Q values. This is illustrated in Figure C-6 which shows three normalized response curves (of identical shape to Franken's curve) corresponding to Q = 5, Q = 50 and Q = 200. These curves are based on Equation (31) which shows that the acceleration response is directly proportional to Q when the modal density is relatively high. Thus an increase in Q by a factor of 10 results in an increase in normalized acceleration response of one decade. The lower curve in Figure C-6 for Q = 5 is in fact Franken's original curve (Reference 8); this value of Q seems reasonable for the closely-spaced ring frames and stringers utilized in the Titan I first stage. If the curves shown in Figure C-6 are overlaid on the vibro-acoustic data of Figure C-4, the specified values of Q are observed to be quite realistic for the structures considered. For example, the normalized response of the Saturn V skin-stringer structure is generally much lower than the response of the Wyle cylinders over most of the frequency range. The damping for the skin-stringer structure would typically be around Q = 5 to Q = 10, whereas the damping for both Wyle cylinders was determined through measurements in the laboratory (Reference 29) to vary from Q = 100 to Q = 200 over much of the frequency range.

It is therefore suggested that the normalized response curves shown in Figure C-6 should be utilized for the prediction of acceleration response of cylindrical vehicle structures.

4.3 Empirical Prediction of Acoustic Mobility

Acoustic mobility is defined as the ratio of the velocity mean-square (power) spectral density to the blocked-pressure mean-square (power) spectral density, i.e., $S_{\dot{u}}(f)/S_p(f)$. The blocked pressure is simply the true surface pressure and thus includes the effects of pressure-doubling. The normalized acceleration spectra shown in Figure C-6 were converted to Acoustic Mobility spectra as shown in Figure C-7. The ordinate of Figure C-7 is $S_{\dot{u}}(f)/S_p(f) \cdot (\mu g)^2/D^2$ and has units of $(in./sec)^2/ft^2$ where D is the vehicle diameter in feet. The abscissa is again frequency times diameter, fD. For each value of Q shown in Figure C-6, the upper curve was utilized in deriving the acoustic mobility spectra shown in Figure C-7.

5.0 CONCLUDING REMARKS

In many practical situations it is necessary to predict the vibration response of a structure to a random pressure field. In certain cases the acceleration response of a final hardware design is required, while in other cases the acceleration response of one or more preliminary designs is required. Often, the selection of a prediction method will be governed by the particular requirements of each situation. For example, the empirical curves of Figure C-6 will be most suitable during preliminary design phases where trade-off studies involving skin thickness, surface density, and ring-frame and stringer construction versus honeycomb sheet construction, may be rapidly achieved. The empirical curves may also be used for evaluating a final design; however, at the final design stage it is also advisable to carry out computerized analyses utilizing either modal analysis or statistical energy analysis or both. These analyses may be repeated for a range of damping values, such that structural Q's can vary from mode to mode, if necessary, in the modal analysis, or can vary between third-octave bands in the statistical energy analysis.

Since both analytical methods have significant advantages and disadvantages, the optimum analytical approach to adopt when predicting vibration response cannot be rigidly defined. Previous studies (Reference 7) have shown that in terms of the final accuracy, both analytical methods can be considered satisfactory. For a typical structure excited by a random pressure field, the basic analytical approach to be adopted is governed primarily by the following:

1) The particular requirements involved. In some cases, the acceleration response is all that is needed, while in other cases both the acceleration response and the noise reduction might be required.

2) The frequency range being considered. Low-order modal response of the structure may be required in one case while in another, higher-order modal response may be required. In yet another case the complete response spectrum may be desired.

3) The type of structure being analyzed. The critical parameters to be considered here would include: modal densities, resonant frequencies and mode shapes. For example, if the mode shapes were difficult to define, but sufficient information was known concerning modal densities (which are additive), then the energy method would be suitable.

REFERENCES

1. Powell, A., "On the Fatigue Failure of Structures Due to Vibrations Excited by Random Pressure Fields," JASA, Vol. 30, No. 12, pp. 1130-1135, December 1958.

2. Powell, A., "On the Approximation to the Infinite Solution by the Method of Normal Modes for Random Vibrations," JASA, Vol. 30, No. 12, pp. 1136-1139, December 1958.

3. Powell, A., "On the Response of Structures to Random Pressures and to Jet Noise in Particular," Chapter 8 of Random Vibration , edited by S.H. Crandall, Technology Press.

4. Manning, J. E., et al., "Transmission of Sound and Vibration to a Shroud-Enclosed Spacecraft," BBN Report 1431, October 1966.

5. Smith, P.N. and Lyon, R.H., "Sound and Structural Vibration," NASA CR-160, March 1965.

6. Maidanik, G., "Response of Ribbed Panels to Reverberant Acoustic Fields," JASA, No. 34, June 1962.

7. Conticelli, V.M. and Cockburn, J.A., "Vibration Response and Noise Reduction of Cylindrical Structures Exposed to Acoustic Environments — A Theoretical and Experimental Investigation," Wyle Laboratories Research Staff Report WR 72-1, January 1972.

8. Franken, P.A., "Sound Induced Vibrations of Cylindrical Vehicles," JASA, Vol. 34, No. 4, pp. 453-454, April 1962.

9. Barnoski, R.L., et al., "Summary of Random Vibration Prediction Procedures," NASA CR-1302, April 1969.

10. Crane, K.L., "A Vibro-Acoustic Transfer Function Manual," Brown Engineering Co. Report, 1969.

11. Bandgren, H.J. and Smith, W.C., "Development and Application of Vibro-Acoustic Structural Data Banks in Predicting Vibration Design and Test Criteria for Rocket Vehicle Structures, NASA TN D-7159, February 1973.

12. Bull, M.K., Wilby, J.F. and Blackman, D.R., "Wall Pressure Fluctuations in Boundary Layer Flow and Response of Simple Structures to Random Pressure Fields," University of Southampton (England), A.A.S.U. Report No. 243, July 1963 (AD 631 521).

13. Crocker, M.J. and White, R.W., "Response of an Aircraft Fuselage to Turbulence and to Reverberant Noise," Wyle Laboratories Research Staff Consulting Report No. WCR 66-11, September 1966.

14. Bozich, D.J. and White, R.W., "A Study of the Vibration Responses of Shells and Plates to Fluctuating Pressure Environments," NASA CR-1515, March 1970.

15. Cockburn, J.A., "Evaluation of Acoustic Testing Techniques for Spacecraft Systems," Wyle Laboratories Reseach Staff Report WR 71-1, June 1971.

16. Cockburn, J.A. and Jolly, A. C., "Structural-Acoustic Response, Noise Transmission Losses and Interior Noise Levels of an Aircraft Fuselage Excited by Random Pressure Fields," WPAFB AFFDL-TR-68-2, August 1968.

17. Miller, D.K. and Hart, F.D., "Modal Density of Thin Circular Cylinders," NASA CR-897, December 1967.

18. Conticelli, V.M., "Study of Vibratory Response of a Payload Subjected to a High Frequency Acoustic Field," Wyle Laboratories Research Staff Report WR-69-9, May 1969.

19. Mahaffey, P.T. and Smith, K.W., "A Method for Predicting Environmental Vibration Levels in Jet-Powered Vehicles," Shock and Vibration Bulletin No. 28, Part IV, pp. 1-14, August 1960.

20. Eldred, K.M., Roberts, W.H. and White, R.W., "Structural Vibration in Space Vehicles," WADD TR-61-62, December 1961.

21. Condos, F. and Butler, W., "A Critical Analysis of Vibration Prediction Techniques," Proceedings of the IES Annual Technical Meeting in Los Angeles, 1963.

22. Barrett, R.E., "Techniques for Predicting Localized Vibration Environments of Rocket Vehicles," NASA TN D-1836, October 1963.

23. Curtis, A.J., "A Statistical Approach to Prediction of the Aircraft Flight Environment," Shock and Vibration Bulletin No. 33, Part I, February 1964.

24. Brust, J.M. and Himelblau, H., "Comparison of Predicted and Measured Vibration Environments for Skybolt Guidance Equipment," Shock and Vibration Bulletin No. 33, Part III, pp. 231-280, March 1964.

25. Winter, E.F. and Van Der Laan, W.F., "Recommended Procedures for Predicting Random Vibration Environments in MSFC Aerospace Vehicles," Measurement Analysis Corporation Report MAC 504-19, September 1967.

26. Chang, K.Y. and White, R.W., "Empirical Evaluation of Vibro-Acoustic Data from MARL/Static Firing Tests," Wyle Laboratories Research Staff Report prepared under Contract No. NAS8-21260 for NASA-Marshall Space Flight Center, February 1971.

27. Peverley, R.W. and Newbrough, D.E., "A Summary of the Acoustic and Vibration Testing in Support of the Apollo Spacecraft Program, Volumes I and II. Report prepared for NASA-MSC by General Electric Co., Apollo Systems, Houston, Texas.

28. Franken, P.A. and Lyon, R.H., "Estimation of Sound-Induced Vibrations by Energy Methods, with Applications to the Titan Missile," Sound and Vibration Bulletin No. 31, Part III, pp. 12-26, April 1963.

29. Conticelli, V.M. and White, R.W., "Experimental Study of Vibro-Acoustic Response of Stiffened Cylindrical Shells," Wyle Laboratories Research Staff Report WR 71-2, January 1971.

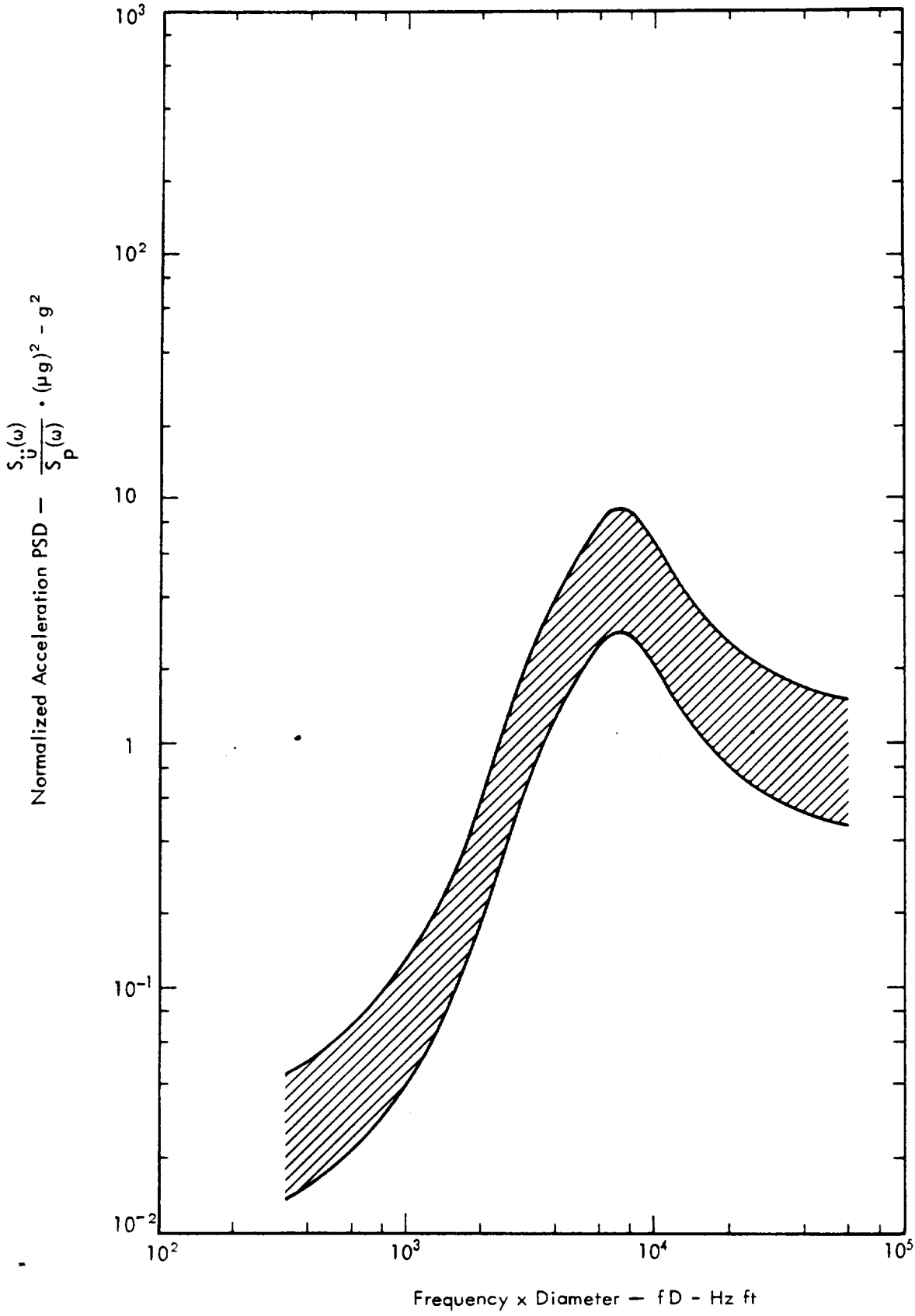

Figure C-1. Franken's Empirical Curve (Reference 8)

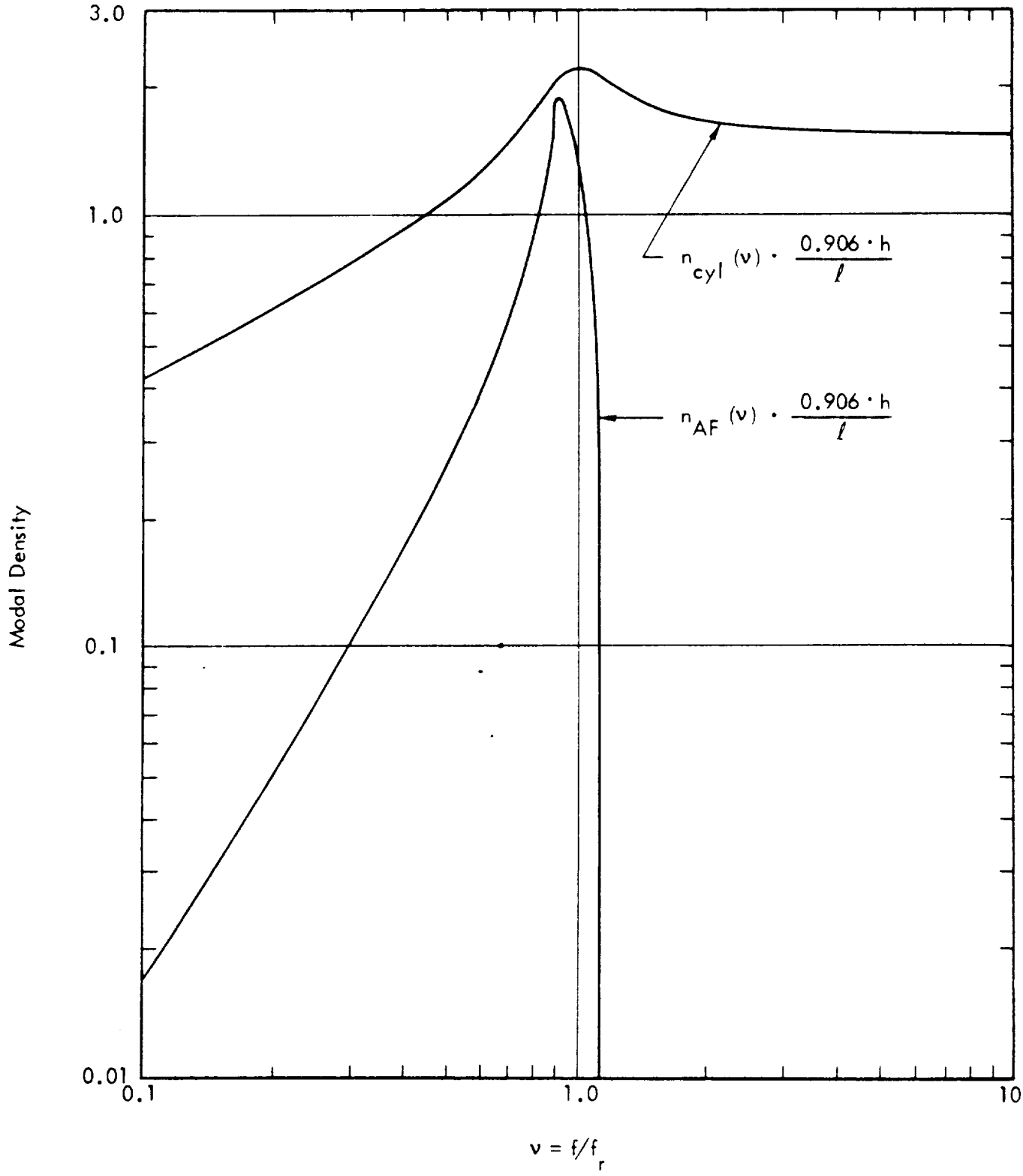

Figure C-2. Analytical Curves for Modal Densities, $n_{cyl}(\nu)$ and $n_{AF}(\nu)$, of a Cylindrical Shell as a Function of Frequency (Reference 17)

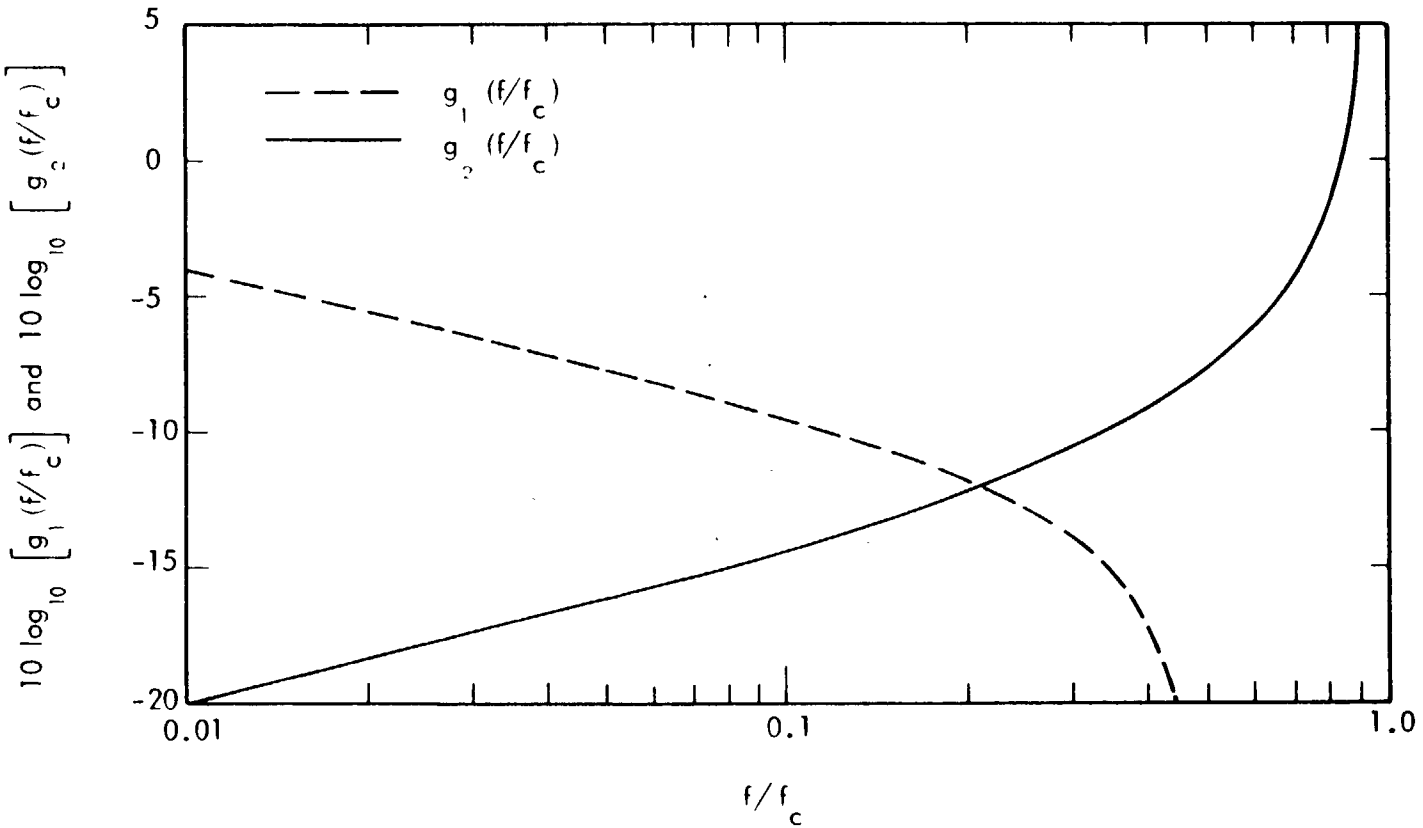

Figure C-3. Graphs of Functions $g_1 (f/f_c)$ and $g_2 (f/f_c)$ (Reference 6)

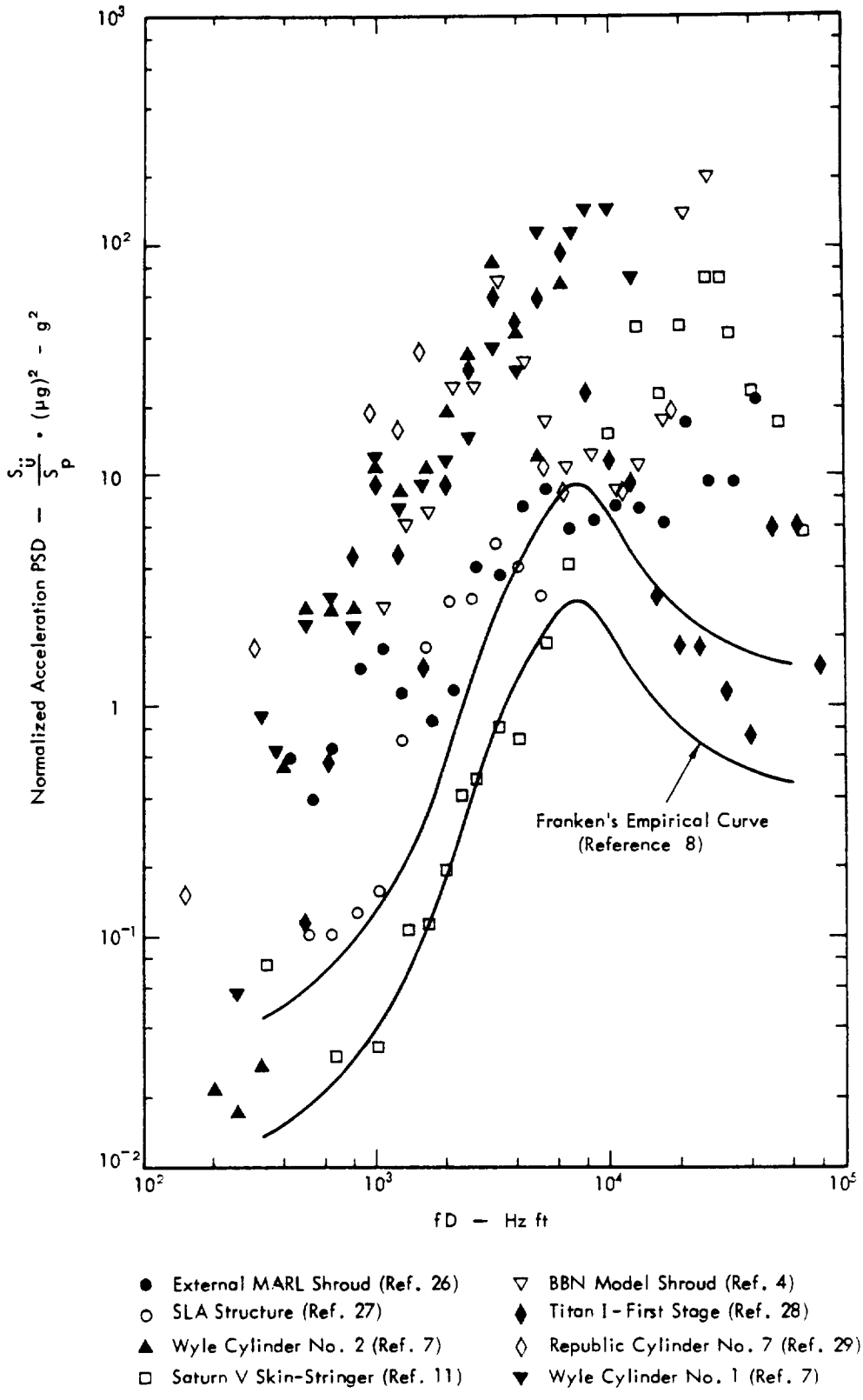

Figure C-4. Comparison Between Vibro-Acoustic Data and Franken's Empirical Curve

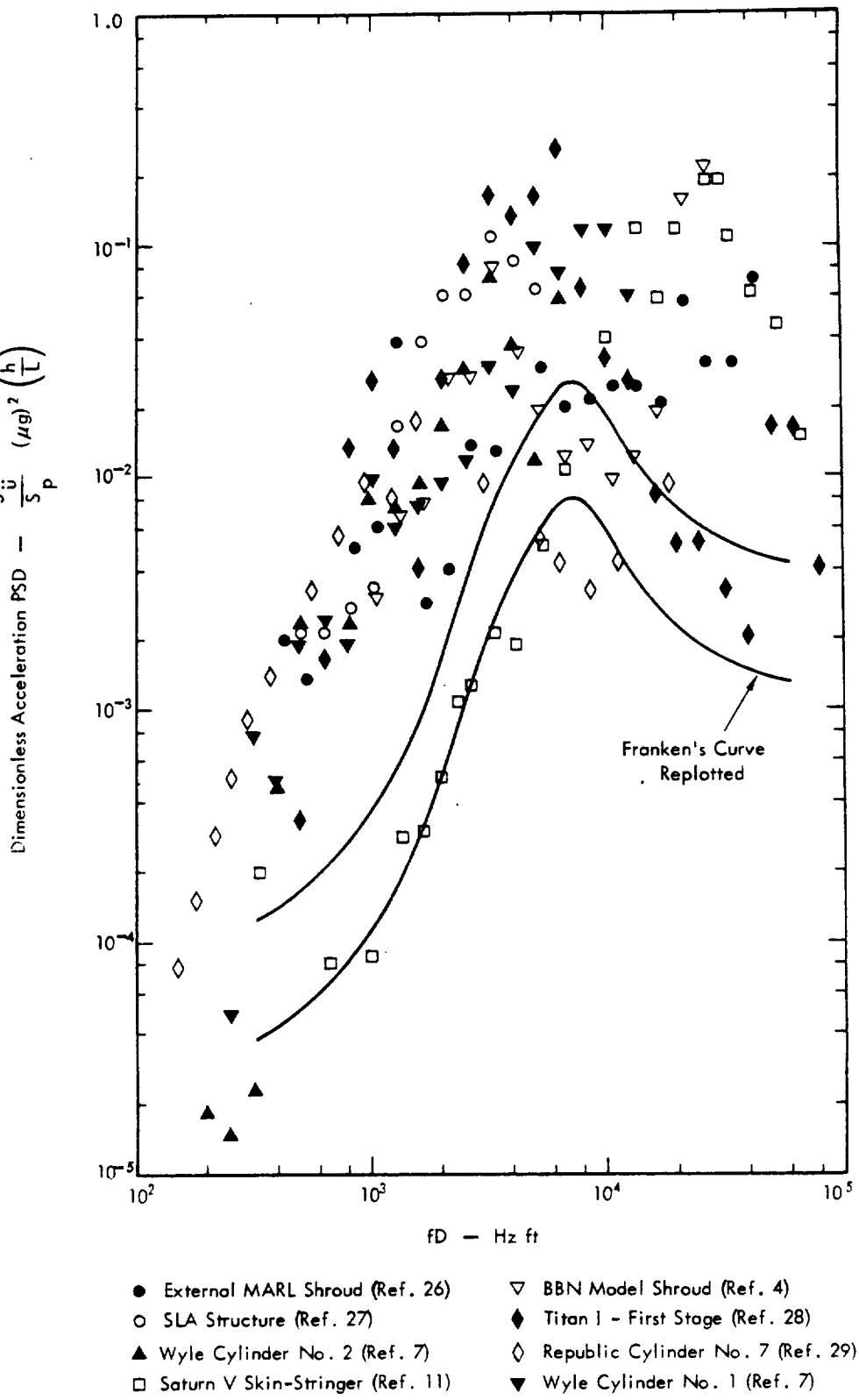

Figure C-5. Alternative Dimensionless Acceleration Spectrum Based on Surface Density, Skin Thickness and a Typical Length

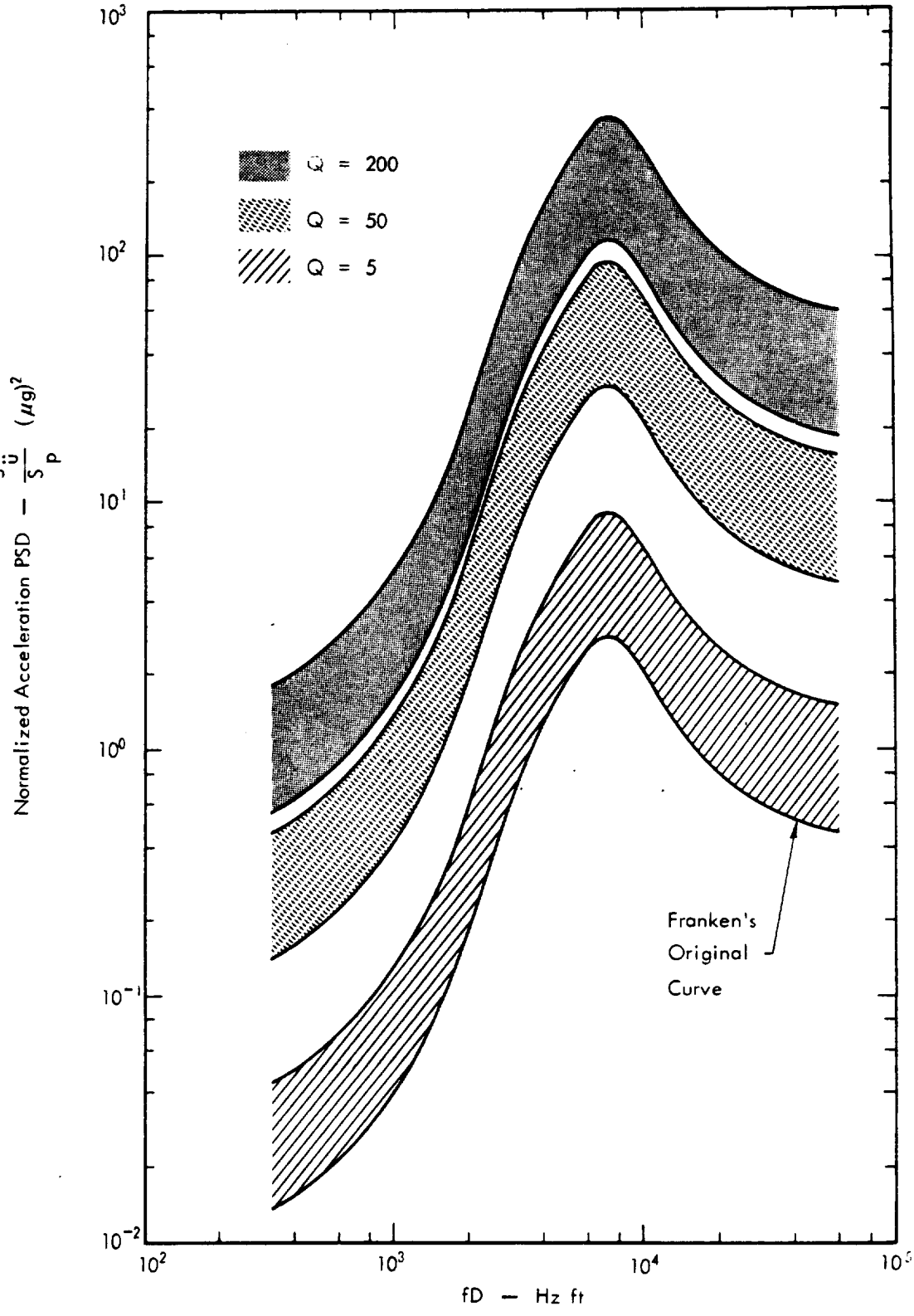

Figure C-6. Normalized Acceleration Response of Cylindrical Structures as a Function of Damping and the Parameter (fD)

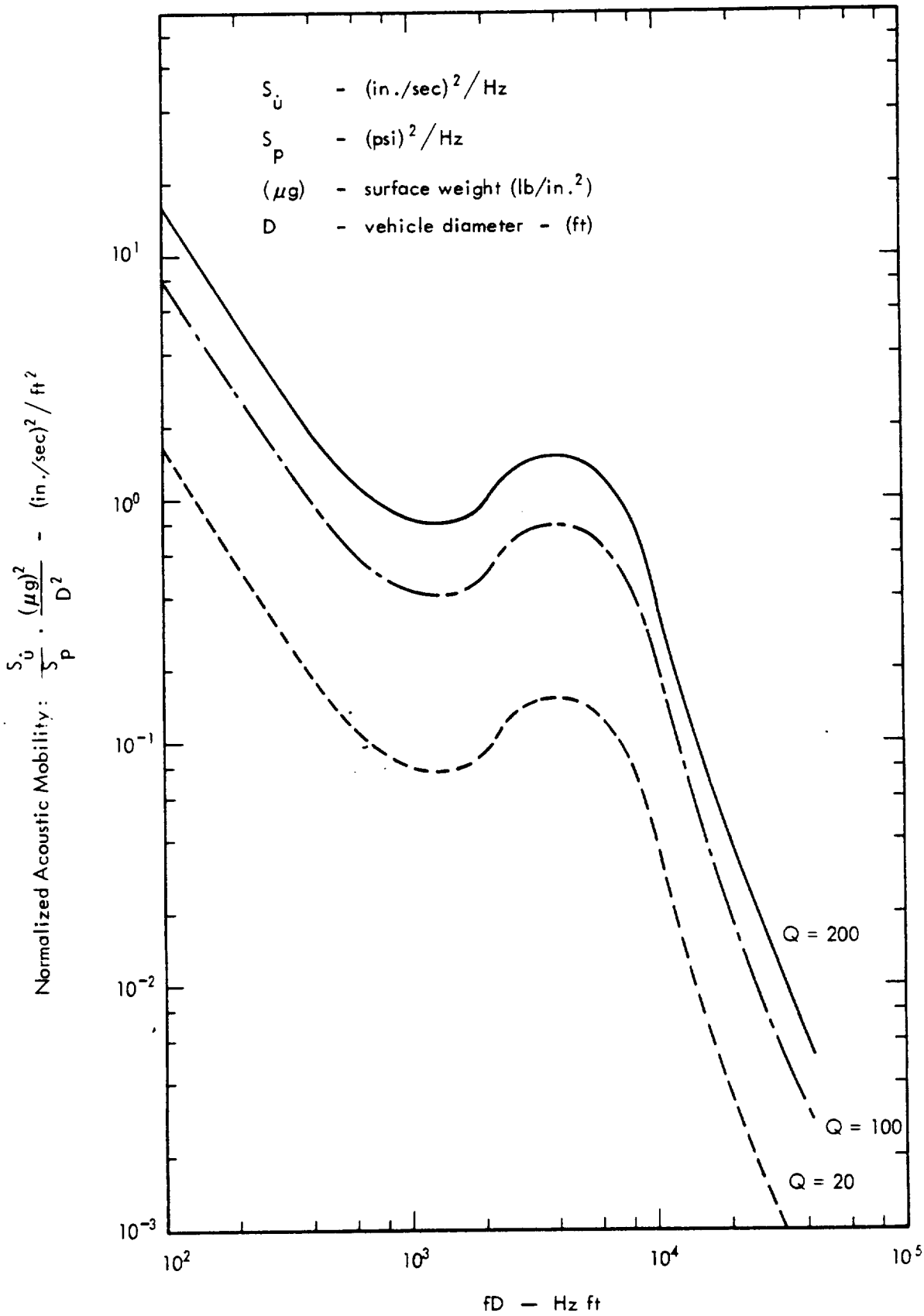

Figure C-7. Acoustic Mobility for Cylindrical Vehicle Structures (Based on Blocked Pressures)

APPENDIX D

DESCRIPTION AND USAGE OF COMPUTER PROGRAMS

APPENDIX D

DESCRIPTION AND USAGE OF COMPUTER PROGRAMS

Four computer programs and one plotting program developed for this study are described in this appendix along with the complete program listing. The computer programs consist of the evaluation of the following equations:

- Input Impedance of a Finite Beam
- Input Impedance of a Ring
- Input Impedance of an Unstiffened Shell
- Input Impedance of a Payload Structure

A type output for a beam impedance is also presented at the end of this appendix.

WYLE LABORATORIES

COMPUTER PROGRAM DESCRIPTION

Program Number	:	73/1001
Author	:	K.Y. Chang
Date	:	3 August 1973
Source Language	:	FORTRAN IV-H
Computer	:	XDS Sigma 5

1.0 PROGRAM TITLE

Beam Impedance Evaluation Program

2.0 PROGRAM FEATURES

Given a suitable geometrical and material parameters of the beam-type structure, this computer program computes and prints the input (velocity) impedance over the specified frequency range at logarithmic increments. The results are stored on a magnetic tape for plotting.

The equations used to evaluate the input impedance have been derived and are given as follows:

$$Z(\omega) = \frac{1}{i\omega}\left[\sum_{m=1}^{\infty} \frac{\phi_m^2(\ell_0)}{0.5\,\ell\rho A\,\omega_m^2} \frac{1-\left(\frac{\omega}{\omega_m}\right)^2 + \frac{i}{Q_m}\left(\frac{\omega}{\omega_m}\right)}{\left[1-\left(\frac{\omega}{\omega_m}\right)^2\right]^2 + \frac{1}{Q_m^2}\left(\frac{\omega}{\omega_m}\right)^2}\right]^{-1}$$

where

$$\phi_m = \sin\frac{m\pi x}{\ell}$$

$$\omega_m^2 = \frac{EI}{\rho A}\,\frac{m^2\pi^4}{\ell^4}$$

and ω represents the angular frequency, Q_m denotes the dynamic magnification factor for the m mode and E, ρ, A, I and ℓ are the parameters of the beam.

This program consists of two subprograms. The first one computes the impedance value and the other one plots the computational results.

3.0 HARDWARE CONFIGURATION

The following computer hardware configuration is required to execute this program:

- Sigma 5 CPU
- 16 K words of core storage
- 1 Magnetic tape transport
- 1 Card reader
- 1 Teletyper
- 1 Line printer

4.0 INPUT INSTRUCTIONS

The input data consists of two input cards punched as follows:

Card 1

Columns 1-10	Number of frequency points to be computed in the specified range. The maximum number should not exceed 200. (Format I10)
Columns 11-20	The lowest frequency in Hz. (Format F10.0)
Columns 21-30	The highest frequency in Hz. (Format F10.0)

Card 2

Columns 1-10	Young's Modulus of beam material in psi. (Format F10.0)
Columns 11-20	Weight density of beam material in $lb/inch^3$. (Format F10.0)
Columns 21-30	Cross-section area of beams in $inch^2$. (Format F10.0)
Columns 31-40	Cross-section moment of inertia of beams in $inch^4$ (Format F10.0)
Columns 41-50	Length of beams in inch. (Format F10.0)
Columns 51-60	Dynamic magnification factor. (Format F10.0)
Columns 61-70	Location of point-driving force in inch. (Format F10.0)

5.0 OUTPUT RESULTS

The computational results are stored on a magnetic tape numbered 1. The printed output have the following form:

First several rows consist of —

- Total weight
- Static stiffness
- Fundamental frequency
- Impedance for infinite length beam

Remaining printed output consists of —

- 1st columns represents the frequency values
- 2nd column represents the normalized frequency values
- 3rd and 4th columns lists the real and imaginary parts of the impedance values
- 4th and 5th columns show the error criterion and number of terms in the summation.

WYLE LABORATORIES

COMPUTER PROGRAM DESCRIPTION

Program Number	:	73/1002
Author	:	K.Y. Chang
Date	:	3 August 1973
Source Language	:	FORTRAN IV-H
Computer	:	XDS Sigma 5

1.0 PROGRAM TITLE

Ring Impedance Evaluation Program

2.0 PROGRAM FEATURES

Given a suitable geometrical and material parameters of the ring frame, this computer program computes and prints the input (velocity) impedance over the specified frequency range at logarithmic increments. The results are stored on a magnetic tape for plotting.

The equations used to evaluate the input impedance have been derived and are given as follows:

$$Z(\omega) = \frac{1}{i\omega}\left[\sum_{n=1}^{\infty} \frac{\left(\frac{n^2}{1+n^2}\right)}{\pi R \rho A \omega_n^2} \frac{1 - \left(\frac{\omega}{\omega_n}\right)^2 + \frac{i}{Q_n}\left(\frac{\omega}{\omega_n}\right)}{\left[1 - \left(\frac{\omega}{\omega_n}\right)^2\right]^2 + \frac{1}{Q_n^2}\left(\frac{\omega}{\omega_n}\right)^2}\right]^{-1}$$

where

$$\omega_n^2 = \frac{EI}{\rho A} \frac{1}{R^4} \frac{n^2(n^2-1)^2}{n^2+1}$$

and ω represents the angular frequency, Q_n denotes the dynamic magnification factor for the nth mode, and E, ρ, A, I and R are the parameters of the ring.

This program consists of two subprograms. The first one computes the impedance value and the other one plots the computational results.

3.0 HARDWARE CONFIGURATION

The following computer hardware configuration is required to execute this program:

- Sigma 5 CPU
- 16 K words of cores
- 1 Magnetic tape transports
- 1 Card reader
- 1 Line printer

4.0 INPUT INSTRUCTIONS

The input data consists of two input cards punched as follows:

Card 1

Columns 1-10	Number of frequency points to be computed in the specified range. The maximum number should not exceed 200. (Format I10)
Columns 11-20	The lowest frequency in Hz. (Format F10.0)
Columns 21-30	The highest frequency in Hz. (Format F10.0)

Card 2

Columns 1-10	Young's modulus of ring material in psi. (Format F10.0)
Columns 11-20	Weight density of ring material in $lb/inch^3$. (Format F10.0)
Columns 21-30	Cross-section area of rings in $inch^2$. (Format F10.0)
Columns 31-40	Cross-section moment of inertia of rings in $inch^4$. (Format F10.0)
Columns 41-50	Mean radius of rings in inch. (Format F10.0)
Columns 51-60	Dynamic magnification factor. (Format F10.0)

5.0 OUTPUT RESULTS

The computational results are stored on a magnetic tape numbered 1. The printed output have the following form:

First several rows consist of —

- Total weight
- Static stiffness
- Fundamental (lowest) frequency
- Impedance for finite length beam
- Breathing (resonanc) frequency

Remaining printed output consists of —

- 1 st column represents the frequency values
- 2nd column represents the normalized frequency values
- 3rd and 4th columns lists the real and imaginary parts of the impedance values
- 4th and 5th columns shows the error criterion and number of terms in the summation.

WYLE LABORATORIES

COMPUTER PROGRAM DESCRIPTION

Program Number	:	73/1003
Author	:	K.Y. Chang
Date	:	3 August 1973
Source Language	:	FORTRAN IV-H
Computer	:	XDS Sigma 5

1.0 PROGRAM TITLE

Unstiffened Shell Impedance Evaluation Program

2.0 PROGRAM FEATURES

Given a suitable geometrical and material parameters of the cylinder-type structure, this computer program computes and prints the input (velocity) impedance over the specified frequency range at logarithmic increments. The results are stored on a magnetic tape for plotting.

The equations used to evaluate the input impedance have been derived and are given as follows:

$$Z(\omega) = \frac{M_0}{i\omega}\left[\sum_{n=0}^{\infty}\sum_{m=1}^{\infty}\frac{\phi_m^2(x_0)}{\zeta_{mn}\,\omega_{mn}^2}\,I_{mn} + \frac{M_0}{K}\right]^{-1}$$

and

$$K = M_0\left[\sum_{n=0}^{\infty}\sum_{m=1}^{\infty}\frac{\phi_m^2(x_0)}{\zeta_{mn}\,\omega_{mn}^2}\right]^{-1}$$

where

$$M_0 = 2\pi R\rho h\ell$$

$$\phi_m(x_0) = \sin \frac{m\pi x_0}{\ell}$$

$$I_{mn} = \frac{\left(\frac{\omega}{\omega_{mn}}\right)^2 \left[1 - \left(\frac{\omega}{\omega_{mn}}\right)^2 - \frac{1}{Q_{mn}^2}\right] + \frac{i}{Q_{mn}}\left(\frac{\omega}{\omega_{mn}}\right)}{\left[1 - \left(\frac{\omega}{\omega_{mn}}\right)^2\right]^2 + \frac{1}{Q_{mn}^2}\left(\frac{\omega}{\omega_{mn}}\right)^2}$$

in which ω_{mn} represents the angular resonance frequency and Q_{mn} is the dynamic magnification factor of the (m,n) mode; and ω represents the angular frequency and E, ρ, h, a and ℓ are the parameters of the shell.

This program consists of two subprograms. The first one computes the impedance value and the other one plots the computational results.

3.0 HARDWARE CONFIGURATION

The following computer hardware configuration is required to execute this program:

- Sigma 5 CPU
- 16 K words of core storage
- 1 Magnetic tape transport
- 1 Card reader
- 1 Teletyper
- 1 Line printer

4.0 INPUT INSTRUCTIONS

The input data consist of two input cards punched as follows:

Card 1

Columns 1-10	Number of frequency points to be computed in the specified range. The maximum number should not exceed 200. (Format I10)
Columns 11-20	The lowest frequency in Hz. (Format F10.0)
Columns 21-30	The highest frequency in Hz. (Format F10.0)

Card 2

Columns 1-10	Young's modulus of shell material in psi. (Format F10.0)
Columns 11-20	Weight density of shell material in $lb/inch^3$. (Format F10.0)
Columns 21-30	Poisson's ratio of shell material. (Format 10.0)
Columns 31-40	Thickness of shells in inch. (Format F10.0)
Columns 41-50	Radius of cylindrical shells in inch. (Format F10.0)
Columns 51-60	Length of shells in inch. (Format F10.0)
Columns 61-70	Dynamic magnification factor. (Format F10.0)
Columns 71-80	Location of point-driving force in inch. (Format F10.0)

5.0 OUTPUT RESULTS

The computational results are stored on a magnetic tape numbered 1. The printed output have the following form:

First several rows consist of —

- Total weight
- Static stiffness
- Impedance for finite plate
- Fundamental frequency
- Breathing (resonance) frequency

Remaining printed output consists of —

- 1st column represents the frequency values
- 2nd column represents the normalized frequency values
- 3rd and 4th columns lists the real and imaginary parts of the impedance values
- 4th and 5th columns shows the error criterion and number of terms in the summation

WYLE LABORATORIES

COMPUTER PROGRAM DESCRIPTION

Program Number	:	73/1004
Author	:	K.Y. Chang
Date	:	3 August 1973
Source Language	:	FORTRAN IV-H
Computer	:	XDS Sigma 5

1.0 PROGRAM TITLE

Component Package Impedance Evaluation Program

2.0 PROGRAM FEATURES

Given a suitable parameters of the point-mass system, this computer program computes and prints the input (velocity) impedance over the specified frequency range at logarithmic increments. The results are stored on a magnetic tape for plotting.

The equations used to evaluate the input impedance have been derived and are given as follows:

$$Z(\omega) = \frac{1}{\frac{1}{i\omega M} + \frac{1}{C + \frac{k}{i\omega}}}$$

and

$$Q = \sqrt{kM} \Big/ C$$

in which ω represents the angular frequency and M is the total mass, k is the stiffness, and C denotes the damping of the system.

This program consists of two subprograms. The first one computes the impedance value and the other one plots the computational results.

3.0 HARDWARE CONFIGURATION

The following computer hardware configuration is required to execute this program:

- Sigma 5 CPU
- 16 K words of core storage
- 1 Magnetic tape transports
- 1 Card reader
- 1 Teletyper
- 1 Line printer

4.0 INPUT INSTRUCTIONS

The input data consist of two input cards punched as follows:

Card 1

Columns 1-10	Number of frequency points to be computed in the specified range. The maximum number should not exceed 200. (Format I10)
Columns 11-20	The lowest frequency in Hz. (Format F10.0)
Columns 21-30	The highest frequency in Hz. (Format F10.0)

Card 2

Columns 1-10	Total mass weight of the payload structure in pounds. (Format F10.0)
Columns 11-20	Static stiffness of the payload structural system in lb/in. (Format F10.0)
Columns 21-30	Dynamic magnification of the payload system. (Format F10.0)

5.0 OUTPUT RESULTS

The computational results are stored on a magnetic tape numbered 1. The printer output has the following form:

First three rows containing —

- Total weight
- Static stiffness
- Fundamental frequency

Remaining printed output consists of —

- 1st column represents the frequency values
- 2nd column represents the normalized frequency values
- 3rd and 4th columns lists the real and imaginary parts of the impedance values

WYLE LABORATORIES

COMPUTER PROGRAM DESCRIPTION

Program Number	:	73/1005
Author	:	K.Y. Chang
Date	:	3 August 1973
Source Language	:	FORTRAN IV-H
Computer	:	XDS Sigma 5

1.0 PROGRAM TITLE

Impedance Plotting Program

2.0 PROGRAM FEATURES

The program plots the impedance results recorded on a magnetic tape which is obtained by Program No. 73/1001 through Program No. 73/1004.

3.0 HARDWARE CONFIGURATION

The following computer hardware configuration is required to execute this program:

- Sigma 5 CPU
- 16 K words of core storage
- 1 Magnetic tape transports
- 1 Card reader
- 1 Teletyper
- 1 Line printer
- 1 Calcomp plotter

4.0 INPUT INSTRUCTIONS

The digital tape recorded from Program 73/1001 must be mounted on Unit 1. This program executes by itself and no data card is needed.

6.0 OUTPUT RESULTS

The impedance data including the modulus and phase angular will be plotted on log-log scale using frequency as the abscissas. No printed output results.

```
      C
      C     PROGRAM NO. 73/1C01
      C     PROGRAM - DRIVING POINT IMPEDANCE OF BEAMS
      C     DEVELOPED BY K.Y. CHANG
      C
            COMPLEX ZM,ZZ
            COMMON HI(201),RL(201),QL(201)
            COMMON S(100)
            KMAX=100
            NERR=200
            RERR=0.001
            PI=3.1415926535
            NF=1
            HI(1)=0.00
        110 FORMAT(I10,2F10.0)
            READ(105,110) NP,FQMIN,FQMAX
      C
      C     NP    = NUMBER OF FREQUENCY POINTS
      C     FQMIN= STARTING FREQUENCY  ( HZ )
      C     FQMAX= ENDING FREQUENCY  ( HZ )
      C
            FQMIN=ALOG(FQMIN)
            DFQ=(ALOG(FQMAX)-FQMIN)/FLOAT(NP)
            DO 3 I=1,NP
            NF=NF+1
            HI(NF)=FQMIN+DFQ*FLOAT(I)
          3 HI(NF)=EXP(HI(NF))
        120 FORMAT(8F10.0)
            READ(105,120) AE,AD,AREA,AI,AL,AQ,ALF
      C
      C     PARMETERS OF FINITE BEAMS
      C     AE    = YOUNG MODULUS OF ELASTICITY  ( PSI )
      C     AD    = WEIGHT DENSITY OF MATERIAL  ( LB/IN**3 )
      C     AREA = CROSS SECTION AREA OF BEAMS  ( IN**2 )
      C     AI    = CROSS SECTION MONENT OF INERTIA OF BEAMS  ( IN**4 )
      C     AL    = LENGTH OF BEAMS  ( IN )
      C     AQ    = DYNAMIC MAGNIFICATION FACTOR
      C     ALF   = LOCATION OF POINT-DRIVING FORCE  ( IN )
      C
            AD=AD/386.1
            AMASS=AL*AD*AREA
            STIFF=48.00*AE*AI/AL/AL/AL
            AK4=AE*AI/AD/AREA
            AK2=SQRT(AK4)
            AK =SQRT(AK2)
            FS= AK*PI/AL
            FS=0.50*FS*FS/PI
            BEAM=4.00*AD*AREA*AK*SQRT(PI)
            WEIT=386.1*AMASS
            WRITE(108,400) WEIT,STIFF,FS,BEAM
        400 FORMAT(20X,'WEIGHT=',E12.4,' LB'
           1   //10X,'STATIC STIFFNESS=',E12.4,' LB/IN'
           1   //10X,'FUNDAMENTAL FREQ=',E12.4,' HZ'
           1   // 3X,'INFINITE BEAM IMPEDANCE=',E12.4,'(F)**0.5'/)
            AMASS2=AMASS/2.00
            PL=PI*ALF/AL
            YI=0.00
            DO 35 I=1,KMAX
            YI=YI+PL
```

```
      YR=SIN(YI)
   35 S(I)=YR*YR
      DO 20 I=1,NF
      AF=2.0*PI*HI(I)
      AF2=AF*AF
      ZZ=(0.0,0.0)
      K=0
   10 INOUT=0
   54 K=K+1
      M=K
      IF (K-KMAX) 55,55,56
   55 SM=S(M)
      GO TO 57
   56 SM=FLOAT(K)*PL
      SM=SIN(SM)
   57 CONTINUE
      AM=FLOAT(M)
      AM=AM*PI/AL
      AM2=AM*AM
      AM4=AM2*AM2
      AW2=AK4*AM4
      AW =SQRT(AW2)
      RI=AF/AW
      RR=1.00-RI*RI
      RI=RI/AQ
      RD=RR*RR+RI*RI
      YR= RR/RD
      YI=-RI/RD
      ZM=CMPLX(SM/AW2,0.0)*CMPLX(YR,YI)
      ZZ=ZZ+ZM
      IF (M .LT. 10) GO TO 10
      RATE=CABS(ZM/ZZ)
      IF (RATE-RERR) 13,4,4
   13 INOUT=INOUT+1
      IF (INOUT-1) 54,54,5
    4 IF (M    -NERR)  10,10,5
    5 CONTINUE
      IF (I-1) 6,6,7
    6 STIFF=AMASS2/REAL(ZZ)
      ZZ=CMPLX(STIFF,0.0)
      GO TO 8
    7 CONTINUE
      ZZ=ZZ*CMPLX(0.00,AF/AMASS2)
      ZZ=(1.0,0.0)/ZZ
      RL(I-1)= REAL(ZZ)
      QL(I-1)=AIMAG(ZZ)
      HI(I-1)=HI(I)
    8 AW=HI(I)/FS
      WRITE(108,100) I,HI(I),AW,ZZ,RATE,M
  100 FORMAT(I9,'  FQ=',F10.4,' (',F10.4,' )',2E15.5,F10.4,'   (',I5,
     1 ' )')
   20 CONTINUE
      NF=NF-1
      REWIND 1
      WRITE (1) NF
      WRITE (1) (HI(I),I=1,NF)
      WRITE (1) (RL(I),I=1,NF)
      WRITE (1) (QL(I),I=1,NF)
      STOP
      END
```

```
      C
      C     PROGRAM NO. 73/1002
      C     PROGRAM - DRIVING POINT IMPEDANCE OF RINGS
      C     DEVELOPED BY K.Y. CHANG
      C
            COMPLEX ZN,ZZ
            COMMON HI(200),RL(200),QL(200)
            NERR=200
            RERR=0.001
            PI=3.1415926535
            NF=0
          110 FORMAT(I10,2F10.0)
            READ(105,110) NP,FQMIN,FQMAX
      C
      C     NP    = NUMBER OF FREQUENCY POINTS
      C     FQMIN= STARTING FREQUENCY  ( HZ )
      C     FQMAX= ENDING FREQUENCY  ( HZ )
      C
            FQMIN=ALOG(FQMIN)
            DFQ=(ALOG(FQMAX)-FQMIN)/FLOAT(NP)
            DO 3 I=1,NP
            NF=NF+1
            HI(NF)=FQMIN+DFQ*FLOAT(I)
          3 HI(NF)=EXP(HI(NF))
          120 FORMAT(8F10.8)
            READ(105,120) AE,AD,AREA,AI,AA,AQ
      C
      C     PARMETERS OF RING FRAMES
      C     AE    = YOUNG MODULUS OF ELASTICITY  ( PSI )
      C     AD    = WEIGHT DENSITY OF MATERIAL  ( LB/IN**3 )
      C     AREA = CROSS SECTION AREA OF RINGS  ( IN**2 )
      C     AI    = CROSS SECTION MONENT OF INERTIA OF RINGS  ( IN**4 )
      C     AA    = RADIUS OF RINGS  ( IN )
      C     AQ    = DYNAMIC MAGNIFICATION FACTOR
      C
            AD=AD/386.1
            AMASS=2.00*PI*AA*AD*AREA
            STIFF=AE*AI/AA/AA/AA/0.15
            AA4=AA*AA*AA*AA
            AK4=AE*AI/AD/AREA/AA4
            AK2=SQRT(AK4)
            AK =SQRT(AK2)
            FS=0.427*AK2
            FE=0.50*SQRT(AE/AD)/AA/PI
            BEAM=4.00*AD*AREA*AA*AK*SQRT(PI)
            WEIT=386.1*AMASS
            WRITE(108,400) WEIT,STIFF,FS,BEAM,FE
          400 FORMAT(20X,'WEIGHT=',E12.4,' LB'
           1   //10X,'STATIC STIFFNESS=',E12.4,' LB/IN'
           1   //10X,'FUNDAMENTAL FREQ=',E12.4,' HZ'
           1   // 3X,'INFINITE BEAM IMPEDANCE=',E12.4,'(F)**0.5'
           2             //12X,'BREATHING FREQ=',E12.4,' HZ'/)
            AMASS2=AMASS/2.00
            DO 20 I=1,NF
            AF=2.0*PI*HI(I)
            AF2=AF*AF
            ZZ=(0.0,0.0)
            N = 0
```

```
      10 N=N+1
         AN=FLOAT(N)
         AN2=AN*AN
         AW2=AK4*AN2*(AN2-1.0)*(AN2-1.0)/(1.0+AN2)
         AW =SQRT(AW2)
         GN=1.00+1.00/AN2
         RI=AF*AW
         RR=AW2-AF2
         RI=RI/AQ
         RD=RR*RR+RI*RI
         YR= RR/RD
         YI=-RI/RD
         ZN=CMPLX(YR,YI)
         ZN=ZN/CMPLX(GN,0.0)
         ZZ=ZZ+ZN
         IF (N .LT. 10) GO TO 10
         RATE=CABS(ZN/ZZ)
         IF (RATE-RERR)  5,4,4
       4 IF (N    -NERR)  10,10,5
       5 CONTINUE
         ZZ=ZZ*CMPLX(0.00,AF/AMASS2)
         ZZ=(1.0,0.0)/ZZ
         AW=HI(I)/FS
         WRITE(108,100) I,HI(I),AW,ZZ,RATE,N
     100 FORMAT(I9,'  FQ=',F10.4,' (',F10.4,' )',2E15.5,F10.4,'   (',I5,
        1 ' )')
         RL(I)= REAL(ZZ)
         QL(I)=AIMAG(ZZ)
      20 CONTINUE
         REWIND 1
         WRITE (1) NF
         WRITE (1) (HI(I),I=1,NF)
         WRITE (1) (RL(I),I=1,NF)
         WRITE (1) (QL(I),I=1,NF)
         STOP
         END
```

```
C
C     PROGRAM NO. 73/1003
C     PROGRAM - DRIVING POINT IMPEDANCE OF SHELLS
C     DEVELOPED BY K.Y. CHANG
C
      COMPLEX ZM,ZN,Z7
      COMMON HI(201),RL(201),QL(201)
      COMMON G(51),W(51,100)
      COMMON S(100)
      COMMON/SHELL/PI,AE,AD,AV,AH,AA,AL,AQ,AB,AC
      JMAX=51
      KMAX=100
      NERR=200
      RERR=0.001
      PI=3.1415926535
      NF=1
      HI(1)=0.00
  110 FORMAT(I10,3F10.0)
      READ(105,110) NP,FQMIN,FQMAX
C
C     NP   = NUMBER OF FREQUENCY POINTS
C     FQMIN= STARTING FREQUENCY  ( HZ )
C     FQMAX= ENDING FREQUENCY  ( HZ )
C
      FQMIN=ALOG(FQMIN)
      DFQ=(ALOG(FQMAX)-FQMIN)/FLOAT(NP)
      DO 3 I=1,NP
      NF=NF+1
      HI(NF)=FQMIN+DFQ*FLOAT(I)
    3 HI(NF)=EXP(HI(NF))
  120 FORMAT(8F10.0)
      READ(105,120) AF,AD,AV,AH,AA,AL,AQ,ALF
C
C     PARMETERS OF FINITE CYLINDRICAL SHELLS
C     AE   = YOUNG MODULUS OF ELASTICITY  ( PSI )
C     AD   = WEIGHT DENSITY OF MATERIAL  ( LB/IN**3 )
C     AH   = THICKNESS OF SHELLS  ( IN )
C     AA   = RADIUS OF SHELLS  ( IN )
C     AL   = LENGTH OF SHELLS  ( IN )
C     AQ   = DYNAMIC MAGNIFICATION FACTOR
C     ALF  = LOCATION OF POINT-DRIVING FORCE  ( IN )
C
      AD=AD/386.1
      AB=AH/AA/SQRT(12.0)
      AC=AE/AD/(1.0-AV*AV)
      AC=SQRT(AC)
      FREQ=AC/AA
      AMASS=2.00*PI*AA*AL*AH*AD
      PLATE=4.00*AD*AH*AH*AC/SQRT(3.00)
      STIFF=2.50*AE*AH*SQRT(AA/AL)*(AH/AA)**1.25
      WEIT=386.1*AMASS
      WRITE(108,400) WEIT,STIFF,PLATE
  400 FORMAT(20X,'WEIGHT=',E12.4,' LB'
     1   //10X,'STATIC STIFFNESS=',E12.4,' LB/IN'
     1   //3X,'INFINITE PLATE IMPEDANCE=',E12.4,'(F)**0.5'/)
      FS=0.375*AC*SQRT(AH/AA)/AL
      FP=0.500*AC/AA/PI
      WRITE(108,410) FS,FP
```

```
      410 FORMAT(10X,'FUNDAMENTAL FREQ=',F12.2,10X,'BREATHING FREQ=',F12.2/)
          PL=PI*ALF/AL
          YI=0.00
          DO 35 I=1,KMAX
          YI=YI+PL
          YR=SIN(YI)
       35 S(I)=YR*YR
          G(1)=0.50
          DO 45 J=1,JMAX
          N=J-1
          IF (J .EQ. 1) GO TO 40
          G(J)=0.25+0.25/FLOAT(N*N)
       40 DO 45 K=1,KMAX
          M=K
          CALL FREQMN(M,N,AW)
       45 W(J,K)=AW
          YRST=0.00
          DO 20 I=1,NF
          AF=2.00*PI*HI(I)
          INDEX=0
          MMAX=1
          ZZ=(0.0,0.0)
          J=0
       10 J=J+1
          N=J-1
          IF (J-JMAX) 51,51,52
       51 GN=G(J)
          GO TO 53
       52 GN=0.25+0.25/FLOAT(N*N)
          INDEX=1
       53 ZN=(0.0,0.0)
          K=0
       30 INOUT=0
       54 K=K+1
          M=K
          IF (K-KMAX) 55,55,56
       55 SM=S(M)
          GO TO 57
       56 SM=FLOAT(K)*PL
          SM=SIN(SM)
          GO TO 63
       57 IF (INDEX) 62,62,63
       62 AW=W(J,K)
          GO TO 64
       63 CALL FREQMN(M,N,AW)
       64 CONTINUE
          RI=AF/AW
          RR=1.00-RI*RI
          RI=RI/AQ
          RD=RR*RR+RI*RI
          YR= RR/RD
          YI=-RI/RD
          YR=YR-YRST
          ZM=CMPLX(SM/AW/AW,0.0)*CMPLX(YR,YI)
          ZN=ZN+ZM
          IF (M .LT. 20) GO TO 30
          RATE1=CABS(ZM/ZN)
          IF (RATE1-REER) 13,14,14
       13 INOUT=INOUT+1
```

```
      IF (INPUT-1) 54,54,15
   14 IF (M    -NERR) 30,30,15
   15 CONTINUE
      IF (MMAX .LT. M) MMAX=M
      ZN=ZN/CMPLX(GN,0.0)
      ZZ=ZZ+ZN
      IF (N .LT. 10) GO TO 10
      RATE=CABS(ZN/ZZ)
      IF (RATE-RERR)  5,4,4
    4 IF (N   -NERR)  10,10,5
    5 CONTINUE
      IF (I-1) 6,6,7
    6 STIFF=AMASS/REAL(ZZ)
      ZZ=CMPLX(STIFF,0.0)
      GO TO 8
    7 CONTINUE
      ZZ=ZZ+CMPLX(AMASS/STIFF,0.0)
      ZZ=ZZ*CMPLX(0.0,AF /AMASS)
      ZZ=(1.0,0.0)/ZZ
      RL(I-1)= REAL(ZZ)
      QL(I-1)=AIMAG(ZZ)
      HI(I-1)=HI(I)
    8 AW=AF/FREQ
      M=MMAX
      WRITE(108,100) I,HI(I),AW,ZZ,RATE,M,N
  100 FORMAT(I9,'  FQ=',F10.4,' (',F10.4,' )',2E15.5,F10.4,'   (',I5,
     1 ',',I3,' )')
    20 YRST=1.00
      NF=NF-1
      REWIND 1
      WRITE (1) NF
      WRITE (1) (HI(I),I=1,NF)
      WRITE (1) (RL(I),I=1,NF)
      WRITE (1) (QL(I),I=1,NF)
    99 STOP
      END
```

```
      SUBROUTINE FREQMN(M,N,AW)
      COMMON/SHELL/PI,AE,AD,AV,AH,AA,AL,AQ,AB,AC
      AM=FLOAT(M)
      AN=FLOAT(N)
      AK=AM*PI*AA/AL
      AK2=AK*AK
      AN2=AN*AN
      ANK2=AN2+AK2
      ANK4=ANK2*ANK2
      AW2=(1.-AV*AV)*AK2*AK2/ANK4+AB*AB*(ANK4-0.5*(AN2*(4.-AV)-2.-AV)/
     1    (1.-AV)  )
      AW=SQRT(AW2)
      AW=AW*AC/AA
      RETURN
      END
```

```
      C
      C     PROGRAM NO. 73/1004
      C     PROGRAM - DRIVING POINT IMPEDANCE OF COMPONENT PACKAGE
      C     DEVELOPED BY K.Y. CHANG
      C
            COMPLEX ZZ
            COMMON HI(200),RL(200),QL(200)
            PI=3.1415926535
            NF=0
        110 FORMAT(I10,2F10.0)
            READ(105,110) NP,FQMIN,FQMAX
      C
      C     NP    = NUMBER OF FREQUENCY POINTS
      C     FQMIN= STARTING FREQUENCY  ( HZ )
      C     FQMAX= ENDING FREQUENCY  ( HZ )
      C
            FQMIN=ALOG(FQMIN)
            DFQ=(ALOG(FQMAX)-FQMIN)/FLOAT(NP)
            DO 3 I=1,NP
            NF=NF+1
            HI(NF)=FQMIN+DFQ*FLOAT(I)
          3 HI(NF)=EXP(HI(NF))
        120 FORMAT(8F10.0)
            READ(105,120) AM,AK,AQ
      C
      C     MASS-SPRING-DASHPOT MODEL
      C     AM    = TOTAL MASS WIGHT OF THE SYSTEM  ( LB )
      C     AK    = STATIC STIFFNESS OF THE SYSTEM  ( LB/IN )
      C     AQ    = DYNAMIC MAGNIFICATION FACTOR OF THE SYSTEM
      C
            AC=SQRT(AK*AM)/AQ
            AMASS=AM
            STIFF=AK
            FS=0.5*SQRT(AK/AM)/PI
            WEIT=386.1*AMASS
            WRITE(108,400) WEIT,STIFF,FS
        400 FORMAT(20X,'WEIGHT=',E12.4,' LB'
           1   //10X,'STATIC STIFFNESS=',E12.4
           1   //10X,'FUNDAMENTAL FREQ=',E12.4//)
            DO 20 I=1,NF
            AF=2.0*PI*HI(I)
            ZZ=(1.0,0.0)/CMPLX(0.0,AF*AM)
            ZZ=ZZ+(1.0,0.0)/CMPLX(AC,-AK/AF)
            ZZ=(1.0,0.0)/ZZ
            AW=HI(I)/FS
            WRITE(108,100) I,HI(I),AW,ZZ
        100 FORMAT(I9,'  FQ=',F10.4,' (',F10.4,' )',2E15.5,F10.4)
            RL(I)= REAL(ZZ)
            QL(I)=AIMAG(ZZ)
         20 CONTINUE
            REWIND 1
            WRITE (1) NF
            WRITE (1) (HI(I),I=1,NF)
            WRITE (1) (RL(I),I=1,NF)
            WRITE (1) (QL(I),I=1,NF)
            STOP
            END
```

PROGRAM NO. 73/1005

```
1               COMMON HI(400),RL(400),QL(400)
2               COMMON/PLOT1/XSTEP,YSTEP
3               COMMON/PLOT2/XSIZE,YSIZE,XUNIT
4               COMMON/PLOT3/XDECADE,YDECADE
5               COMMON/REF1/NUMBER,YMIN,YMAX,XAXIS,XSCALE,YSCALE
6               XSTEP=1.00
7               YSTEP=-2.00
8               XUNIT=1.00
9               YSIZE=1.00
10              XDECADE=3.33
11              YDECADE=1.38
12              XDECADE=2.00
13              YDECADE=2.00
14              XDECADE=1.50
15              YDECADE=1.50
16              CALL PLOT(0.0, 12.0,25)
17              NUMBER=0
18              REWIND 1
19            20 CONTINUE
20              READ (1) NF
21              READ (1) (HI(I),I=1,NF)
22              READ (1) (RL(I),I=1,NF)
23              READ (1) (QL(I),I=1,NF)
24              CALL PHASE(NF,RL,QL,+1)
25              CALL POTPHS(HI,QL,NF)
26              IF (NUMBER .GT. 0) GO TO 30
27              CALL SYMBOL(0.50,-6.0,0.125,90.,1.0,
28             1    32,'MODULUS OF IMPEDANCE (LB-SEC/IN)')
29            30 CONTINUE
30              XSTEP= 0.00
31              YSTEP=-7.50
32              CALL POTLOG(HI,RL,NF)
33              YSTEP= 7.50
34              XSTEP=-XAXIS-1.00
35              NUMBER=NUMBER+1
36              STOP
37              GO TO 20
38              END
```

SUBPROGRAMS

BF:PIN	PLOT	BF:ST	BF:S2	BF:II	BF:SF	BF:FI	PHASE
POTPHS	SYMBOL	POTLOG	BF:SX				

PROGRAM ALLOCATION

AR.0	NF	A9.0	I

PROGRAM SIZE AA

/F4:COM / ALLOCATION ARC WORDS

0.0	HI	190.0	RL	320.0	QL

```
      SUBROUTINE PBTPHS(X,Y,N)
C     DEVELOPED BY K.Y. CHANG
      DIMENSION X(1),Y(1)
      COMMON/PLOT1/XSTEP,YSTEP
      COMMON/PLOT2/XSIZE,YSIZE
      COMMON/PLOT3/XDECADE,YDECADE
      COMMON/REF1/NUMBER,DMIN,DMAX,XAXIS,XSCALE,YSCALE
      COMMON/AXIS/ TT(8)
      DATA  TT/0.0458,0.0969,0.1549,0.2218,0.301,0.3979,0.5229,0.699/
      YSTEP=YSTEP-YSIZE
      CALL PLOT (XSTEP,YSTEP,25)
      ECOEF=2.302585963
      XCON=XDECADE/ECOEF
      YMIN=-180.00
      YMAX= 180.00
      IF (NUMBER.GT.0) GO TO 220
      XSCALE=1.00
      II=IFIX(ALOG(X(1))/ECOEF)
      IF (X(1)-1.0) 1,3,2
    1 II=II-1
    2 XSCALE=1.0/10.0**FLOAT(II)
    3 CONTINUE
      IA=IFIX(ALOG(X(N))/ECOEF)+1
      XAXIS=FLOAT(IA-II)*XDECADE
      YUPI=YMAX/YSIZE
      CALL SYMBOL(0.60,0.00,0.10,0.00,1,2,-1,YMIN)
      CALL PLOT (1.0,0.0,3)
      YY=(YMAX-YMIN)/YUPI
      CALL PLOT (1.0,YY,2)
      YY=YY-0.10
      CALL SYMBOL(0.68,  YY,0.10,0.00,1,2,-1,YMAX)
      CALL SYMBOL(0.50,0.40,0.125,90.,1,0,11,'PHASE (DEG)')
      YY=-YMIN/YUPI
      CALL SYMBOL(0.85,  YY,0.10,0.00,1,0,1,'0')
      CALL PLOT (1.0,YY,3)
      XX=XAXIS+1.00
      CALL PLOT(XX,YY,2)
      ND=IFIX(XAXIS/XDECADE+0.5)
      DO 19 I=1,ND
      CALL PLOT(XX,YY+0.125,3)
      CALL PLOT(XX,YY,2)
      DO 18 J=1,8
      XD=XX-TT(J)*XDECADE
      CALL PLOT(XD,YY+0.0625,3)
   18 CALL PLOT(XD,YY,2)
   19 XX=XX-XDECADE
  220 CONTINUE
      XX= ALOG(X(1)*XSCALE)*XCON
      XX=XX+1.00
      YY=(Y(1)-YMIN)/YUPI
      CALL PLOT(XX,YY,3)
      DO 22 I=2,N
      XX= ALOG(X(I)*XSCALE)*XCON
      XX=XX+1.00
      YY=(Y(I)-YMIN)/YUPI
      NI=2
      CC=ABS(Y(I)-Y(I-1))
      IF (CC-180.) 22,22,21
```

```
      21    NI=3
      22    CALL PLOT  (XX,YY,NI)
            CALL PLOT (0.0,YSIZE,25)
            XSTEP=0.00
            RETURN
            END
```

```
            SUBROUTINE PHASE(N,RR,RI,KK)
      C     DEVELOPED BY K.Y. CHANG
            DIMENSION RR(1),RI(1)
            IF (KK) 2,4,1
          1 RMAX=0.00
            DO 6 I=1,N
            PR=RR(I)
            PI=RI(I)
            DD=SQRT(PR*PR+PI*PI)
            IF (DD-RMAX) 6,6,5
          5 RMAX=DD
          6 CONTINUE
            RMAX=RMAX/1000000.
            DO 20 I=1,N
            PR=RR(I)
            PI=RI(I)
            IF (PR) 13,10,13
         10 IF (PI) 11,12,11
         11 DD=90.*PI/ABS(PI)
            GO TO 14
         12 DD=0.00
            GO TO 14
         13 DD=ATAN2(PI,PR)
         14 RR(I)=SQRT(PR*PR+PI*PI)
            IF (RR(I)-RMAX) 16,16,15
         15 IF (ABS(DD) -3.1416) 17,16,16
         16 DD=0.00
         17 RI(I)=57.2957795*DD
         20 CONTINUE
            GO TO 4
          2 CONTINUE
            DO 3 I=1,N
            PR=RR(I)
            PI=RI(I)
            DD=0.0174533*PI
            RR(I)=PR*COS(DD)
          3 RI(I)=PR*SIN(DD)
          4 CONTINUE
            RETURN
            END
```

```
      SUBROUTINE PGTLOG(X,Y,N)
C     LEVEL0FED BY K.Y. CHANG
      DIMENSION X(1),Y(1)
      COMMON/PLOT1/XSTEP,YSTEP
      COMMON/PLOT3/XDECADE,YDECADE
      COMMON/REF1/NUMBER,YMIN,YMAX,XAXIS,XSCALE,YSCALE
      COMMON/AXIS/ TT(8)
      DATA  TT/0.0458,0.0969,0.1549,0.2218,0.301,0.3979,0.5229,0.699/
      XSTEP=XSTEP+1.00
      CALL PLOT (XSTEP,YSTEP,25)
      ECOEF=2.302585963
      XCON=XDECADE/ECOEF
      YCON=YDECADE/ECOEF
      IF (NUMBER.GT.0) GO TO 20
      IQ=IFIX( 6.5/YDECADE)
      XSCALE=1.00
      II=IFIX(ALOG(X(1))/ECOEF)
      IF (X(1)-1.0) 1,3,2
    1 II=II-1
    2 XSCALE=1.0/10.0**FLOAT(II)
    3 CONTINUE
      IA=IFIX(ALOG(X(N))/ECOEF)+1
      XMAX=10.0**FLOAT(IA)
      XAXIS=FLOAT(IA-II)*XDECADE
      YMAX=Y(1)
      DO 6 I=2,N
    4 IF(Y(I)-YMAX) 6,6,5
    5 YMAX=Y(I)
    6 CONTINUE
      IA=IFIX(ALOG(YMAX)/ECOEF)+1
      IF (YMAX-1.0) 7,8,8
    7 IA=IA-1
    8 YMAX=10.0**FLOAT(IA)
    9 II=IA-IQ
   10 YMIN=10.0**FLOAT(II)
      YAXIS=FLOAT(IA-II)*YDECADE
      YSCALE=1.00
      IF (II) 14,15,14
   14 YSCALE=1.0/10.0**FLOAT(II)
   15 CONTINUE
      CALL PLOT (0.0,0.0,3)
      YY=YAXIS
      CALL PLOT(0.0,YY,2)
      NY=IFIX(YAXIS/YDECADE+0.5)
      DO 17 I=1,NY
      CALL SYMBOL(-0.40,YY-0.15,0.10,0.00,1.0,2,'10')
      CALL SYMBOL(-0.27,YY,0.10,0.00,1,1,-1,IA)
      IA=IA-1
      CALL PLOT(0.125,YY,3)
      CALL PLOT(0.0,YY,2)
      DO 16 J=1,8
      YD=YY-TT(J)*YDECADE
      CALL PLOT(0.0625,YD,3)
   16 CALL PLOT(0.0,YD,2)
   17 YY=YY-YDECADE
      CALL SYMBOL(-0.40,YY-0.05,0.10,0.00,1.0,2,'10')
      CALL SYMBOL(-0.27,YY+0.10,0.10,0.00,1,1,-1,IA)
      CALL PLOT(0.0,0.0,3)
```

```
      XX=XAXIS
      CALL PLOT(XX,0.0,2)
      NX=IFIX(XAXIS/XDECADE+0.5)
      IK=-1
      DO 19 I=1,NX
      CALL SYMBOL(XX-0.10,-0.20,0.10,0.00,1,2,IK,XMAX)
      XMAX=XMAX/10.0
      IF (XMAX .LT. 1.5) IK=IK+1
      CALL PLOT(XX,0.125,3)
      CALL PLOT(XX,0.0,2)
      DO 18 J=1,8
      XD=XX-TT(J)*XDECADE
      CALL PLOT(XD,0.0625,3)
   18 CALL PLOT(XD,0.0,2)
   19 XX=XX-XDECADE
      CALL SYMBOL(      XX,-0.20,0.10,0.00,1,2,IK,XMAX)
      XX=XAXIS/3.00+0.25
      YY=-0.50
      CALL SYMBOL(XX,YY,0.125,0.00,1,0,14,'FREQUENCY (HZ)')
   20 IK=3
      DO 23 I=1,N
      XX=ALOG(X(I)*XSCALE)*XCON
      YY=ALOG(Y(I)*YSCALE)*YCON
      IF (Y(I) .GT. YMAX) YY=YAXIS
      IF (Y(I) .LT. YMIN) YY=0.00
      CALL PLOT(XX,YY,IK)
   23 IK=2
      IF (NUMBER.GT.0) GO TO 30
      XX=XAXIS
      YY=0.00
      DO 27 I=1,NY
      YY=YY+YDECADE
      DO 26 J=1,8
      IK=9-J
      YD=YY-TT(IK)*YDECADE
      CALL PLOT(XX-0.0625,YD,3)
   26 CALL PLOT(XX,YD,2)
      CALL PLOT(XX-0.125,YY,3)
   27 CALL PLOT(XX,YY,2)
      DO 29 I=1,NX
      DO 28 J=1,8
      XD=XX-TT(J)*XDECADE
      CALL PLOT(XD,YY-0.0625,3)
   28 CALL PLOT(XD,YY,2)
      XX=XX-XDECADE
      CALL PLOT(XX,YY-0.125,3)
   29 CALL PLOT(XX,YY,2)
      CALL PLOT(0.00,YAXIS,3)
      CALL PLOT(XAXIS,YAXIS,2)
      CALL PLOT(XAXIS,0.00,2)
   30 CONTINUE
      CALL PLOT(XAXIS,0.00,25)
      XSTEP=1.50
      RETURN
      END
```

WEIGHT= 0.1181E+01 LB

STATIC STIFFNESS= 0.6510E+01 LB/IN

FUNDAMENTAL FREQ= 0.1046E+02 HZ

INFINITE BEAM IMPEDANCE= 0.5595E-01(F)**0.5

1	FQ=	0.0000	(0.0000)	0.65110E+01	0.00000E+00	0.0001	(11)
2	FQ=	1.2589	(0.1203)	0.97815E-02	-0.81138E+00	0.0001	(11)
3	FQ=	1.5849	(0.1515)	0.97836E-02	-0.63904E+00	0.0001	(11)
4	FQ=	1.9953	(0.1907)	0.97870E-02	-0.50073E+00	0.0001	(11)
5	FQ=	2.5119	(0.2401)	0.97924E-02	-0.38908E+00	0.0001	(11)
6	FQ=	3.1623	(0.3023)	0.98010E-02	-0.29814E+00	0.0001	(11)
7	FQ=	3.9811	(0.3806)	0.98146E-02	-0.22306E+00	0.0001	(11)
8	FQ=	5.0119	(0.4791)	0.98364E-02	-0.15983E+00	0.0001	(11)
9	FQ=	6.3096	(0.6032)	0.98717E-02	-0.10504E+00	0.0000	(11)
10	FQ=	7.9433	(0.7593)	0.99294E-02	-0.55707E-01	0.0000	(11)
11	FQ=	10.0000	(0.9559)	0.10025E-01	-0.90615E-02	0.0000	(11)
12	FQ=	12.5892	(1.2035)	0.10188E-01	0.37672E-01	0.0000	(11)
13	FQ=	15.8489	(1.5151)	0.10478E-01	0.87602E-01	0.0001	(11)
14	FQ=	19.9526	(1.9074)	0.11025E-01	0.14475E+00	0.0002	(11)
15	FQ=	25.1188	(2.4012)	0.12163E-01	0.21533E+00	0.0004	(11)
16	FQ=	31.6227	(3.0230)	0.14923E-01	0.31133E+00	0.0006	(11)
17	FQ=	39.8106	(3.8057)	0.23625E-01	0.46375E+00	0.0006	(13)
18	FQ=	50.1186	(4.7911)	0.70765E-01	0.79943E+00	0.0008	(15)
19	FQ=	63.0956	(6.0316)	0.21989E+01.	0.25588E+01	0.0007	(23)
20	FQ=	79.4326	(7.5934)	0.21499E+00	-0.44017E+00	0.0007	(15)
21	FQ=	99.9997	(9.5595)	0.76086E-01	0.10508E+00	0.0008	(11)
22	FQ=	125.8922	(12.0347)	0.60775E-01	0.42240E+00	0.0006	(17)
23	FQ=	158.4889	(15.1508)	0.97468E-01	0.84102E+00	0.0010	(19)
24	FQ=	199.5257	(19.0737)	0.12337E+01	0.23334E+01	0.0009	(27)
25	FQ=	251.1878	(24.0123)	0.32387E+00	-0.16612E+00	0.0007	(19)
26	FQ=	316.2266	(30.2297)	0.14963E+00	0.70119E+00	0.0008	(23)
27	FQ=	398.1060	(38.0570)	0.58165E+00	0.19457E+01	0.0008	(31)
28	FQ=	501.1855	(47.9109)	0.56775E+00.	-0.80123E-01	0.0010	(23)
29	FQ=	630.9551	(60.3162)	0.33113E+00	0.13948E+01	0.0009	(31)
30	FQ=	794.3252	(75.9336)	0.18712E+01	-0.46473E+00	0.0010	(35)
31	FQ=	999.9963	(95.5947)	0.52251E+00	0.17496E+01	0.0009	(37)
32	FQ=	1258.9207	(120.3466)	0.10802E+01	0.31151E+00	0.0009	(35)
33	FQ=	1584.8867	(151.5073)	0.25910E+01	0.30668E+01	0.0009	(51)
34	FQ=	1995.2537	(190.7364)	0.10221E+01	0.24518E+01	0.0009	(49)
35	FQ=	2511.8767	(240.1230)	0.10779E+01	0.19795E+01	0.0009	(49)
36	FQ=	3162.2627	(302.2966)	0.13588E+01	0.19739E+01	0.0009	(53)
37	FQ=	3981.0537	(380.5688)	0.16102E+01	0.25289E+01	0.0009	(59)
38	FQ=	5011.8477	(479.1077)	0.23129E+01	0.36773E+01	0.0009	(69)
39	FQ=	6309.5430	(603.1611)	0.42790E+01	0.30535E+01	0.0009	(77)
40	FQ=	7943.2383	(759.3342)	0.28060E+01	0.36818E+01	0.0009	(79)
41	FQ=	9999.9492	(955.9456)	0.41487E+01	0.33394E+01	0.0010	(85)

NSTOP

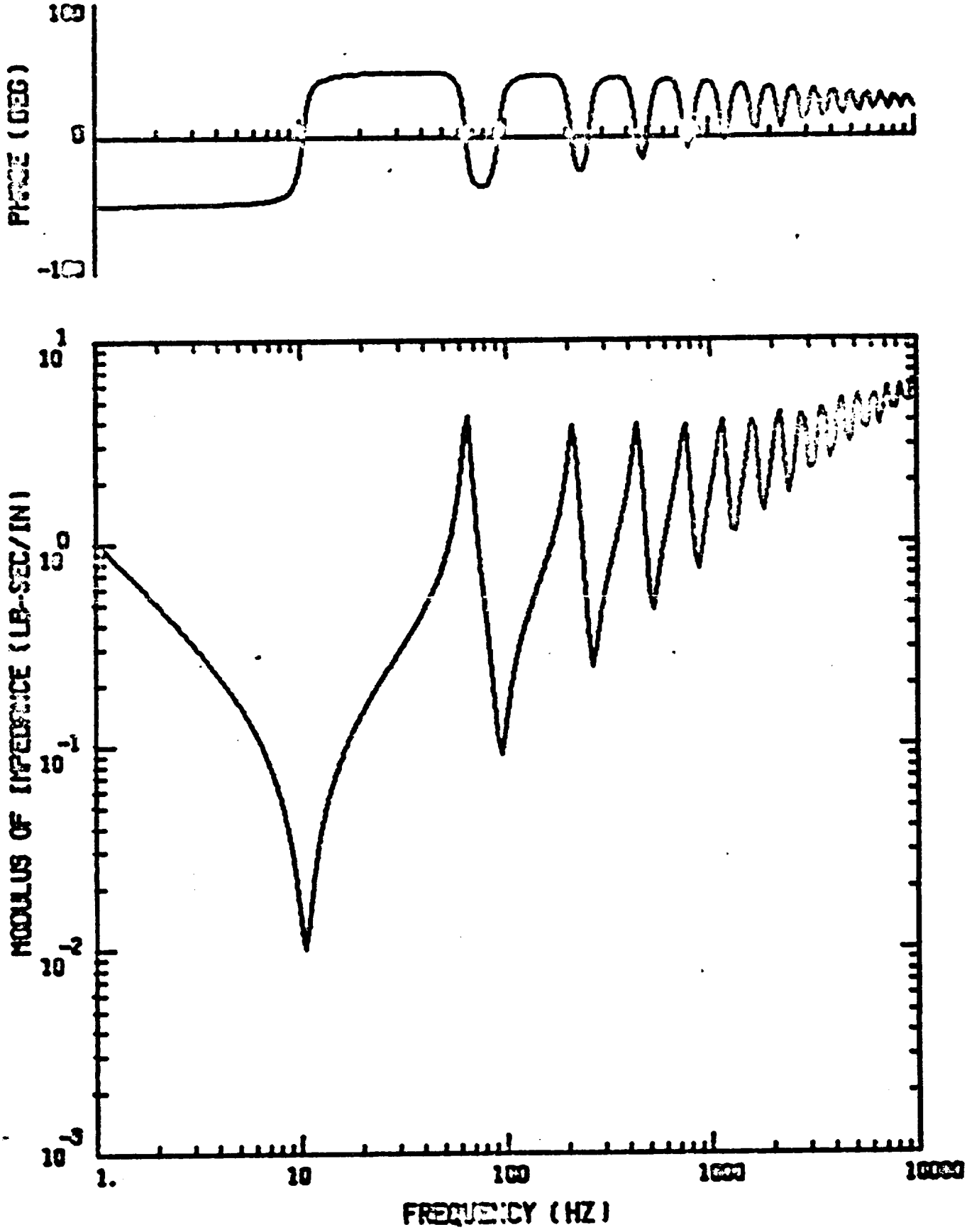
PHASE (DEG)
10
0
-10
MODULUS OF IMPEDANCE (LB-SEC/IN)
10^{1}
10^{0}
10^{-1}
10^{-2}
10^{-3}
1.
10
100
1000
10000
FREQUENCY (HZ)

WYLE WR 73-9

PREDICTION OF VIBRO-ACOUSTIC LOADING CRITERIA FOR SPACE VEHICLE COMPONENTS

K.Y. Chang, J.C. Cockburn, G.C. Kao; September 1973
Wyle Laboratories, Research Staff, Huntsville, Alabama

This report presents a technique to estimate driving force spectra of equipment packages attached to cylindrical structures subjected to broadband random acoustic excitations. This procedure is considered indicative of the present state-of-the-art and will provide satisfactory predictions of the vibratory environment.

The force-spectrum equation was derived from a one-dimensional mechanical impedance model and is expressed in terms of structural impedance, acoustic mobility and blocked pressure spectra. A set of nomograms and computational charts was developed to compute the force spectrum graphically with a minimum amount of manual computation. Two example problems with different structural configurations were used to demonstrate computation procedures. Satisfactory agreements between analytical predictions and experimental measurements were observed.

I. K. Y. CHANG
J. C. COCKBURN
G. C. KAO

II. WR 73-9

III. NAS8-25811

1. Stiffened Shells
2. Mechanical Impedance
3. Acoustic Mobility
4. Structural Dynamics
5. Force Spectrum
6. Nomograms
7. Computation Techniques

WYLE WR 73-9

PREDICTION OF VIBRO-ACOUSTIC LOADING CRITERIA FOR SPACE VEHICLE COMPONENTS

K.Y. Chang, J.C. Cockburn, G.C. Kao; September 1973
Wyle Laboratories, Research Staff, Huntsville, Alabama

This report presents a technique to estimate driving force spectra of equipment packages attached to cylindrical structures subjected to broadband random acoustic excitations. This procedure is considered indicative of the present state-of-the-art and will provide satisfactory predictions of the vibratory environment.

The force-spectrum equation was derived from a one-dimensional mechanical impedance model and is expressed in terms of structural impedance, acoustic mobility and blocked pressure spectra. A set of nomograms and computational charts was developed to compute the force spectrum graphically with a minimum amount of manual computation. Two example problems with different structural configurations were used to demonstrate computation procedures. Satisfactory agreements between analytical predictions and experimental measurements were observed.

I. K. Y. CHANG
J. C. COCKBURN
G. C. KAO

II. WR 73-9

III. NAS8-25811

1. Stiffened Shells
2. Mechanical Impedance
3. Acoustic Mobility
4. Structural Dynamics
5. Force Spectrum
6. Nomograms
7. Computation Techniques

WYLE WR 73-9

PREDICTION OF VIBRO-ACOUSTIC LOADING CRITERIA FOR SPACE VEHICLE COMPONENTS

K.Y. Chang, J.C. Cockburn, G.C. Kao; September 1973
Wyle Laboratories, Research Staff, Huntsville, Alabama

This report presents a technique to estimate driving force spectra of equipment packages attached to cylindrical structures subjected to broadband random acoustic excitations. This procedure is considered indicative of the present state-of-the-art and will provide satisfactory predictions of the vibratory environment.

The force-spectrum equation was derived from a one-dimensional mechanical impedance model and is expressed in terms of structural impedance, acoustic mobility and blocked pressure spectra. A set of nomograms and computational charts was developed to compute the force spectrum graphically with a minimum amount of manual computation. Two example problems with different structural configurations were used to demonstrate computation procedures. Satisfactory agreements between analytical predictions and experimental measurements were observed.

I. K. Y. CHANG
J. C. COCKBURN
G. C. KAO

II. WR 73-9

III. NAS8-25811

1. Stiffened Shells
2. Mechanical Impedance
3. Acoustic Mobility
4. Structural Dynamics
5. Force Spectrum
6. Nomograms
7. Computation Techniques

WYLE WR 73-9

PREDICTION OF VIBRO-ACOUSTIC LOADING CRITERIA FOR SPACE VEHICLE COMPONENTS

K.Y. Chang, J.C. Cockburn, G.C. Kao; September 1973
Wyle Laboratories, Research Staff, Huntsville, Alabama

This report presents a technique to estimate driving force spectra of equipment packages attached to cylindrical structures subjected to broadband random acoustic excitations. This procedure is considered indicative of the present state-of-the-art and will provide satisfactory predictions of the vibratory environment.

The force-spectrum equation was derived from a one-dimensional mechanical impedance model and is expressed in terms of structural impedance, acoustic mobility and blocked pressure spectra. A set of nomograms and computational charts was developed to compute the force spectrum graphically with a minimum amount of manual computation. Two example problems with different structural configurations were used to demonstrate computation procedures. Satisfactory agreements between analytical predictions and experimental measurements were observed.

I. K. Y. CHANG
J. C. COCKBURN
G. C. KAO

II. WR 73-9

III. NAS8-25811

1. Stiffened Shells
2. Mechanical Impedance
3. Acoustic Mobility
4. Structural Dynamics
5. Force Spectrum
6. Nomograms
7. Computation Techniques

WYLE WR 73-9

PREDICTION OF VIBRO-ACOUSTIC LOADING CRITERIA FOR SPACE VEHICLE COMPONENTS

K.Y. Chang, J.C. Cockburn, G.C. Kao; September 1973
Wyle Laboratories, Research Staff, Huntsville, Alabama

This report presents a technique to estimate driving force spectra of equipment packages attached to cylindrical structures subjected to broadband random acoustic excitations. This procedure is considered indicative of the present state-of-the-art and will provide satisfactory predictions of the vibratory environment.

The force-spectrum equation was derived from a one-dimensional mechanical impedance model and is expressed in terms of structural impedance, acoustic mobility and blocked pressure spectra. A set of nomograms and computational charts was developed to compute the force spectrum graphically with a minimum amount of manual computation. Two example problems with different structural configurations were used to demonstrate computation procedures. Satisfactory agreements between analytical predictions and experimental measurements were observed.

I. K. Y. CHANG
J. C. COCKBURN
G. C. KAO

II. WR 73-9

III. NAS8-25811

1. Stiffened Shells
2. Mechanical Impedance
3. Acoustic Mobility
4. Structural Dynamics
5. Force Spectrum
6. Nomograms
7. Computation Techniques

WYLE WR 73-9

PREDICTION OF VIBRO-ACOUSTIC LOADING CRITERIA FOR SPACE VEHICLE COMPONENTS

K.Y. Chang, J.C. Cockburn, G.C. Kao; September 1973
Wyle Laboratories, Research Staff, Huntsville, Alabama

This report presents a technique to estimate driving force spectra of equipment packages attached to cylindrical structures subjected to broadband random acoustic excitations. This procedure is considered indicative of the present state-of-the-art and will provide satisfactory predictions of the vibratory environment.

The force-spectrum equation was derived from a one-dimensional mechanical impedance model and is expressed in terms of structural impedance, acoustic mobility and blocked pressure spectra. A set of nomograms and computational charts was developed to compute the force spectrum graphically with a minimum amount of manual computation. Two example problems with different structural configurations were used to demonstrate computation procedures. Satisfactory agreements between analytical predictions and experimental measurements were observed.

I. K. Y. CHANG
J. C. COCKBURN
G. C. KAO

II. WR 73-9

III. NAS8-25811

1. Stiffened Shells
2. Mechanical Impedance
3. Acoustic Mobility
4. Structural Dynamics
5. Force Spectrum
6. Nomograms
7. Computation Techniques

WYLE WR 73-9

PREDICTION OF VIBRO-ACOUSTIC LOADING CRITERIA FOR SPACE VEHICLE COMPONENTS

K.Y. Chang, J.C. Cockburn, G.C. Kao; September 1973
Wyle Laboratories, Research Staff, Huntsville, Alabama

This report presents a technique to estimate driving force spectra of equipment packages attached to cylindrical structures subjected to broadband random acoustic excitations. This procedure is considered indicative of the present state-of-the-art and will provide satisfactory predictions of the vibratory environment.

The force-spectrum equation was derived from a one-dimensional mechanical impedance model and is expressed in terms of structural impedance, acoustic mobility and blocked pressure spectra. A set of nomograms and computational charts was developed to compute the force spectrum graphically with a minimum amount of manual computation. Two example problems with different structural configurations were used to demonstrate computation procedures. Satisfactory agreements between analytical predictions and experimental measurements were observed.

I. K. Y. CHANG
J. C. COCKBURN
G. C. KAO

II. WR 73-9

III. NAS8-25811

1. Stiffened Shells
2. Mechanical Impedance
3. Acoustic Mobility
4. Structural Dynamics
5. Force Spectrum
6. Nomograms
7. Computation Techniques

WYLE WR 73-9

PREDICTION OF VIBRO-ACOUSTIC LOADING CRITERIA FOR SPACE VEHICLE COMPONENTS

K.Y. Chang, J.C. Cockburn, G.C. Kao; September 1973
Wyle Laboratories, Research Staff, Huntsville, Alabama

This report presents a technique to estimate driving force spectra of equipment packages attached to cylindrical structures subjected to broadband random acoustic excitations. This procedure is considered indicative of the present state-of-the-art and will provide satisfactory predictions of the vibratory environment.

The force-spectrum equation was derived from a one-dimensional mechanical impedance model and is expressed in terms of structural impedance, acoustic mobility and blocked pressure spectra. A set of nomograms and computational charts was developed to compute the force spectrum graphically with a minimum amount of manual computation. Two example problems with different structural configurations were used to demonstrate computation procedures. Satisfactory agreements between analytical predictions and experimental measurements were observed.

I. K. Y. CHANG
J. C. COCKBURN
G. C. KAO

II. WR 73-9

III. NAS8-25811

1. Stiffened Shells
2. Mechanical Impedance
3. Acoustic Mobility
4. Structural Dynamics
5. Force Spectrum
6. Nomograms
7. Computation Techniques